SBORNÍK GEOLOGICKÝCH VĚD
JOURNAL OF GEOLOGICAL SCIENCES

užitá geofyzika

applied geophysics

25

Publikace a.s. Geofyzika, Brno

Vědecký redaktor

RNDr. KAREL CIDLINSKÝ, CSc.

Diskuse o pracích se konala na vědecké radě a.s. Geofyzika, Brno,
dne 3. února 1990

SBORNÍK GEOLOGICKÝCH VĚD
JOURNAL OF GEOLOGICAL SCIENCES

užitá geofyzika

applied geophysics

25

VYDAL ČESKÝ GEOLOGICKÝ ÚSTAV
PRAHA 1992

ISBN 80-7075-110-X
ISSN 0036-5319

OBSAH

Sborník geologických věd	Užitá geofyzika 25	Pages 9 – 48	6 figs.	– tab.	4 pls.	Praha 1992 ISBN 80-7075-110-X ISSN 0036-5319

Geophysical prospecting for hydrocarbons in the Intracarpathian Paleogene and in the East Slovak Flysch Belt

Geofyzikální průzkum na uhlovodíky v centrálněkarpatském paleogénu a flyšovém pásmu východního Slovenska

Milan Mořkovský[1] - Josef Novák[1] - Regina Lukášová[1]

Received October 20, 1988

1 : 50,000
27-41, 27-43,
27-44, 28-33

Seismic methods
Common-depth-point method
Interpretation

Mořkovský, M. - Novák, J. - Lukášová, R. (1992): Geophysical prospecting for hydrocarbons in the Intracarpathian Paleogene and in the East Slovak Flysch Belt. – Sbor. geol. Věd, užitá Geofyz., 25, 9–48. Praha.

Abstract: Results are presented of geophysical, namely CDP seismic measurements carried out in the period 1972-84 in the Intracarpathian Paleogene and in the East Slovak Flysch Belt. For interpretation were also used refraction seismic, gravity and magnetic data, results of well-shooting, acoustic and electrologging in deep boreholes, and data on physical properties of rocks obtained by measurements on drill core samples. The well-shooting data were used for velocity studies in the area. Based on reflection seismic data are the time map and the depth structural scheme of the buried Mesozoic relief of the Central Carpathians in the broader environs of Lipany. Seismic measurements indicated numerous tectonic faults, NE-SW striking reverse faults, and normal faults.

[1]*Geofyzika, a.s., Brno, Ječná 29a, 612 46 Brno*

Introduction

In the present article we attempt to summarize the results of geophysical, namely seismic, survey accomplished in 1984 for hydrocarbon prospecting in the Intracarpathian Paleogene, the Klippen Belt, the East Slovak Flysch Belt and their basement. Most valuable data were obtained by CDP measurements on seismic profiles.

The Intracarpathian Paleogene is composed of several lithofacial sequences, from pre-flysch, wild flysch to typical flysch development (Chmelík 1957), often with giant bodies of badly sorted conglomerates of alluvial fan (Marschalko 1965, 1981). After geological mapping, geophysical survey and deep drilling the Intracarpathian Paleogene

is at the present prospecting stage relatively most investigated. Results from boreholes (Lipany-1,2,3,4 and 5, PU-Šambron, Plavnica-1) at the southern border of the Klippen Belt confirmed larger tectonic deformation (Nemčok et al. 1977) and presence of irregular breccia series built of Lower Cretaceous and Jurassic rocks in the deeper part of the Intracarpathian Paleogene which Rudinec (1981) regards as olistoliths. Besides the scale-fold structure, the Paleogene strata are affected by the youngest Neogene normal faults.

According to drilling, the basement of the Paleogene in the peri-Klippen zone is Mesozoic. Its entire relief (Cretaceous to Lower Triassic) was verified by borehole Šariš-1 in the interval 1,340–3,836 m. It is the Mesozoic of the Krížna nappes (Koráb et al. 1986) with strongly tectonized crystalline rockc in its basement (3,836–5,000 m).

The Klippen Belt forms a narrow strip between the Flysch Carpathians and the Intracarpathian Paleogene. Mainly in consequence of Neogene folding it takes on the tectonic style of the Carpathian flysch area (Leško-Salaj-Samuel 1963). Within the Klippen Belt in the Hanušovce horst, the borehole Hanušovce-1 penetrated Upper Cretaceous sediments and the Klippen Belt Paleogene to the depth of 4,000 m. Paleogene sediments are represented by the Proč series. To the final depth of 6,000 m were drilled the Eocene sediments (Strihovce, Beloveža and Zlín series) of the Krynica and Rača units of the Magura nappes (Leško et al. 1984).

The flysch belt of the Czechoslovak Carpathians in the eastern part consists of two units, the Magura nappes and the Dukla unit. From S to N the Magura nappes contain the partial Krynica, Bystrica and Rača unit between Smilno and Nižný Mirošov, the tectonic basement crops out to the surface in the form of a window – the Dukla unit. Deep boreholes Smilno-1 and Zboj-1 yielded geological data on the Flysch belt. The borehole Smilno-1 (Leško 1986) struck to the depth of 4,600 m the Rača unit of the Magura nappes formed by the Upper Paleocene to Lower Eocene Beloveža series and the inoceramus series and Upper Senonian to Paleocene breccia. In the depth interval 4,600–5,700 m the Outer Flysch Belt was struck represented by the black flysch series and Eocene breccia, and by Upper Miocene menilite series. The borehole Zboj-1 (Ďurkovič et al. 1982) confirmed down to the depth of 3,800 m the structure of the Dukla unit formed by submenilite Paleocene to Middle Eocene series, by the Cisna Paleocene series and by the Lupkov Upper Cretaceous to Paleocene series. The tectonic basement of the Dukla unit is mainly built of the psammitic Zboj series struck by drilling in the interval 3,800–5,002 m. It is now assumed that the Zboj series is of Upper Eocene to Lower Oligocene age.

Compared to the East Slovak Basin, for example, oscillographic and analog reflection seismic measurements were conducted on a smaller scale in the area of interest because of hard seismological conditions and complicated interpretation. A change came with the arrival of digital recording and processing. In the period 1972–84, 50 seismic CDP profiles at the total length of 477 km were shot for oil and gas prospection in the Intracarpathian Paleogene and in the East Slovak Flysch Belt. Seismic measuremets concentrated in the peri-Klippen area in the broader environs of Lipany (Šambron-Lipany-Kapušany). Large-scale reflection seismic surveys were carried out in the area of Smilno and Zboj. In the area of Adidovce and Zubné three short reconnaissance profiles

were situated. Seismic profiles were also stretched near Starina, Tokajík and S of Jakubany.

A relatively dense network of CDP profiles was set in the peri-Klippen area and eight deep boreholes were drilled there (Lipany-1,2,3,4 and 5, Plavnica-1, PU-1 Šambron and Šariš-1). Well- shooting was conducted in six boreholes. A structural scheme of the relief of Triassic dolomites in the basement of the Intracarpathian Paleogene was constructed.

Besides CDP and drilling information, results of refraction seismic, gravity and magnetic measurements, logging in deep boreholes (seismic, sonic, electric) and of measurements of physical properties of rocks on core samples were interpreted.

Application of individual geophysical methods and results

Gravity survey

Leaving aside the gravity measurements of Meinhold-Scheele (1943), Běhounek (1950), Běhounek-Válek (1951) which covered the southern and western margins of the study area only, the first systematic survey in the area was the regional gravity survey conducted by the Research Oil Institute, Brno in the period 1954–57, with one point of measurement per 2–3 km^2. Since 1970 a detailed gravity survey has been carried out in the study area with 3–6 points of measurement per km^2.

The regional gravity measurements were processed and interpreted by Menčík (1957), Čekan-Šutor (1960), Šutor-Čekan (1965) and Tomek in Kadlečík et al. (1977). In the framework of regional gravity survey and of surveys over the entire Czechoslovak territory the Intracarpathian Paleogene and the East Slovakian flysch were investigated by Ibrmajer-Doležal-Mottlová (1959), Ibrmajer-Doležal (1962) and Ibrmajer (1963, 1978).

Fusán et al. (1971) used the maps of Bouguer anomalies and maps of regional and residual anomalies, drilling data and data obtained by other geophysical methods to compile a map of the basement relief of the covered areas in the southern part of the Inner West Carpathians. The map includes only the southernmost margin of our study area.

Results of a deatiled gravity survey in the area between Šambron and Lipany (Váca et al. 1971) were used by Čekan-Mořkovský (1982) to compile maps of residual anomalies. The map of residual anomalies of the gravity field with the radius of averaging ring r = 2 km reflects (at the thickness of Paleogene sediments around 2.3 km) the lithological changes in rocks of the Intracarpathian Paleogen. Residual anomalies plotted in the map often correlate with outcrops of rocks exhibiting different densities. On the contrary, the map of residual anomalies of the gravity field with the radius of the averaging ring r = 2–16 km mainly characterizes (as documented by reflection seismic measurements) the relief of the basement dolomites (the Krížna unit). It is noteworthy that the positive residual anomaly corresponding to an elevation of dolomites south of Šambron-Krásna Lúka extends without major deformations to the area north of the Klippen Belt.

The gravity field in the broader area of the Humenné Mesozoic subunit was interpreted

by Pospíšil-Filo (1982). They concluded that NW of Prešov the Klippen Belt dips to the NE and together with the Magura flysch group is thrust over the Intracarpathian Paleogene, deforming it in the contact zone. The authors assumed that between Prešov and Vranov the Klippen Belt had been strongly deformed by displacement of Mesozoic rocks and that its position is vertical. In the area of Humenné the authors again assumed a dipping of the Klippen Belt to the NE. In their opinion its deformations due to the displacement of Mesozoic blocks were so extensive that they might have caused "disruption" of the Klippen Belt.

Regarding the intricate structure and tectonics of the East Slovakian flysch and its basement, the interpretation is very difficult though numerous problems have been solved. However, the shallow character of the Klippen Belt and of most gravity anomalies in the Flysch Carpathians was confirmed (Tomek in Kadlečík et al. 1977). Only the most important anomalies, e.g. the Snina-Stakčín anomaly and the positive anomaly near Kurimka – perhaps the core zonee of the Smilno window – are probably associated with the flysch relief.

Magnetic survey

The first magnetic measurements in the study area were conducted by Scheele (1944). However, only small parts of the study area were covered (the area between Slovenská Kajňa and Lieskovec and a small area N of Vranov). A systematic magnetic survey was carried out in the period 1955–1957 over the greater part of the study area. It was a regional survey with points of measurement at intervals of 2–3 km. The obtained results were interppreted by Ibrmajer-Doležal-Mottlová (1959), Čekan-Šutor (1960), Šutor-Čekan (1965) and Šutor in Kadlečík et al. (1977).

The geomagnetic field is rather monotonous (± 20 nT). It is most probably due to the low susceptibility of the flysch complexes and their basement, or to their low differential susceptibility. Considering that the mean error of measurement was ± 4 nT, it is obvious that the interpretation of the geomagnetic field is not easy.

Geoelectric survey

A large-scale survey was carried out in the study area for enginering-geoelectric purposes. For investigations of the deep structure which is the subject of the present paper they are not of special importance.

Physical properties of rocks

The studies of rock densities carried out in the period 1953–1964 by the Institute of Applied Geophysics, Brno and by Geological Survey, Prague resulted in compilation of Map of rock densities in Czechoslovakia on the scale of 1:500,000 (Eliáš-Uhmann 1968).

The densities were mainly determined by measurements on samples collected on the surface, but drill cores were also used. According to the map, bulk densities of rocks in the study area range from 2,350 to 2,750 kg/m^3.

Measurements of physical properties of surface rock samples yield data loaded with errors (depending on the degree of weathering, leaching of the calcitic component, etc.). Therefore, measurements on drill cores are more reliable and the changes of physical properties of rocks with depth can be observed.

The measurements of physical properties of rocks currently carried out in Geofyzika Brno include: measurements of density parameters (bulk, mineralogical, natural density, porosity), velocity of propagation of longitudinal elastic waves (vertical and parallel to lamination), magnetic susceptibility, natural gamma activity and U, Th and K contents.

In the study area, physical properties of rocks were determined on drill cores from boreholes PU-1 Šambron, MLS-1 Humenné, Zboj-1, Lipany-1, 2, 3, 4 and 5, Hanušovce-1, Smilno-1, Šariš-1, Prešov-1 (Pl.1). Píchová (1985) summarized the results in tables of physical parameters of individual geologic-tectonic units. Píchová (ibid.) also summarized results of measurements (density and porosity) on surface samples (Mikuška-Chrumová 1983, 1984, Uhmann et al. 1977). The density and magnetic susceptibility of rocks from the western part of the East Slovak Magura flysch were higher than in the eastern part. The porosity of surface samples is considerably higher (due to weathering) and therefore bulk density is lower. Measurements on surface samples were carried out in 1984 and 1985 (Mikuška-Chrumová 1985, 1986). Physical properties of rocks in the area of interest have recently been studied by Ondra-Hanák (1989). They found that samples collected on the surface generally exhibit higher densities in the Klippen Belt including Cretaceous complexes and Paleogene cover – the Proč series – as compared with the Krynica unit and with the adjacent Intracarpathian Paleogene. Thus they contributed to the studies of Menčík (1963).

Stránská et al. (1986) compiled a 1:200,000 map of rock densities for the West Carpathians on the Czechoslovak territory. Besides graphical representation, it contains comprehensive tables of bulk, mineralogical and natural densities and porosities. In the opinion of the authors bulk densities decrease from the Levočské pohorie hills to the E.

The density and radioactivity of the main lithological types and stratigraphic units of the West Carpathians (measurements on 213 drill cores) were described by Husák (1986). He contended that the densities of rocks of the Intracarpathian Paleogene do not depend on the thickness of overlying beds.

Odstrčil (1985) investigated the possibilities of determining densities of near-surface rocks (or the average natural density of the Bouguer slab) from gravity measurements.

Aerial and satellite measurements

An aerial magnetometric and radiometric survey on the scale of 1:200,000 is described in the report of Mašín et al. (1960). The magnetic field in the study area is generally monotonous. A detailed aerial survey on the scale of 1:25,000 covered the southern margin of the area of interest where the magnetic field is monotonous, with the prevailing

value of −10 nT. Striking anomalies can be observed in the broader environs of Radatice over an area of approx. 6 km^2. According to Gnojek (1987) these anomalies are due to a basic body at the depth of approx. 1,900 m (under the surface). Radiometric measurements did not reveal any anomalies.

New information about the geologic structure of the East Slovakian flysch was yielded by remote seensing. A ring structure in the area Svidník-Stropkov, i.e. in the margin of the Zborov anticlinal belt, was detected. Pospíšil-Němčok-Feranec (1982) and Pospíšil (1983, 1985) explained the origin of this structure by the presence of deep tectonic lines, or by a collision zone of different basement blocks.

Refraction seismic survey

Refraction seismic survey was commenced in 1970 with measurements on profile 1(R)/70 between Nová Sedlice and Podhoroď (Hrdlička et al. 1971). In the period 1970–1981 a large-scale survey was carried out in the Intracarpathian Paleogene, in the Klippen Belt and in the Flysch Belt on seven profiles stretched in the direction of the Carpathians and on seven profiles vertical to it, at the total length of 826 km (Pl. 1). The results were – besides evaluation in annual reports – further interpreted by Leško-Mořkovský (1975), Plíva et al. (1976, 1977), Wojas (1977) and Kadlečík et al. (1977).

Owing to the seismogeological features of the intricate fold-nappe structure of the Flysch Carpathians the interpretation was not easy. The processing and interpretation were also complicated by small differences in densities and velocities of elastic waves between deep flysch complexes and their basement. The velocity boundaries traced by refraction seismic in the flysch can be interpreted as gradient changes of elastic waves velocities, or as different flysch complexes (Kadlečík et al. 1977). The general interpretation of refraction seismic data in regard to drilling and geophysical results obtained on the territories of Poland, the USSR and Czechoslovakia led to the conclusion that the basement of flysch complexes might be a refraction boundary with a velocity of over 6,000 m/s (Kadlečík et al. 1977). However, this opinion was not supported by the results from borehole Smilno-1 which at the depth of the measured boundary (5,000 m) struck basal beds of black flysch. Because of these contradictory results refraction seismic measurements were stopped in the Flysch Carpathians on the territories of Poland, the USSR and Czechoslovakia.

More reliable results were obtained by refraction seismic measurements in the Intracarpathian Paleogene where the data yielded by the borehole Lipany-4 correlated with the depth of the refraction boundary and were in agreement with reflection seismic data.

Refraction measurements in boreholes

The refraction seismic method was employed in boreholes MLS-1 Humenné and Lipany-1 (Pl. 1).

Refraction seismic measurements in the borehole MLS-1 Humenné were carried out

to trace the contact of Albian-Cenomanian marl schists and the Lias-Aptian Limestone complex struck by drilling at the depth of 470 m (Filková-Mořkovský-Pernica 1973). The interpreted relief of Aptian limestones of the Humenné Mts. forms a ridge whose axis parallels the line Ptičie-Kamienka.

In the borehole Lipany-1 refracted waves propagated along the velocity boundary between Keuper and Upper Triassic dolomites (Filková-Pernica 1978). The results showed striking anomalies in propagation of refracted waves. Therefore, the refraction method was not applied in other boreholes in the area. The results indicated the presence of a larger number of boundaries that could not be identified until Mořkovský et al. (1987) showed that the boundaries correspond with the relief of dolomites in the Intracarpathian Paleogene basement, and with the tectonic planes (overthrusts) in the Intracarpathian Paleogene or in the Klippen Belt. But their separation from refraction measurements in boreholes is not possible.

Well-shooting and vertical seismic profiling

Well-shooting measurements are of great importance for processing of reflection seismic results and especially for transforming the time data of seismic sections into deep scale. Unlike well-shooting measurements, where only direct waves are registered, in the vertical seismic profiling reflected, or multiple reflected, and transform waves are registered as well. Thus the lithophysical boundaries, from which the waves are reflected, the multiple reflections and the ratio of longitudinal and transverse waves can be considered. These facts are very important for interpretation of profile seismic measurements.

Well-shooting results are presented as a dependence of time on depth (vertical time curves) and as a dependence of velocities (average, layer, interval) on depth or time. The data are computer-processed, as well as vertical seismic data which are presented in the form of time sections.

In the study area, well-shooting was conducted in eleven deep boreholes (Lipany-1, 2 and 3, Šariš-1, PU-1 Šambron, Plavnica-1, Hanušovce-1, Smilno-1, Zboj-1, MLS-1 Humenné, Prešov-1, see Pl. 1) and VSP was carried out in all of them except MLS-1 Humenné.

Reflection seismic survey

The first reflection seismic survey in the East Slovak Flysch (in the environs of Adidovce and S of Stropkov – Pl. 1) was conducted in the period 1959–1960 (Jurga - Cidlinský 1961, Jurga 1962). An oscillographic seismic unit was used and the RNP method ("regulirujemyj napravlennyj prijom", Rjabinkin) was applied. However, the measurements, even with grouping of geophones and shotholes, did not yield satisfactory results.

In 1970, a reflection seismic survey was conducted along a 3 km long parametric

profile within the Dukla unit in the area of Ruský Potok (Adamovský et al. 1970). The measurements were carried out in the modification of continuous profiling using the 24-channel analog seismic unit RX 24 S II. The grouping of shotholes (1–3), of different depths of shotholes (10–35 m), masses of explosives (50–100 kg) and geophone intervals in a group (0–5 m) was tested. The obtained material was difficult to interpret and contained only indications of continuous reflections in the range 1.6–2.1 s.

Profile 3/71 was situated between Nová Sedlica and Podhoroď. Measurements were carried out in 1971 (Adamovský et al. 1972a) using the analog seismic unit RX 24 S II. Time sections were constructed using the analog processing system SWZ-1. Field methodology was chosen on the basis of results of parametric measurements near Ruský Potok in 1970. Later on, the original analog records from profiles 1/70 and 3/71 were digitized and digitized time sections were constructed (Lukášová et al. 1974). Thus the seismic material was completed up to times around 3 s.

Since 1972, reflection seismic measurements in the study area were done in the CDP modification. This method of multiple coverage, digital registration and processing yielded much more information.

Besides the profiles measured until 1984, Pl. 1 contains CDP profiles from the period 1985–1986. Until the end of 1986 measurements had been conducted on 64 profiles at the total length of 669 km.

Reflection seismic data obtained in the East Slovak Flysch until 1973 were studied by Kadlečík et al. (1977) and by Leško et al. (1979). They concluded that most events aree of interference character. Some boundaries with strong reflections most probably correspond to tectonic planes. In seismic sections the authors distinguished an upper part with abundant reflections and a lower, relatively monotonous part with less reflection elements. In accordance with interpretation profiles they identified the boundary between the two parts of time section with the flysch basement relief.

Reflection seismic measurements in CDP modification

Parametric measurements

Already the first CDP measurements in the *East Slovak Flysch* in 1972 (profiles 4/72 and 6B/72) showed the absence of continuous reflections and often relatively high noise level. The CDP measurements were therefore followed by parametric measurements carried out on a large scale in 1973, predominantly in the environs of the villages Adidovce and Zubné on short profiles 5B/73, 8B/73 and 9/73 (Pl. 1). Different configurations, explosives, groups of geophones, linear groups of three to seven shallow boreholes, and the effect of filtering on the instrument operation were tested. To determine the signal/noise ratio, wave patterns within the distance of 2,650 m from the shotpoint were measured.

To enhance the suppression of interference waves, weighted groups of geophones at approx. 100 m intervals were tested. This relatively long group did not bring a notable

improvement. Nevertheless, the suppression of interference waves was better as compared with the common 50 m intervals. Analogous was the objective of testing linear groups of shallow shotholes. It was found out that the effectivity of such a group equals the effectivity of one deep shothole. Because of unfavourable drilling conditions the testing did not include the expensive grouping of deep boreholes. Experiments with grouping of shallow shotholes showed that this technique might yield favourable results.

Applications of different systems of measurements on profiles – split spread, end-on and reversed end-on spreads – did not stress special advantages of one system over another. Similarly, recording at greater distances from the shotpoint (in the interval 1,325–2,475 m) tested on profile 8B/73 did not yield better results.

Experiments in the environs of Adidovce and Zubné showed that location of 20–30 kg explosives in shotholes on average 25 m deep was most effective.

In 1981 recording to 10 s was tested on profiles situated near the deep boreholes Smilno-1 and Zboj-1 (37/81, 38/81). However, on both profiles a drop in seismic energy to noise level was observed at times over 5 s. Therefore the recording length of 5–6 s was chosen as optimal.

The comparison of results obtained in the environs of Smilno on profiles 34/81 (50 m intervals of points of arrival) and 34A/84 (25 m intervals of points of arrival) favoured the 25 m interval (96-channel recording), namely for measurements to the depth of 3,000–4,000 m. At greater depths the 50 m interval will be predominantly applied. Application of a large coverage which means a greater filtration effect of CDP summation and an improved signal/noise ratio is expected to provide better results.

Parametric measurements were also carried out in the surrounding of Bardejov and Starina (1972), Smilno (1972 and 1981), Matiaška (1975) and Zboj (1973 and 1981) – cf. Pl. 1.

The seismological conditions on the surface are analogous in the *Intracarpathian Paleogene* and in the Flysch Belt. Therefore, analogous experiments were carried out in the two areas. Despite the seismogeological similarity of the surface structure of both areas, recordings from the Intracarpathian Paleogene contained abundant reflections and parametric measurements in the area yielded much better results. The methodology of seismic measurements in the Flysch Belt was modified using results from the Intracarpathian Paleogene. Parametric measurements in the Intracarpathian Paleogene were carried out in the environs of Bajerovce (1974), Hanušovce and Šambron (1975), Šarišské Sokolovce (1976) – cf. Pl. 1.

In the *Klippen Belt* parametric measurements were conducted N of Bystré nad Topľou (1975) – cf. Pl. 1.

Methodology of field works and used instrumentation

Field parameters for CDP seismic measurements were chosen on the basis of results of parametric measurements.

Waves were generated by dynamite technology. In the period 1972–1975 mainly the

six-fold coverage was used, later 12-fold coverage. A split spread with 50 m intervals between groups of geophones was used, in 1984 also 25 m intervals.

Arrivals of reflected waves were recorded by digital seismic units SN 338, SN 328 and DFS IV with input filter 16–125 Hz, 12.5–125 Hz or 18–124 Hz respectively, sampling interval 2 ms and record length 5 or 6 s.

Elastic waves were generated by blasting 20–30 kg explosives located in 25–30 m deep holes. Geophones GSC-11D with frequency of 10 Hz were grouped by 24.

Seismic data processing

Until 1978 digitally recorded data had been processed on the EMR 6070 Advance computer with plotter TNR 91. Standard seismic software was used for demultiplexion, amplitude recovery, static corrections, time variable filtration and deconvolution. Seismic waves were migrated through weighted diffraction summation. Kinematic correction were calculated on the basis of velocity tests using 18 chosen velocities. Deconvolution was performed according to the character of the seismic material – before, after or before and after stacking.

Since 1979 seismic data have been processed on the RDS 500 computer with APOLLO processor, controlled by the program system GEOMAX (registered trade mark CGG). Graphic representation of results is done by plotters VERSATEC and TNR 95. Compared with the EMR system GEOMAX is more versatile. It can be used for automatic calculation of residual static corrections, for processing of SLALOM line seismic data (registered trade mark CGG), for enhancement of the wavefield coherency, for migration of seismic information (program WEMIG). For a correct function of the program WEMIG the inclinations of reflecting horizons must not be larger than 45°. Migration by means of wave equations much better preserves the dynamics and frequency content of the time section. As a rule, deconvolution is performed after summation.

Digital processing of seismic data including its final stage, i.e. graphic representation in the form of migrated time sections is performed in the department of seismic data digital processing, Geofyzika Brno.

Velocities

Well-shooting

For reflection seismic data processing the knowledge of velocities is essential for time/depth conversion. Most reliable information is provided by well-shooting. Fig. 1 shows the dependences of average velocities on depth for individual deep boreholes situated in the study area and chosen for the conversion. It follows from Fig. 1 that average velocities attain the highest values in boreholes PU-1 Šambron, MLS-Humenné, Plavnica-1 and Hanušovce-1. The curve for the borehole Smilno-1 shows the lowest average velocities. Velocities measured in the borehole Šariš-1 and Zboj-1 range between

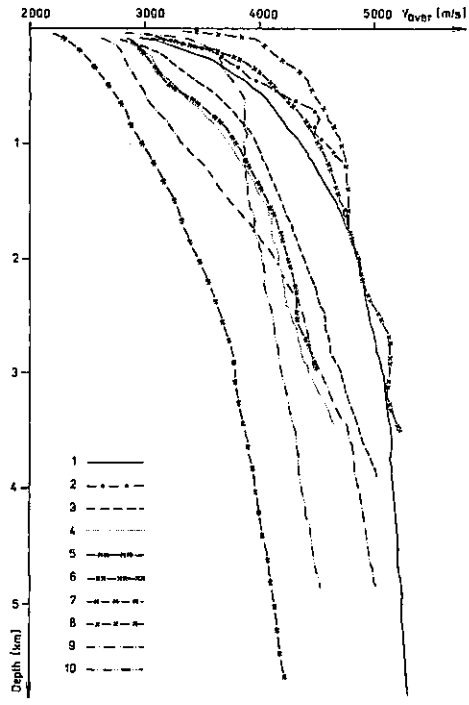

1. Depth-dependences of average velocities according to well-shooting.
1 – Hanušovce-1, 2 – MLS-1 Humenné, 3 – Lipany-1, 4 – Lipany-2, 5 – Lipany-3, 6 – Plavnica-1, 7 – Smilno-1, 8 – PU-1 Šambron, 9 – Šariš-1, 10 – Zboj-1.

them. The curve of average velocities Lipany-1 demonstrates higher velocities than curves Lipany-3, Lipany-2 and Šariš-1 for the same depths. The curves from boreholes Šariš-1, Lipany-1 and 2 reflect at the depth of 1,350 m, 2,750 m and 2,870 m respectively a striking change of velocity gradients characterizing the influence of the Intracarpathian Mesozoic basement. Similarly the curve of average velocities from boreholes Plavnica-1 demonstrates a larger velocity gradient due to the presence of a block of fractured dolomites at the depth of 2,300 m.

In the Paleogene complex average velocities of elastic waves strikingly decrease from NW to SE, which is due to the lithology of sediments.The Intracarpathian Paleogene in the vicinity of the borehole PU-1 Šambron contains numerous sandstone layers with higher velocities of seismic waves propagation as compared with Paleogene rocks with a higher content of pelitic sediments in the environs of Lipany (Mořkovský-Filková 1985) and in the vicinity of the borehole Šariš-1. At a depth of approx. 1,000 m the curve $V_{aver}(H)$ of the borehole Šariš-1 shows an increased velocity gradient due to calcareous rocks in the basement of the Šambron formation.

Layer velocities in the *Intracarpathian Paleogene complex* range from 2,600 to 5,600 m/s. The exceptionally high values 5,600–5,800 m/s recorded in the borehole Lipany-2

in the depth interval 2,400–2 660 m, and the velocity of 6,300 m/s recorded in the borehole Lipany-5 in the depth intervals 2,560–2,720 m and 2,810–2,900 m are due to the presence of displaced blocks of older rocks (olistoliths?). Layer velocities of individual curves generally increase with increasing depth though the positive character of the increase is locally affected by lithological changes or by tectonic deformation of rocks. For instance, a local decrease in velocities in the depth interval 1,360–1,750 m in the borehole PU-1 Šambron is due to very porous interformational conglomerates in the basement of the Šambron formation. Lower layer velocities can also be observed in intervals 1,620–1,770 m in the borehole Lipany-2 and 2,450–2,560 m in the borehole Lipany-3.

Layer velocities in the *Mesozoic* and *crystalline basement* of the Intracarpathian Paleogene in the boreholes Lipany-1,2, Šariš-1 and Plavnica-1 range from 5,800 to 7,500 m/s. A striking decrease to 5,000 m/s occurs in Lower Lias-Keuper rocks, in variegated Werfenian schists and in Lower Triassic quartzites. For the Humenné Mesozoic formation well-shooting in thee borehole MLS-1 Humenné recorded velocities ranging from 4,000 to 4,140 m/s (pelites, psammites) and 6,100 m/s (limestones, dolomites).

Layer velocities recorded within the *Klippen Belt*, where the borehole Hanušovce-1 reached the depth of 4,000 m, range from 3,400 to 5,700 m/s.A noticeable decrease of velocities within the interval 3,450–3,800 m is obviously due to tectonic deformation.

In the *Magura nappe* reached by the borehole Smilno-1 in the depth interval 0–4,600 m, layer velocities first gradually increase with depth (from 2,700 to 4,950 m), then from 1,750 m downwards the recorded range is 4,950–5,000 m/s, except the depth interval 2,850–3,100 m where the velocities are substantially lower. It may be due to tectonic dissection. Layer velocities within the Rača and Krynica unit of the Magura nappes struck by the borehole Hanušovce-1 in the depth interval 4,000–6,003 m beneath the Klippen Belt range from 5,500 to 5,700 m/s.

For the *Outer Flysch Belt* penetrated by the 5,700 m deep borehole Smilno-1 in the basement of the Magura nappes, layer velocities around 5,000 m/s are characteristic.

Layer velocities recorded in the borehole Zboj-1 in the *Dukla nappe unit* range from 3,800 to 5,000 m/s (in the interval 100–3,800 m). Layer velocities in the *Zboj series* struck by the borehole Zboj-1 range from 5,000 to 5,700 m/s in the depth interval 3,800–5,002 m.

Subsurface velocities

The above presented well-shooting data provided only separate pieces of information about acoustic waves velocities. To gain more comprehensive knowledge about the changes of velocities of elastic waves propagation throughout the area of interest, subsurface velocity values yielded by reflection seismic profiling were considered.

For processing, all the numerous secondary factors affecting the propagation of elastic waves must be taken into account. It is e.g.the tangential tectonics which may directly influence the physical properties of rocks, and by displacing stratigraphic formations

significantly influence the velocities (Mořkovský-Filková 1985). At the same time it must be assumed that the relative dependences of velocities, despite the differentiated effect of lithology on the rate and intensity of weathering, are preserved. A diagram was constructed of the distribution of subsurface velocities in the Intracarpathian Paleogene, in the Klippen Belt, and in the adjacent part of the Magura Flysch (Pl. 2). Studies of subsurface velocities and the assumed vertical and horizontal distribution of lithostratigraphic complexes helped to delimit the areas of the industrial model velocity curves. They were, of course, based on well-shooting data.

The highest subsurface velocities (4,200–4,600 m/s) in the *Intracarpathian Paleogene* were measured south of Jakubany and in the strip of outcrops of the Šambron formation (calcareous sandstones prevailing over claystones with beds of conglomerates), stretching from the borehole PU-1 Šambron to the ESE. Towards the north and south the subsurface velocities strikingly decrease to 2,800–3,600 m/s which is connected with the presence of the prevailingly claystone Paleogene facies. The increase in velocities south of Jakubany is due to the top sandstone Paleogene series. In the broader environs of Lipany, subsurface velocities range from 3,300 to 3,900 m/s. East of Lipany, in the broader environs of Sabinov, the velocities range from 3,000 to 3,300 m/s. In the area east of Šarišské Sokolovce and Gregorovce a decrease to 2,500–3,000 m/s was recorded. The same values occur in Lower Miocene complexes in the environs of Kapušany. Farther eastwards, in the area Kapušany-Bystré nad Topľou, the subsurface velocities again increase. In the southernmost parts of the western section of the Intracarpathian Paleogene near Šarišské Michaľany a gradual decrease from NW (via Medzany) to SE can be observed. Also this phenomenon can be related to the lithofacial changes within the Palaeogene, most probably to claystone series which prevail over sandstone beds.

In the *Klippen Belt*, between Kamenica and Šarišské Sokolovce, subsurface velocities range roughly from 3,900 to 4,200 m/s. Near Terňa, Hanušovce and Údol subsurface velocities are lower (3,000–3,600 m/s). Generally, subsurface velocities of elastic waves in the Klippen Belt are higher as compared with the adjacent part of the Intracarpathian Paleogene. An exception is the area of Údol and Plaveč, covered by Upper Eocene graywacke and calcareous, often slightly diagenetically lithificated sandstones and calcareous claystones of the Ujak development – Malcov series – where the velocities are practically the same as in the Intracarpathian Paleogene.

In the *Magura Flysch* the highest subsurface velocities (4,200–4,600 m/s) were observed in the Čergov massif, south-west of Hertník. For this area, coarse-grained calcareous Čergov sandstones are typical. Striking drops of velocities (2,700–3,300 m/s) at the northeastern ends of profiles 46/83 and 74/85, south of Hertník are associated with the contact of sandstone layers with the prevailingly pelitic Malcov series.

Generally, the diagram of subsurface velocities confirms the relations between velocities of elastic waves propagation in the Intracarpathian Paleogene revealed by well-shooting (Mořkovský-Filková 1985), i.e. the gradual decrease in velocities from the Šambron area towards the southeast due to lithofacial changes. However, this may also manifest the differences in compaction which have been described for the Intracarpathian Paleogene by Ondra-Hanák (1989). The change in velocities was also indicated by refraction seismic data (Jarý et al. 1976).

The areas of the individual model velocity curves in the Intracarpathian Paleogene

For application of velocity models (based on well-shooting data) on reflection seismic profiles, the areas of individual velocity curves, or the transition zones between them had to be delimited. For this purpose not only subsurface velocities, but also results of analysis of geophysical information in time sections, and data on stratigraphy and structure (Pl. 2) were used.

The *velocity curve PU-1 Šambron* covers the area where subsurface velocities range from 4,200 to 4,500 m/s. The velocity V_o obtained by well-shooting in the borehole PU-1 Šambron is 4,200 m/s. Although in the environs of Plaveč a drop in subsurface velocities can be observed, we use, with regard to the assumed small thickness of the here outcropping Ujak claystones – the Malcov series – the velocity curve PU-1 Šambron for the whole area east of the borehole PU-1 Šambron towards the Klippen Belt.

The area of the *velocity curve Šariš-1* was delimited on the basis of prevailing occurrences of subsurfaces velocities in the range 2,900–3,000 m/s (well-shooting in the borehole Šariš-1 yielded velocities V_o ranging from 2,000 to 3,000 m/s).

Velocity curves Lipany-1, 2 and *3* apply for an area of velocities ranging from 3,000 to 3,600 m/s. Regarding the evident drop in velocities of elastic waves in the area east of the Lipany boreholes, the velocity data yielded by measurements in the boreholes were corrected. Layer velocities obtained in the borehole Prešov-1 were also taken into account (in the Intracarpathian Paleogene complex the layer velocity was 3,950 m/s). The lowest velocities were observed between Terňa and Šarišská Poruba, i.e. in an area where the Čelovce depression Neogene rocks crop out. Farther to the east an increase in velocities of elastic waves is assumed.In the broader surroundings of Hanušovce the velocity distribution will probably be very similar to that in the environs of Lipany.

Velocity analyses would not be suitable for the areas of interest (the Intracarpathian Paleogene and the Flysch Belt) contrary to less tectonized regions as e.g. the East Slovakian Neogene Basin. The reasons are thee high order of velocities and lack of larger reflections corresponding to layer boundaries. Continuous reflection horizons are usually due to fault tectonics – overthrusts. Because of lack of seismic data such an analysis can hardly be objective. Therefore, velocity analyses were only used to substitute other velocity data.

A short review of results of processing the data on velocities of seismic waves propagation in the Intracarpathian Paleogene, in the Klippen Belt, and in the East Slovak Flysch

Velocities of elastic waves propagation in the *Intracarpathian Paleogene* were documented by well-shooting in boreholes PU-1 Šambron, Šariš-1, Lipany-1, 2 and 3, Plavnica-1, and Prešov-1 (which in the basement of Neogene sediments verified the Intracarpathian strata).

The studies of velocities in the *basement of the Intracarpathian Paleogene* were based

on seismic data from boreholes Lipany-1, Lipany-2, Šariš-1 and Plavnica-1 drilled in the Mesozoic basement. There the layer velocities were 6,300 m/s in the borehole Lipany-1, 6,000 m/s and 7,200 m/s in the borehole Lipany-2. In the upper, pelitic layers (Middle Cretaceous) in the borehole Šariš-1 in the depth interval 1,340–1,450 m (not present in the Lipany area) layer velocities attain 4,800 m/s. The deeper Middle Cretaceous to Jurassic strata down to the depth of 2,605 m and Keuper claystones down to the depth around 2, 800 m exhibit average layer velocity of 5,800 m/s. In the Middle Triassic dolomite complex layer velocities range from 6,000 to 7,500 m/s, while in the Werfenian formation they drop to 5,000 m/s. The Mesozoic rocks in the borehole Plavnica-1 exhibit layer velocities of 5,000 m/s, 6,500 m/s and 7,400 m/s. The crystalline complex in the borehole Šariš-1 is characterized by relatively low "layer" velocity of 5,850 m/s, which is due to strong tectonic deformation.

Velocity data from the *Klippen Belt* were produced by well-shooting in the borehole Hanušovce-1 (points A,C).

Velocities in the *Flysch Belt* in the area of the Smilno tectonic window were reliably measured in the borehole Smilno-1. Reliable are also the seismic results from the borehole Zboj-1. They were used for evaluation of velocities on profiles stretched in thee area of Zboj and Starina, Adidovce and Zubné.

For *extrapolation of traveltime curves* (at depths without well-shooting data) for the pelitic-carbonatic complex of the Upper Mesozoic we utilized layer velocities in the range from 4,800 to 5,800 m/s, for extrapolation in the carbonatic complex the velocity of 6,300 m/s was used. This layer velocity value was obtained by averaging the velocity values measured in boreholes Lipany-1, 2, Šariš-1 and Plavnica-1. We also considered the thickness of the drilled interval and its lithological composition. Further, refraction seismic results from the profile 12/R/74,75 where a velocity boundary with boundary velocity of 6,300 m/s was considered. The boundary can be regarded as the surface of Central Carpathian carbonate series covered by Paleogene strata. The given layer velocities were compared with seismic data from boreholes Ďurkov-1 (Filková-Moťkovský-Pernica 1969) and Kecerovské Pekľany-1 (Pernica-Filková 1974a) in the Košická kotlina depression.

Velocity studies in the crystalline complex are not easy because of lack of seismic data. To determine the characteristic "layer" velocities, we consider data typical of the crystalline complex built of granodiorites and gneisses in the study area in the borehole Šariš-1, in the Košická kotlina depression in boreholes Rozhanovce-1 (Filková-Moťkovský-Pernica 1971) and Kecerovské Pekľany-1 (Pernica-Filková 1974a), in the Danube Basin and on the southeastern slopes of the Bohemian Massif, e.g. in boreholes Kolárovo-3 (Jakeš et al. 1978), Osvětimany-1 (Pernica-Filková 1975) and Ždánice-4 (Pernica-Filková 1974b). Taken into account were also the average values from measurements of velocities of longitudinal elastic waves propagation on samples of rocks similar to the rocks in the study area (Uhmann 1974).

It should be noted that because of a limited amount of information and data about velocities of elastic waves in deep-seated complexes we often had to make conclusions on the basis of separate or not quite explicit information.

Using the above given information about velocities of elastic waves and using

geological models we constructed graphs $2t_o(H)$ for seismic CDP profiles. They were used for time-depth conversion of data from seismic sections. An example of the simplified dependence $2t_o(H)$ for profile 42/82 is in Pl. 3.

Methodology of interpretation

Geological interpretation of reflection seismic profiles included incorporation of stratigraphic data from deep boreholes in time and depth sections, tying up the horizons corresponding to stratigraphic data, and identification of indications of fault tectonics. Tectonic lines were located according to discontinuities of continuous boundaries, anomalous dipping of reflections, and according to all available geological and geophysical data.

Correlation of reflection horizons and stratigraphic boundaries and identification of faults were done in migrated version with deconvolution and with enhancement of wave field coherency. Also unmigrated materials were used for interpretation. They were utilized namely for verification of geophysical reliability of reflection elements, for study of diffracted and interference waves, etc. In this way obtained geophysical material for time sections was by means of graphs $2t_o(H)$ converted to depth.

In the course of interpretation of seismic data from the broader environs of Lipany it was found that the only boundary for reliable study is the relief of Triassic dolomites in the Intracarpathian Paleogene basement. In the intricate tectonic structure, CDP data alone are not sufficient for a serious evaluation of the fault tectonics and for tracing the tectonic lines in the area. The studied boundary, i.e. the Triassic dolomites relief, was in the broader environs of Lipany interpreted on individual seismic profiles and consequently a structural scheme of the area was compiled.

The used stratigraphic data were provided by Moravské naftové doly, k.p. Hodonín, branch Michalovce and by the Geological Institute of Dionýz Štúr, Bratislava. Other sources are quoted in the text.

Geophysical and geological information

The Intracarpathian Paleogene and peri-Klippen area in the broader surroundings of Lipany

It should be noted that the *opinions on the tectonic structure of the Intracarpathian Paleogene* changed many times. In the 1950s the first information about tectonics was connected with geological mapping works of J. Ilavský, B. Leško and O. Samuel, which were focused on lithostratigraphy mainly. Then followed the team work on the geological map of Czechoslovakia on the scale of 1:200,000, sheets Vysoké Tatry Mts. and Košice-Zborov, edited by O. Fusán and A. Matějka. The works were continued within the framework of detailed mapping and prospection for hydrocarbons by T. Ďurkovič, P. Gross, F. Chmelík, T. Koráb, B. Leško, R. Marschalko, J. Nemčok, and others.

In 1963, E. Menčík summarized the geophysical data from the flysch belt in eastern Slovakia (incl. the Intracarpathian Paleogene) for the purposes of oil prospection. The author observed the direct relation between gravity anomalies and the surface structure of the Klippen Belt, and pointed out the scope of interpretation. Of basic importance were the works by R. Marschalko, explaining the development of the Intracarpathian sedimentation area from the viewpoint of dynamic sedimentology.

In summary it can be stated that many authors studying the tectonic structure on Polish and Czechoslovak territories assumed a comparatively simple brachysynclinal structure of the Intracarpathian Paleogene. The assumption was mainly supported by small inclinations of layers known from outcrops. Numerous normal faults and the reverse thrust of the Klippen Belt over the Intracarpathian Paleogene were assumed – Fusán et al. (1963), Matějka et al. (1964), Stráník (1965). A larger tectonic deformation of the Intracarpathian Paleogene was assumed near the Klippen Belt and confirmed by Nemčok et al. (1977).

In his works from the period 1952–1959 Golab (fide Chmelík 1963) described nappe dislocations in the Polish part of the area. Other authors, however, do not share his opinion. Chmelík (1963) and Chmelík in Buday et al. (1967) in his study of the Intracarpathian Paleogene between Ružomberok and Prešov mentioned only overthrusts and normal fault sections, not nappes. In agreement with Leško (1958), Chmelík (1963) revealed the tectonic contact of basal and higher Paleogene series along the northern margin of Branisko. But he emphasized overthrusting of younger complexes over older ones, including the Mesozoic. The author paid attention especially to the Hromoš-Šambron anticlinal zone which he considered the most important post-Paleogene structure predisposed by WNW-ESE directions disturbing the anticlinal zone. He assumed steep dipping to the SSW and overthrusting to the NNE. Chmelík (ibid.) further assumed that a similar dislocation is followed by the flow of the Torysa river between Krivany and Sabinov. In the course of Styrian movements the Klippen series and the Magura Flysch were thrust back over the Intracarpathian Paleogene and thus most megasynclines and megaanticlines originated. It should be noted that many of the opinions and problems forwarded by Chmelík (1963) or by Chmelík in Buday et al. (1967) have been further studied and led to drilling the deep borehole Šariš-1 (Leško-Chmelík-Rudinec 1982).

An entirely new aspect in these works is the interpretation of significant Old Styrian movements in the Intracarpathian Paleogene, described as the Lipany overthrusts. Most important for a progressive evaluation of seismic data was the identification of the main elements of the tectonic style of reverse overthrusts. In many cases this interpretation completed the interpretation of the above mentioned field mapping finds of Chmelík.

Interpreting the data from the borehole Lipany-1, Leško-Nemčok (1979) mentioned a generally lower intensity of folding in the Intracarpathian Paleogene as compared with the borehole PU-1 Šambron. The contact proper of the Paleogene base with the Mesozoic has the character of sediment deposited in situ. The upper part of the basal lithofacies incorporates sliding bodies, indicating a general change in sedimentation. Later, Leško et al. (1982) did not study tectonic problems.

Closely related to the discussed problems is the structure of the peri-Klippen zone. At the contact with the Intracarpathian Paleogene and at the contact with the Krynica unit,

it was explained by Nemčok by the overthrusting of the Magura Flysch and the Klippen Belt over the Central Carpathians, or by the thrusting of the Central Carpathians under the Klippen Belt and outer flysch (1961, 1978). Thus he also explained the double-vergency of the Magura nappe (1983, 1984). Previous regional geophysical works concerned with these problems were evaluated by Kadlečík et al. (1977) and Leško et al. (1979). Of recent works regarding the peri-Klippen zone, Polish results must be mentioned. Using data from deep boreholes Maruszyna IG-1 and Banska IG-1, and from geological field work, Birkenmajer (1985) constructed a geological section implying the author's conception of only south-vergent overthrusts. He does not assume the existence of north-vergent reverse faults neither at the northern margin of the Klippen Belt, nor in the Magura nappes. It should be noted that data from the Polish boreholes do not exclude that the tectonic style is that of the Lipany area, i.e. submersion of sub-Tatra nappes in the basement of the Intracarpathian Paleogene towards the north. Regarding the lack of data about the character and course of the Paleogene-Mesozoic boundary, namely south of the borehole Banska IG-1, also this interpretation, i.e. rather steep submersion of the Mesozoic under the floor of the borehole Maruszyna IG-1 is possible.

Interpretation of tectonics in reflection seismic profiles

As the general conception of the tectonics of the study area was based on qualitative evaluation of reflection seismic data, we shall outline the reasons that complicated the identification of extensive seismic boundaries as tectonic planes:

– transgressive lithofacies (incl. numulite limestones) 150 and 100 m thick in boreholes Lipany-1, Banska IG-1 and Zakopane IG-1 found on the Paleogene base suggested regional distribution of a physically distinct boundary

– tectonic zones in Neogene basins represent boundaries, in the time section accompanied by a system of diffracted waves.

Diffractions cannot be observed with overthrusts in the Intracarpathian Paleogene. It is obviously due to several factors:

– small physical contrast along dislocations in strongly compacted rocks

– due to strong compaction and therefore high velocities of elastic waves diffracted envelope waves are only slightly curved and cannot be distinguished from other curved layer boundaries. To a certain extent it relates to the relatively small dip of tectonic boundaries

– computer velocity analyses did not show striking changes of velocities of the observed boundaries.

As it has already been said, new views on tectonization of the Intracarpathian Paleogene were forwarded by Nemčok, and namely confirmed the basic conception published by Leško-Chmelík-Rudinec (1982).

Now to the reasons which led us to localization of reverse overthrusts in the Intracarpathian Paleogene to the SW, approximately parallel to the surface structure of the Klippen Belt. First of all it was the discrepancy of dippings of layers found on cores from the surroundings of Lipany, with dips of large seismic reflections, often with large

amplitudes. Another reason was the zonal arrangement of reflections, especially noticeable on profiles parallel to the young structure of the Klippen Belt (e.g. profiles 42/82, 19/76) and tested by perpendicular profiles. The overthrusts are well demonstrated by data from the boreholes Lipany-1, 3, 2 in combination with seismic section of profile 42/82 (Pl. 3). There, around the borehole Lipany-3 at 1.0–1.2 s subhorizontal arrangement of reflections can clearly be observed. In the respective depth interval, i.e. 2,100 –2,500 m, dark-grey to black-grey consolidated calcareous claystones with dips of layers 15–43° prevail. In their base at the depth 2,925–2,929 m, calcite-healed fractures form horizontally oriented systems (Rudinec-Řeřicha 1983). Tectonic deformation from the depth 2,100 m upwards is documented by drill cores and by anomalies on average velocities curve. Also the complex of subhorizontal reflections on profile 22/78 (0.78–1.0 s) corresponding to the depth interval 1,550–2,150 m is documented by core from 2,126–2,129 m of the borehole Lipany-2 where very strong tectonization and inclinations up to 62° are described. Then the continuous reflections in the vicinity of the borehole Lipany-5 at 1.16 s on profile 15/75 (the depth of 2,500 m) confirm the existence of an extensive reflection area. The surface of the Mesozoic was struck at the depth of 2,957 m (Rudinec 1986).

It should generally be noted that with this structural style the lithostratigraphic boundaries are mostly conditioned by the tectonics and by different competence of layers.It is possible to determine the character of stratigraphic boundaries either in the close vicinity of deep boreholes or where significant lithostratigraphic complexes can be distinguished by other geophysical methods (see the positive gravity anomaly Krásna Lúka).

The presented seismic sections (Figs. 2–5, Pl. 3) show that despite the doubtful character of the material available we interpreted numerous faults, prevailingly overthrusts. However, owing to the differences in their seismic manifestations and to the relatively thin network of profiles we often could not tie the indications with one another. For the same reason we did not include in the sections the youngest normal faults, evidently deforming the Klippen Belt as well as the Intracarpathian Paleogene.

In the Intracarpathian Paleogene and in the Mesozoic the seismic manifestations of normal faults are, compared with overthrusts, less distinct. It is obviously due to a strong rock compaction.

Profile 19/76 (Fig. 2)

The NW-SE striking profile runs from the southern margin of the village of Šambron to the area south of Rožkovany, roughly parallel to the Klippen Belt outcrops, at the distance of 7–8 km. Seismic data from the profile enabled comparatively reliable interpretation of the Intracarpathian Paleogene base, of the relief of Triassic dolomites, and of the crystalline basement.

In the area of crossing with profiles 20/78 and 32/80 it can be well observed where the movements of eastern overthrusts ended on the line of displacement of the upper floor of the Intracarpathian Paleogene, i.e. on the Lipany overthrust fault. Owing to the

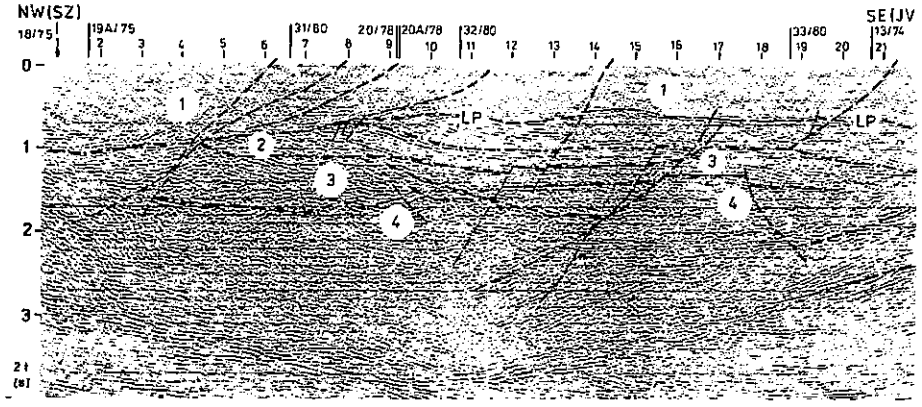

2. Seismic profile 19/76, time section with geologic interpretation (12-fold coverage, interval between the points of arrival 50 m, time-variable filtration and deconvolution, wave field coherency, wave migration). 1 – Intracarpathian Paleogene, 2 – Upper Mesozoic, pelitic-carbonatic complex (Albian-Keuper); 3 – Middle Triassic dolomites (or varied schists and Lower Triassic quartzites); 4 – crystalline complex; LP – Lipany overthrusts.

mentioned structural elements the elevation Bajerovce-Krásna Lúka is ranged with a system of N-S striking overthrust faults and thus related to the Branisko elevation (Leško-Chmelík-Fusán 1980). It is confirmed by the course of gravity isoanomalies. The north-western part of the profile near the crossing with the profile 31/80 was affected by fault dislocations called by Leško-Chmelík-Fusán (1980) north-southern western overthrust faults and regarded younger as compared to the eastern overthrusts. Contrary to these authors we suppose that the foundation of N-S overthrusts cannot be identified with the continuation of the Muráň-Divín fault towards the NE. They are rather independent tectonic zones, both in terms of genesis and direction.

As regards the longitudinal structural elements, i.e. approximately parallel to the profile, the Lipany overthrust fault, overlapping the N-S striking eastern overthrust faults, is clearly indicated. The Lipany overthrust fault has been affected by recent normal faults which apparently offset dislocations of the overthrust zone. The contact of the Upper (pelitic-carbonatic) Mesozoic with the Paleogene is most probably tectonic. Directions of reflections and their size within the Upper Mesozoic inner structure are obviously affected by eastern overthrusts. Using data from crossing profiles and from boreholes Šariš-1 and PU-1 Šambron we investigate the extent of the Upper Mesozoic conditioned by tectonics and by denudation.

According to data on the thickness of the Middle to Lower Triassic complex from borehole Šariš-1, the complex is ranged with typical seismofacies. As on profiles 20/78, 20A/78, etc., it is a series of mostly 100–200 m long events with large amplitudes. Along the profile 19/76 they often subhorizontally dip to the SE, i.e. dip parallel with the eastern overthrusts. The Lower Mesozoic boundary is well indicated as in the crystalline complex reflections of the described character disappear (see profiles 20/78 and 20A/78

in Fig. 5). The contact proper between the Mesozoic and crystalline complex may be tectonic. Towards the NW of station 4.0 km, i.e. of the indication of the Muráň fault and western overthrust faults, the indications become less and less evident. In sense of Čekan-Mořkovský (1982) we regard these parts as the culmination of the Krížna dolomite relief in the zone Bajerovce-Krásna Lúka. Also the increased thickness of dolomite westwards of the crossing with profile 32/80 interpreted from seismic data are in accordance with gravity data.

Profile 22/78 (Fig. 3)

The profile is stretched perpendicular to the principal structural elements of the area. It runs from the outcrops of the sandstone series S of Červenica towards the NE through the deep borehole Lipany-2 crossing the southern margin of the Klippen Belt. The number and quality of reflection seismic elements from the Intracarpathian Paleogene are in accordance with near profiles of the same trend. The zone of joint reflections at the time 1.0–1.1 s in the south-western part of the profile indicates the Lipany overthrust fault. NW of the profile 22/78, the Lipany fault is even better indicated in the seismic material, while towards the SE the indications fade out. Generally, it can be said that the indications of the Lipany fault become clearer with distance from the Klippen Belt, i.e.

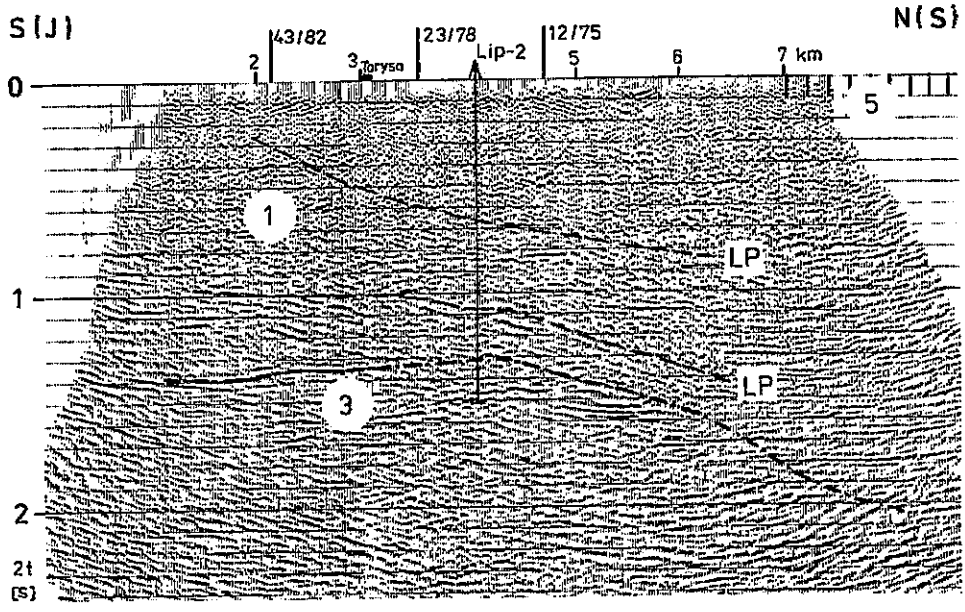

3. Seismic profile 22/78, time section with geologic interpretation (12-fold coverage, 50 m interval between the points of arrival, time-variable filtration and deconvolution, wave field coherency, wave migration).
1 – Intracarpathian Paleogene; 3 – Middle Triassic dolomites; 5 – Klippen Belt outcrops; LP – Lipany overthrusts.

towards the SW (profiles 21/78, 33/80). In the borehole Lipany-2 at the depth of 2,365 m (i.e. at the time approx. 1.09 s) a great loss of mud occurred. Considering the negligible primary porosity of rocks, it testifies to the existence of a crushed zone along a significant tectonic zone. We are of the opinion that related to this significant zone – the Lipany overthrust fault – are most occurrences of Mesozoic rocks, so far regarded as elements transferred by sedimentation – olistoliths. From results obtained on the profile 22/78 and on other seismic profiles in the area it follows that the Lipany fault represents only part of a whole system of reverse movements that affected e.g. the northern margin of the sandstone series at the southern termination of the profile 22/78, predisposed the Torysa river valley and displayed other effects.

The Mesozoic relief in the Intracarpathian Paleogene basement reached by the borehole Lipany-2 can be comparatively well traced to the Klippen Belt outcrops. The dipping of the relief towards the N was also confirmed by the boreholes Lipany-4 and Lipany-5. The stretch of the Klippen Belt at depth cannot be drawn in seismic section.

Profile 26/79 (Fig. 4)

The profile runs from Šarišské Michaľany roughly towards the NNE closely behind the northern margin of the Klippen Belt outcrops. The dolomite relief in the Intracarpathian Paleogene basement is indicated by the presence of reflections with large ampli-

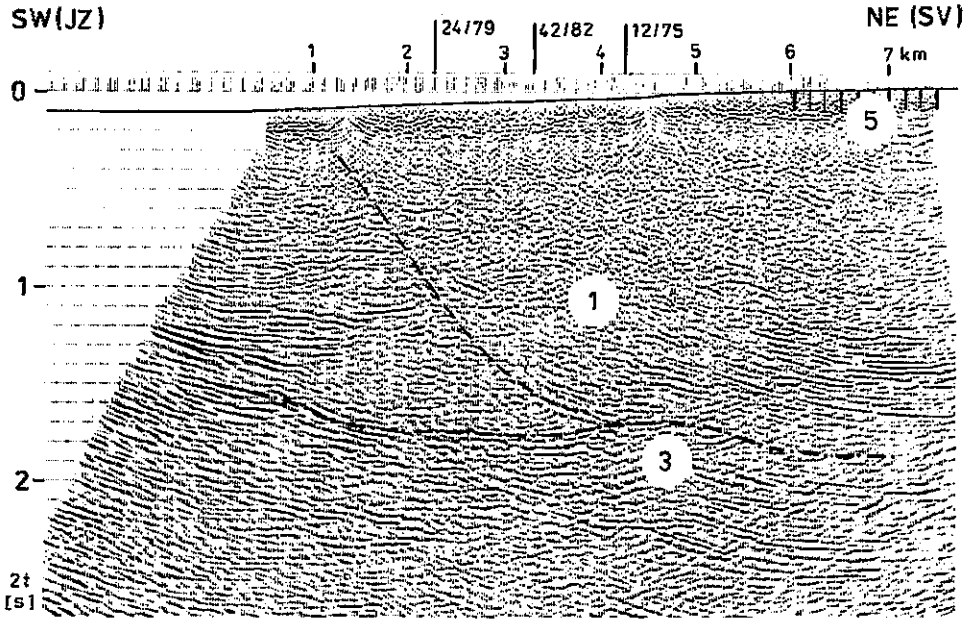

4. Seismic profile 26/79, time section with geologic interpretation (12-fold coverage, 50 m interval between the points of arrival, time-variable filtration and deconvolution, wave field coherency, wave migration).
1 – Intracarpathian Paleogene; 3 – Middle Triassic dolomites; 5 – Klippen Belt outcrops.

tudes. In the central part of the profile a local arching of the relief can be observed. It is probably the front part of the high block of the Inner Carpathians, along which overthrusting from NE to SW took place.

Some elements observed on the profile 42/82 at the crossing with profile 26/79 (e.g. the subhorizontal reflection zone at the time interval 0.9–1.0 s which might indicate overthrust tectonics) do not appear on the described profile. A striking phenomenon on the profile 26/79 in the time interval 1.2–1.6 s beneath the Klippen Belt outcrops is a group of subparallel reflections with large amplitudes. They are interpreted as manifesting intensive imbrications of deep sequences of the Intracarpathian Paleogene. The dips of reflections in the marginal parts of profile 26/79, similarly as with the profile 22/78, are not reliable. Distortion due to migration played a role there.

Profile 20/78 - 20A/78 - 20B/80 (Fig. 5)

When interpreting the reflection seismic profiles we made some changes in the interpretation of stratigraphy of the borehole Šariš-1 done by Koráb et al. (1986).

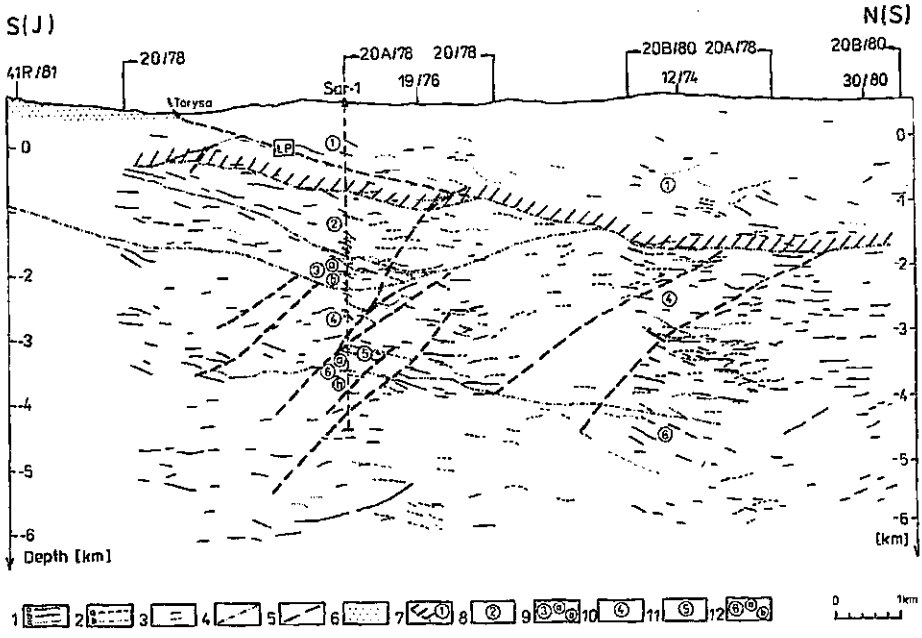

5. Seismic profile 20/78-20A/78-20B/80, depth section with geologic interpretation.
1 – events on profiles 20/78 and 20B/80: a – very strong reflections, b – strong reflections, c – weak reflections; 2 – events on profile 20A/78: a – strong reflections, b – weak reflections; 3 – dippings of beds revealed by borehole Šariš-1; 4 – stratigraphic boundaries; 5 – faults; 6 – sandstone series of the Intracarpathian Paleogene (its base is indicated by inclined hatching); 7 – Intracarpathian Paleogene (its base is indicated by inclined hatching; 8 – Albian–Lias; 9 – Lower Lias–Keuper (Upper Mesozoic pelitic-carbonatic complex): a – Lower Lias, b – Keuper; 10 – Middle Triassic (dolomite with anhydrite layers); 11 – Lower Triassic (coloured Werfenian schists, quartzites); 12 – crystalline complex: a – granodiorites, b – gneisses; LP – Lipany overthrusts.

Because of lack of drill cores (first in the depth interval 1,735–1,740 m) and of small reliability of drill cuttings for stratification of the drilled series we emphasized the geophysical boundaries traced in the borehole and on reflection seismic profiles 20/78 and 20A/78 as well as in other well log data. Further we considered the tectonic structure in general. The depth data obtained by seismic interpretation of stratigraphic and tectonic boundaries must be regarded with tolerance considering especially the anisotropy of velocities of elastic waves propagation and the complex development of the Intracarpathian Paleogene in general. Anisotropy of velocities in folded areas expresses the ratio of structural difference of rocks in longitudinal direction and in direction perpendicular to the youngest tangential tectonics, which is the limiting factor affecting also the velocities of elastic waves. In the further description of the seismic profile 20/78-20A/78-20B/80 the depth data are taken from the collar of the borehole Šariš-1.

0–1,340 m the Intracarpathian Paleogene

On the profile 20/78 in the Intracarpathian Paleogene single fragmented reflections prevail. The only continuous system is the zone of reflections in the borehole Šariš-1 at the depth of 995 m, dipping towards the NNE. In our opinion these reflections correspond to the Lipany overthrusts, i.e. to the fault zone which we regard as one of the most important overthrust dislocations in the Intracarpathian Paleogene. In the area of the Lipany boreholes we encounter older rocks (often tectonic shreds), containing Mesozoic microfauna. In agreement with Ďurkovič in Koráb et al. (1986) we consider the interval 0–950 m or 0–955 m as corresponding to a complex with prevailing claystones. The ratio of sandstones and claystones is 1:8 to 1:10. In the interval 1,075–1,080 m, Ďurkovič (ibid.) also identifies nummulites determined by E. Koehler in drill cuttings. Results of resistivity and radioactivity well logging also prove a lithological boundary at the depth of 995 m.

In regard to increasing velocities and to the character of electric logs it may be expected that sandy calcareous claystones to calcareous sandstones prevail in the interval 995–1,150 m, i.e. under the overthrust surface. It also correlates with an increased content of $CaCO_3$ in fragments of rocks in the mud.

The Paleogene-Mesozoic boundary can be identified only with difficulty because of lack of cores. At the depth of 1,080 m, however, Gašparíková (ibid.) identifies ?Middle Cretaceous foraminifers s which Kullmanová (ibid.) ranges to the depth of 1,280 m. These finds, however, should be explained similarly as the finds of Mesozoic faunas in the Intracarpathian Paleogene near Lipany, or by redeposition. The Paleogene boundary-Mesozoic can presumably be traced in the borehole Šariš-1 at the depth of 1,340 m where electric logs show a horizon with increased apparent resistivity. It cannot be excluded, however, that it is an indication of fault tectonics. Nevertheless, contrary to overlying series the complexes at depth are manifested as different seismofacies.

1,340–3,836 m Mesozoic

Regarding the interpretation of the time section of profile 20/78 and other available

data, we distinguish three complexes of typical seismofacies in the Mesozoic in the borehole Šariš-1.

In the *upper complex*, corresponding to the Albian–Lias (1,340–2,350 m), strong conspicuous events prevail. Of a similar character are the seismic reflections on profile 19/76. The increased content of $CaCO_3$ in the drill cuttings corresponds to strikingly increased velocities of elastic waves ant to increased apparent resistivity in the interval 1,340–1,710 m. At the depth of 1,435 m Kullmanová in Korán et al. (1986) identifies calcareous siltstones, at the depths of 1,640 and 1,720 m organodetrital limestones – calcarenites. In the rock complex from 1,370 to 1,710 m the high layer velocities (over 6,000 m/s) should indicate overwhelming prevalence of limestones. In the interval 1,710–2,300 m oscillations of layer velocities correspond to alternation and predominance of marly limestones over calcarous claystones.

In contrast to the upper complex, no strong events can be observed in the *middle complex* representing Lower Lias to Keuper (2,350–2,860 m), namely around the borehole Šariš-1, maybe with the exception of the upper tectonized boundary. Towards the NE of the borehole Šariš-1 the complex is entirely tectonically reduced at the crossing of profiles 20A/78 and 19/76. Towards the SW, on the contrary, the thickness of the complex greatly increases, this being valid mainly for the upper part of the complex. Lithologically, the upper part contains prevailingly a series of calcareous claystones with inclusions of limestones where layer velocities, obviously in dependence on the content of carbonates, range from 5,000 to 5,800 m/s. According to sonic logs, velocities of elastic waves strikingly increase at the depth of 2,605 m as compared with the upper part of the complex. As the sonic curve from 2,605 m downwards, i.e. in Keuper intervals confirmed by drill cores, is of a similar character, the boundary Lias-Keuper can be safely set in the depth. It should also be noted that the curve of layer velocities at the depth of 2,600 m shows an increase to 6,000 m/s. The boundary Keuper-Middle Triassic in the basement is evident from sonic log and well-shooting.

The *lower complex*, Middle to Lower Triassic (2,860–3,836 m), is in the upper part built of Middle Triassic dolomite strata with anhydrite layers, in the seismic section indicated as a set of short, dynamically striking seismic boundaries. They are based at the depth of 3,739 m, i.e. in a zone of a notable decrease of elastic waves velocities indicated both by well shooting and by sonic log. An increased content of claystone-anhydrite admixture in dolomites is indicated by sonic measurements in the intervals 3,465–3,533 m, 3,600–3,620 m and presumably also in the interval 3,690–3,739 m, which is in accordance with the lithological content of drill cuttings. According to Rudinec-Řeřicha in Korán et al. (1986), not only gypsum, but also variegated claystones appear at the depth of 3,735 m. According to seismic data, we regard dolomite strata in the borehole Šariš-1 as tectonically reduced. It is indicated by high, nevertheless "oscillating" acoustic values suggested in the interval 3,675–3,690 m. Towards the NE and the SW of the interpreted dislocation the thickness of the dolomite complex increases.

In the basement of dolomites, down to the depth of 3,836 m, Korán et al. (1986) identified a series of coloured Werfenian schists and stratigraphically unclassified quartzites. According to acoustic log, the top of the Werfenian series occurs at the depth

of 3,739 m. The lower boundary is not, similarly as at Branisko, sharp. Obviously, it is a gradual transition and the quartzites can also be ranged to the Werfenian as it is indicated by lower velocities from the depth of 3,774 m. This transition to depth is manifested as an increase in numbers of quartzite layers 0.5–1.0 m thick. The sharp decrease in elastic waves velocities in the Werfenian was recorded also by well-shooting and is evident in ultrasonic checking of quartzite samples from the depth of 3,794.5 m. The sonic log shows a continuous layer of quartzites in the interval 3,800–3,825 m, with only scarce intercalations of claystones. In dependence on the content of the clayey admixture layer velocities in dolomites range between 6,000 and 7,500 m/s, in the Werfenian they drop to 5,000 m/s.

3,836–5,000 m crystalline complex

According to Koráb et al. (1986) in granodiorites the interval 3,836–4,125 m occurs in the final section of the borehole, in muscovite-biotite gneisses in the depth interval 4,125–5,000 m. In physical terms these rocks do not differ substantially, with the exception of a higher anisotropy in gneisses. Gneisses of predominantly migmatite type exhibit slightly increased densities and substantially increased magnetic susceptibility values. Granodiorites from the depth interval 4,126–4,129 m exhibit anomalously increased gamma activity and increased U-content (Píchová-Plička-Mitevová 1986). This fact as well as the lower velocities of elastic waves measured on samples can be best explained as indications of deep tectonics. In the interval 3,836–3,885 m sonic log recorded oscillating velocities, which may correspond to a zone of intensive weathering.

Profile 42/82 (Pl. 3)

Profile 42/82 stretches from the northern environs of the village of Krivany towards the SE, north of Lipany and Sabinov to the area south of Terňa. It is situated roughly 3–4 km from the Klippen Belt outcrops. The profile passes near boreholes Lipany-1 and Lipany-3, and the borehole Lipany-2 was located on it. Reflections in the Intracarpathian Paleogene are weak, with small amplitudes. Stronger events occur at the base of the complex. In the Mesozoic relief reflections are in places dynamically intensive and sometimes, in larger segments, continuous. The seismic contrast between the sporadic events in the Paleogene and the abundant, strong and continuous reflections from the Mesozoic relief can be with advantage used to trace the relief. Similarly, the inner structures of the Mesozoic basement or the deeper complexes produce more or less strong events.

In the seismic section, the Paleogene-Mesozoic boundary is studied on data from the boreholes Lipany-1, 2 and 3, and also (using data from the transverse profile 15/75) from the borehole Lipany-5. Towards the SE the boundary rises to the area of the Lipany boreholes from where it gradually falls.

In the time interval 1.1–1.15 s, i.e. the start of the profile – station – 19.3, subhorizontal events indicate the Lipany overthrust fault. It is considered to be one of the youngest faults. Approximately to the E from the crossing with the profile 53/83

subhorizontal events, like on the profile 12/75, become weaker. It might indicate a change in the intensity or in the time plan of the Lipany overthrust faults. Overthrusting is evidenced by the tectonic deformation of the Intracarpathian Paleogene noticeable on drill cores (slickensides of cores from the borehole Lipany-1, 2, 550 m, etc.).

In the time interval 0.5–0.7 s and also in other intervals the reflections are subhorizontal and traces of correlation of reflection elements can be observed. It indicates partial, less intensive reverse movements (from NW to SE) within the upper parts of the Intracarpathian Paleogene. At the station around 25.0 km a fault is interpreted. It may be the Fričovce fault (Matějka et al. 1964).

Time map of the relief of Triassic dolomites (Fig. 6)

The map is based on time sections, more exactly on the course of the relief of Triassic dolomites in them.

The map illustrates the morphology of Triassic dolomites at an approximation only. The interval of isolines is large (the interval of isochrones 0.05 s corresponds to nearly 150 m at the depths of interest). It must be taken into account that the map does not document the variability of velocities in the area.

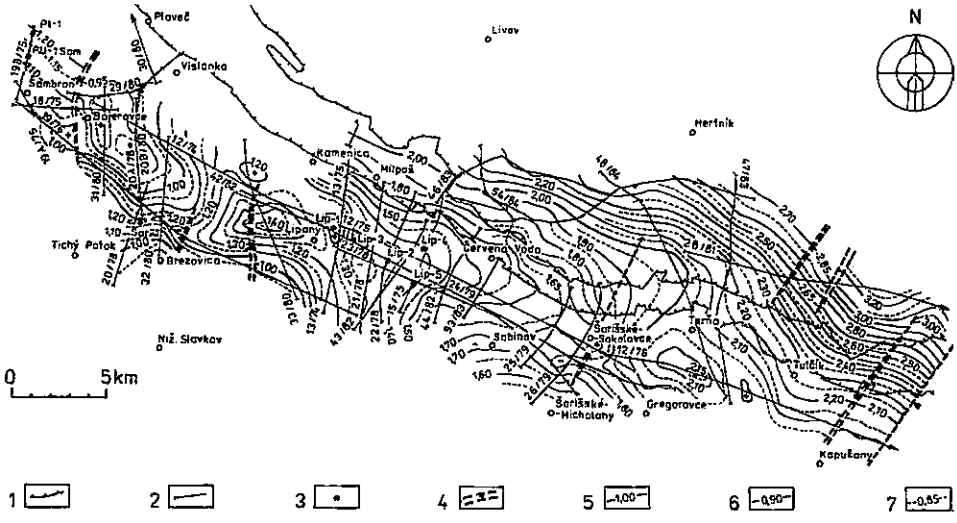

6. Time map of the relief of Triassic dolomites. 1 – Klippen Belt, 2 – CDP seismic profiles; 3 – deep boreholes; 4 – faults; 5 – isochrones of two-way time at 1.0 s intervals; 6 – as above, at 0.1 s intervals; 7 – as above, at 0.05 s intervals.

Relief of Triassic dolomites (Pl. 4)

Depth sections were used to construct a structural scheme in isonormals. Later it was transformed into a map of isohypses, using the system of auxiliary orthogonal profiles

(Gurvič 1964). The structural scheme in isohypses illustrates the vertical depths of the studied boundary.

In the southernmost part of the area, between Brezovica and Gregorovce, the isolines demonstrate a dipping of the relief towards the N and NE into a striking depression zone, stretching from the borehole Šariš-1 towards the E to Lipany. There, WNW of Lipany, the interpreted boundary reaches the maximum depth −2,850 m. The depression zone continues farther to the ESE. It can be further followed from the southern environs of the borehole Lipany-5 to the surroundings of Sabinov. In the area S of Sabinov the depression is rather shallow and wide. It is bounded by the isonormal −3,100 m. Farther to the E the depression deepens and S of Terňa attains the maximum depth of 3,950 m. Presumably, it continues to the SE, into the area of the sunken block of the Prešov fault in the northern part of the Prešovská kotlina depression.

The course of the described depression coincides quite well with the distinct Sabinov gravity low in the map of residual anomalies for r = 2 km and r = 2–16 km (Čekan-Mořkovský 1982).

In the western part of the area, SE of Šambron, dominates the arching of the complex of Triassic dolomites. Its top part stretches from WNW to ESE and is well demonstrated on profiles 31/80 and 20A/78. The elevation character of the relief corresponds to a striking, W-E trending gravity anomaly in the map of residual gravity anomalies with the radius of averaging ring r = 2–16 km (Čekan-Mořkovský 1982) and in the map of residual anomalies for $r = 8\sqrt{5}$ km (Váca et al. 1971). A continuation of the ridge can be observed in the area SW and SSE of Kamenica. There the structure has two highs. SW of Kamenica it is delimited by isoline −2,450 m, in the environs of borehole Lipany-1 its highest value is −2,300 m (borehole Lipany-1 struck Triassic dolomites at the depth −2,299 m). Farther to the E, in the vicinity of borehole Lipany-2, isonormals form an enclosed local elevation with a minimum depth of 2,450 m. On the inconspicuous ridge, extending from the elevation area towards the SE, the borehole Lipany-5 is situated. Similarly, on an extension stretching from the borehole Lipany-2 towards the ENE, the borehole Lipany-4 is located. Towards the E, an extensive elevation structure can be observed. It is elongated, trending from WNW to ESE and delimited by the highest isoline −2,850 m. The ridge extending to the SE can be followed to the area SE of Šarišské Sokolovce.

The tectonic structure of the study area has been discussed above. In Pl. 4 some tectonic lines are drawn as interpreted on reflection seismic profiles. They are Neogene normal faults which can either be observed on several seismic profiles or are illustrated in schemes.

The tectonic structure of the area W of Lipany is characterized by normal faults, N-S to NE-SW trending, dipping to the W, with amplitudes up to 500 m. It is likely that the local N-S isohypses of the relief of Triassic dolomites correspond to these tectonic features or at least were predisposed by them. In the area of Šarišské Sokolovce a dip to the SE with a step of approx. 300 m has been interpreted. On seismic profiles 42/82 and 12/75 the fault is well indicated, while on the profile 24/79 thee indications are rare. It cannot be excluded that it is the Fričovce fault, or one of the parallel faults located more to the W (Matějka et al. 1964). The fault may continue to the NNE. Because of absence

of seismic profiles this continuation is only indicated. On the profile 12/76 in the environs of Hanušovce, two faults dipping to the W are assumed. The easternmore of them was interpreted (Adamovská et al. 1977) as the Pavlovce fault (cf. Matějka et al. 1964). A comparison with the tectonic line is presumably the Lipnice fault. On the profile 28/81 the faults are not indicated. It can therefore be assumed that they fade out to the S. On the profile 28/81 two faults with a considerable step, dipping to the SE, are interpreted. They probably fade out N of the Klippen Belt. The indicated continuation of the faults towards the S and N coincides with orientations of faults revealed by geological mapping (Matějka et al. 1964).

The isohypses in the structural scheme indicate a general dipping of the relief of Intracarpathian dolomites to the N and NE, and its dipping beneath the outcrops of the Klippen Belt. This trend is interrupted by a striking ridge with the axis southern Šambron–Bajerovce–Krásna Lúka–northern Krivany–Lipany–Červená Voda–Šarišské Sokolovce. Boreholes Plavnica-1 and Plavnica-2 (personal communication R. Rudinec) revealed that in the southwestern part of the area, between Šambron and Vislanka, the tectonic structure is rather complicated. As compared with the structural scheme (Pl. 4) the dipping of the relief of dolomites to the N may be even steeper.

The area of Smilno

In the surroundings of the Smilno tectonic window where the Dukla series emerge from the basement of the Magura Flysch, reflection seismic surveys were conducted in 1972, 1981 and 1984 (Adamovský et al. 1972b, Mořkovský et al. 1982, Novák et al. 1985).

In seismic sections only short, weak and dipping reflections can be observed. There are ample interferences and low-frequency disturbances and numerous diffracted waves.

We shall discuss in more detail the section of profile 34A/84 in close vicinity of the borehole Smilno-1. The profile 34A/84 (interval between the points of arrival 25 m) was measured on a line very near the profile 34/81 (interval 50 m).

The upper part of the seismic section (the top of Beloveža series in the Dukla unit) is characterized by absence of reflections. The reflections appear at approx. 1.0 s.

A comparison with drilling data showed that inclinations of recorded events do not agree with inclinations of layers. At times 2.0–2.2 s strong events with large amplitudes occur. In the segment S of the borehole they dip steeply to the N. In close vicinity of the borehole they are subhorizontal. North of the borehole they slightly rise to the N and their amplitudes are less distinct. This range of reflections may coincide with the deeper part of submarine slide, i.e. with the boundary between the Magura and Outer Flysch (Leško 1986). Let us note, however, that in well-shooting and VSP data (Filková 1983) the boundarry is not manifested as a velocity boundary and does not reflect elastic waves. In this time interval (2.0–2.2 s), corresponding to the depth interval 3,840–4,330 m, 15–80° dipping of beds was documented on drill cores (Leško 1986).

At the time around 3.4 s a range of strong events, subhorizontal or slightly dipping to the N, can be observed near the borehole. According to extrapolated well-shooting results from the borehole Smilno-1 (Filková 1983) they are at the depth of approx.

7,400 m. Leško (1986) regarded this group of reflections (on profile 34/81) as an indication of basis for menilite flysch strata separated from the basement sediments by a tectonic overthrust surface. The crushed zone described by Leško (1986) at a depth of around 3,000 m demonstrated in seismic logs (Filková 1983) by a decrease in layer velocities from 5,000 m/s to 3,700 m/s in the interval 2,850–3,100 m is in the seismic logs indicated only sporadically (e.g. in the northern margin of the section, obviously at the time around 0.9 s, at the stem of the borehole at the time 1.64).

It can be said that the results obtained on profiles 34A/84 and 34/81 are not identical. This can be demonstrated on the above described event at around 3.4 s. On the profile 34A/84 it is subhorizontal and slightly dips to the N, while on the profile 34/81 the event is subhorizontal and rises towards the N. It is so because the profiles run through different terrains. This fact, however, makes a reliable interpretation of individual events on different seismic profiles impossible. It was proved that compared with the profile 34/81 the group of events at 3.4 s on the profile 34A/84 can be correlated in a much longer segment. On the profile 34/81 more events can be observed in the interval 1.6–3.0 s.

Seismic data document a tectonic diversity due to several phases of fold-overthrust and Neogene normal fault tectonics. It results in a very complicated pattern of interfering waves from sources in seismic profile which is further complicated by intesive side reflecting. Larger seismic interfaces may be due to tectonic faults which, however, cannot be observed at greater distances. It must be noted that inclinations of events larger than 45° cannot be recorded after migration. Direct correlation of drilling and seismic data is therefore difficult.

The surroundings of Zboj

In the surroundings of the deep borehole Zboj-1 reconnaissance profiles 6D/73, 3/75 and 38/81 (Adamovská et al. 1974, Adamovská et al. 1977, Mořkovský et al. 1982) were situated.

In the seismic time section of profile 38/81 only short reflections with small amplitudes can be observed. Numerous diffracted waves often overlap regular events. In close vicinity of Zboj-1 to the N a tectonic line dipping to the NE can be interpreted. The flat character of the line together with other phenomena indicates overthrust style of displacement. Further, a dull boundary dipping from 1.8 s at the start of the profile towards the NE to 2.16 s is interpreted. The boundary may coincide with the contact of the Dukla unit and the Zboj series struck by the borehole Zboj-1 at the depth of 3,800 m (Ďurkovič et al. 1982). Reflections on the profile 38/81 are either subhorizontal, or slightly dipping, which contrasts with the large inclinations of the series as they were revealed by Zboj-1 (up to 90°). It is likely that the seismic elements coincide with partial tectonic elements whose inclinations differ from the layer structure itself.

Conclusions

The present paper summarizes the results of geophysical, mainly CDP seismic

measurements conducted in the Intracarpathian Paleogene and in the East Slovak Flysch in the period 1972–84. The survey focussed on the environs of Lipany. In the area of Zboj and Smilno only a small-scale surveys were carried out.

In intensively folded areas the CDP method does not yield satisfactory results as it was shown by the evaluation of reflection seismic data (Kadlečík et al. 1977) and by investigations in the area of the Smilno window in 1981 and 1984. More detailed measurements outlined some younger slightly inclined overthrust planes, which are practically the only continuous reflection elements. Besides intensive folding and younger fault deformation, another factor influencing the origin of useful reflected waves is the great thickness of flysch complexes. The origin of interference waves is accompanied by great loss of energy. Therefore a majority of reflections generated by the surface of substratum are not recorded. In this rspect a negative role is played by the very probable intensive imbrication of the flysch basement.

From this point of view more favourable appears the outer part of the peri-Klippen zone N of Sabinov where the relief of Middle Triassic dolomites can be traced from the Intracarpathian Paleogene to the NE beyond the Klippen Belt to the Čergov mountain top parts.

In the broader area of the Intracarpathian Paleogene CDP measurements yield information, though not very reliable, about the relief of Mesozoic carbonates and about the overthrust structure of both the Mesozoic and Paleogene. However, it is hardly possible to distinguish Paleogene sediments and Keuper pelites. The gravity anomaly Bajerovce-Krásna Lúka is regarded as the culminating zone of the relief of dolomites.

CDP seismic data from the broader area of Lipany were used to construct a time scheme and a depth structural scheme of the buried Mesozoic relief of the Inner Carpathians. Interpretation of CDP data indicated, namely in the Intracarpathian Paleogene, numerous faults, in vast majority reaching the recent relief. They are mostly post-Eocene, presumably Old Styrian NE-SW striking overthrust faults which significantly influenced the structure of the Intracarpathian Paleogene, of the Klippen Belt and of the Krynica unit. Leško-Chmelík-Fusán (1980) called these tectonic lines along the inner margin of the Klippen Belt the Lipany overthrust faults. To verify them and to solve the problems connected with young overthrust tectonics will require close cooperation with specialists in mapping the area of interest. Seismic indications of normal faults are in the Intracarpathian Paleogene and in the Mesozoic less noticeable as compared with overthrusts. Obviously, it can be explained by strong compaction of rocks and by shortage of reflections from fault planes due to their large steep inclination.

An important point of the presented concept is the interpretation of the Intracarpathian Paleogene basement continuation to the NE beyond the Klippen Belt. It can be more or less reliably traced up to the top parts of Čergov. In regard to the basement dipping to the N, the southern and top parts of Čergov become an elevation zone divided by young overthrust faults. The northernmost of them can function as barriers for accumulation of hydrocarbons.

K tisku doporučil T. Koráb
Přeložila D. Malíková

References

Adamovská, V. et al. (1974): Seizmický průzkum metodou SRB v roce 1973, oblast východoslovenský neogén, východoslovenský flyš. – MS Geofond. Bratislava.

Adamovská, V. et al. (1977): Zpráva o reflexně-seizmickém měření v centrálněkarpatském paleogénu a flyši východního Slovenska v roce 1975 a 1976. – MS Geofond. Bratislava.

Adamovský, L. et al. (1970): Seizmický průzkum východoslovenské neogenní oblasti v roce 1970. – MS Geofond. Bratislava.

Adamovský, L. et al. (1972a): Seizmický průzkum ve východoslovenském flyši. – MS Geofond. Bratislava.

Adamovský, L. et al. (1972b): Zpráva o seizmickém průzkumu východoslovenského flyše. Profily RS 1(R)/72, 4/72. – MS Geofond. Bratislava.

Běhounek, R. (1950): Zpráva o tíhových měřeních v oblasti středního Slovenska. – MS Geofyzika. Brno.

Běhounek, R. - Válek R. (1951): Závěrečná zpráva o tíhových měřeních v oblasti středního Slovenska.– MS Geofyzika. Brno.

Birkenmajer, K. (1985): Main Geotraverse of the Polish Carpathians (Cracow - Zakopane).–Guide to excursion 2. Carpatho - Balkan Geological Association, XIIIth Congress. Kraków.

Buday, T. et al. (1967): Regionální geologie ČSSR, díl II., Západní Karpaty, sv. 2. – Ústřední ústav geologický. Praha.

Čekan, V. - Mořkovský, M. (1982): Zhodnocení tíhových a seizmických měření v centrálněkarpatském paleogénu mezi Šambronem a Lipany. – MS Geofond. Bratislava.

Čekan, V. - Šutor, A. (1960): Zpracování regionálních gravimetrických a magnetických měření provedených v letech 1952–1957 v oblasti východního Slovenska.–MS Geofond. Bratislava.

Chmelík, F. (1957): Zpráva o geologických výzkumech centrálněkarpatského paleogénu v Šariši mezi Šambronem a Sabinovem. – Zpr. geol. Výzk. v Roce 1957. Praha.

Chmelík, F. (1963): Geologie vnitrokarpatského paleogénu mezi Ružomberokem a Prešovem. – MS Geofond. Bratislava.

Ďurkovič, T. et al. (1982): Hlboký štruktúrny vrt Zboj-1. – Region. Geol. Západ. Karpát, 16, 1-76. Bratislava.

Eliáš, M. - Uhmann, J. (1968): Hustoty hornin v ČSSR. – Ústřední ústav geologický. Praha.

Filková, V. (1983): Seizmokarotážní měření a vertikální seizmické profilování na hlubinném vrtu Smilno-1. – MS Geofond. Bratislava.

Filková, V. - Mořkovský, M. - Pernica, J. (1969): Vrtně-refrakční měření v oblasti Košické kotliny na hlubinném vrtu Ďurkov-1. – MS Geofond. Bratislava.

Filková, V. - Mořkovský, M. - Pernica, J. (1971): Vrtně-refrakční měření v oblasti Košické kotliny na hlubinném vrtu Rozhanovce-1. – MS Geofond. Bratislava.

Filková, V. - Mořkovský, M. - Pernica, J. (1973): Vrtně refrakční měření v širším okolí hlubinného vrtu Humenné (MLS)-1. – MS Geofond. Bratislava.

Filková, V. - Pernica, J. (1978): Vrtně refrakční měření v okolí vrtu Lipany-1. – MS Geofond. Bratislava.

Fusán, O. et al. (1963): Vysvetlivky k prehladnej geologickej mape ČSSR 1:200 000, list Vysoké Tatry. – Ústřední ústav geologický. Bratislava.

Fusán, O. et al. (1971): Geologická stavba podložia zakrytých oblastí južnej časti vnútorných Západných Karpát. – Zbor. geol. Vied, Západ. Karpaty, 15, 1-173. Bratislava.

Gnojek, I. (1987): Magnetická anomálie u Bzenova, jz. od Prešova. – Miner. Slov., 19, 2, 169-173. Spišská Nová Ves.

Gurvič, I. I. (1964): Sejsmorazvedka. – Nedra. Moskva.

Hrdlička, A. et al. (1971): Zpráva o refrakčně seizmickém měření na profilu R 1/70 v oblasti východoslovenského flyše v roce 1970. – MS Geofond. Bratislava.

Husák, L. et al. (1986): Mapa přirozených hustot hornin Západních Karpat. – Geol. Průzk., 28, 4, 117. Praha.

Ibrmajer, J. (1963): Gravimetrické mapy ČSSR v měřítku 1:200 000.– Věst. Ústř. Úst. geol., 28, 4, 217-226. Praha.

Ibrmajer, J. (1978): Tíhové mapy ČSSR a jejich geologická interpretace. (Doktor. disert. práce). – MS Geofond. Praha.

Ibrmajer, J. - Doležal, J. (1962): Souborné zpracování a interpretace gravimetrických měření ve flyšové oblasti ČSSR. – Užitá Geofyz., Sborník prací ÚGF, 37-79. Praha.

Ibrmajer, J. - Doležal, J. - Mottlová, L. (1959): Zhodnocení geofyzikálních materiálů ve flyši. –MS Geofond. Bratislava.

Jakeš, O. et al. (1978): Zpráva o reflexně-seizmickém měření v Podunajské pánvi v roce 1977. – MS Geofyzika. Brno.

Jarý, J. et al. (1976): Zpráva o refrakčním seizmickém průzkumu ve flyši a centrálněkarpatském paleogénu východního Slovenska v roce 1975. – MS Geofond. Bratislava.

Jurga, B. (1962): Výsledky pokusných seizmických měření v oblasti flyše. – Geol. Práce, Zoš., 63. Bratislava.
Jurga, B. - Cidlinský, K. (1961): Seizmický výzkum v podmínkách flyšového útvaru. – MS GÚDŠ. Bratislava.
Kadlečík, J. et al. (1977): Komplexní interpretace geofyzikálních materiálů z východoslovenského flyše. – MS Geofond. Bratislava.
Koráb, T. et al. (1986): Výskum vnútrokarpatského paleogénu a jeho podložia v Šarišskej vrchovine a v Levočskom pohorí. Záverečné naftovo-geologické zhodnotenie oblasti na základe vrtu Šariš-1. – MS Geofond. Bratislava.
Leško, B. (1958): Prehľad geológie paleogénu južnej časti Levočského pohoria a priľahlých kotlín. – Geol. Práce, Zpr., 12. Bratislava.
Leško, B. (1986): Geologické a naftovoložiskové zhodnotenie vrtu Smilno-1, severovýchodné Slovensko. – Miner. slov., 18, 3, 193-212. Spišská Nová Ves.
Leško, B. et al. (1979): Podložie flyšových Karpát na východnom Slovensku interpretované z geofyzikálnych meraní. – Miner. slov., 11, 2, 97-114. Spišská Nová Ves.
Leško, B. et al. (1982): Opomý vrt Lipany-1 (4000 m). – Region. Geol. Západ. Karpát, 18, 1-77. Bratislava.
Leško, B. et al. (1984): Geologické zhodnotenie vrtu Hanušovce-1. – Miner. slov., 16, 3, 217-255. Spišská Nová Ves.
Leško, B. - Chmelík, F. - Fusán, O. (1980): Výskum hlbokých štruktúr Západných Karpát z hľadiska výskytu ropy a zemného plynu. Návrh na hlboký opomý vrt Šariš-1 (5500–6000 m). – MS Geofond. Bratislava.
Leško, B. - Chmelík F. - Rudinec, R. (1982): Perspektívne územie na ropu a zemný plyn východne od Vysokých Tatier. – Geol. průzk., 24, 2, 37-39. Praha.
Leško, B. - Mořkovský, M. (1975): Príspevok ku geológii podložia východoslovenských flyšových Karpát. – Geol. Práce, Spr., 64, 219-236. Bratislava.
Leško, B. - Nemčok, J. (1979): Opomý vrt Lipany-1, záverečné geologické a naftovogeologické vyhodnotenie. – MS Geofond. Bratislava.
Leško, B. - Salaj, J. - Samuel, O. (1963): Paleogene of Slovak Carpathians Klippen Belt. Resumes des communications, Ass.Geol. Karp. - Balk., VIth Congress. – Warszawa, Kraków.
Lukášová, R. et al. (1974): Technická zpráva o digitálním zpracování analogových záznamů z oblasti východoslovenského neogénu a flyše. – MS Geofond. Bratislava.
Marschalko, R. (1965): Sedimentárne textúry a paleoprúdenie v okrajových flyšových litofáciach. – Geol. Práce, Zpr. 34, 75-102. Bratislava.
Marschalko, R. (1981): Podmorské náplavové kužele v paleogéne Centrálnych Karpát a rozšírenie flyša pod neogénom východného Slovenska. In: Geologická stavba a nerastné suroviny hraničnej zóny Východných a Západných Karpát. – Geologický prieskum. Košice.
Mašín, J. et al. (1960): Zpráva o leteckém geofyzikálním měření 1:200 000 v roce 1959. – MS Geofyzika.Brno.
Matějka, A. et al. (1964): Vysvetlivky k prehľadnej geologickej mape ČSSR 1:200 000 Zborov–Košice. – Ústredný ústav geologický. Bratislava.
Meinhold, R. - Scheele, H. (1943): Bericht über gravimetrischen Untersuchungen in der östlichen Slowakei. – MS Geofond. Bratislava.
Menčík, E. (1957): Komplexní hodnocení průzkumných prací ve flyšových oblastech ČSSR. Dílčí úkoly: 1. Geologická stavba v oblasti Turzovka-Čadca - jejich vztah k průběhu tíhového pole. 2. Regionální stavba východoslovenského flyše. – MS Geofond. Bratislava.
Menčík, E. (1963): Geologické zhodnocení gravimetrických a magnetických měření v karpatském flyši na východním Slovensku. – MS Geofond. Bratislava.
Mikuška, J. - Chrumová, E. (1983): Geofyzikálny prieskum flyšového pásma a vnútrokarpatských jednotiek. Gravimetrické mapovanie. Fyzikálne vlastnosti hornín. Ročná technická správa za rok 1982. – MS Geofond. Bratislava.
Mikuška, J. - Chrumová, E. (1984): Geofyzikálny prieskum flyšového pásma a vnútrokarpatských jednotiek. Gravimetrické mapovanie. Fyzikálne vlastnosti hornín. Ročná technická správa za rok 1983. – MS Geofond. Bratislava.
Mikuška, J. - Chrumová, E. (1985): Geofyzikálny prieskum flyšového pásma a vnútrokarpatských jednotiek. Gravimetrické mapovanie. Fyzikálne vlastnosti hornín. Ročná technická správa za rok 1984. – MS Geofond. Bratislava.
Mikuška, J. - Chrumová, E. (1986): Geofyzikálny prieskum flyšového pásma a vnútrokarpatských jednotiek. Gravimetrické mapovanie. Fyzikálne vlastnosti hornín. Ročná technická správa za rok 1985. – MS Geofond. Bratislava.
Mořkovský, M. et al. (1982): Zpráva o reflexně seizmickém měření ve východoslovenském flyši v roce 1981. – MS Geofond. Bratislava.
Mořkovský, M. et al. (1987): Komplexní zpracování reflexně seizmických měření SRB v centrálněkarpatském paleogénu a flyšovém pásmu východního Slovenska. – MS Geofond. Bratislava.

Mořkovský, M. - Filková, V. (1985): The relation of longitudinal seismic waves velocities to the geology of the Inner Carpathian Paleogene of eastern Slovakia. – Sbor. geol. Věd, užitá Geofyz., 19, 31-49. Praha.
Nemčok, J. (1961): Vznik a výplň depresií v magurskom flyši na východnom Slovensku. – Geol. Sbor. Slov. Akad. Vied Umení, 12, 2. Bratislava.
Nemčok, J. (1978): Deformácie flyšových sedimentov ako odraz dynamiky podložia. – Západ. Karpaty, Sér. geol., 3, 35-58. Bratislava.
Nemčok, J. (1983): Pohyb flyšovej masy na východnom Slovensku. – Geol. Práce, Spr., 79, 141-152. Bratislava.
Nemčok, J. (1984): Magurský príkrov a bradlové pásmo na východnom Slovensku. – Geol. Práce, Spr., 81, 119-129. Bratislava.
Nemčok, J. et al. (1977): Štruktúrny vrt PU-1 Šambron (Lubovnianska vrchovina). – Region. Geol. Západ. Karpát, 8, 1-72. Bratislava.
Novák, J. et al. (1985): Technická zpráva o reflexně seizmickém měření ve flyši a centrálněkarpatském paleogénu východního Slovenska v roce 1984. – MS Geofond. Bratislava.
Odstrčil, J. (1985): Mapa středních přirozených hustot ČSSR odvozených z tíhových měření 1:25 000. – MS Geofond. Bratislava.
Ondra, P. - Hanák, J. (1989): Petrofyzikální studium sedimentů východoslovenského flyše. – Geol. Práce, Spr. 89, 67 - 97. Bratislava.
Pernica, J. - Filková, V. (1974a): Seizmokarotážní měření na hlubinném vrtu Kecerovské Pekľany-1. – MS Geofond. Bratislava.
Pernica, J. - Filková, V. (1974b): Seizmokarotážní měření na hlubinném vrtu Ždánice-4. – MS Geofond. Bratislava.
Pernica, J. - Filková, V. (1975): Seizmokarotážní měření na hlubinném vrtu Osvětimany-1. – MS Geofond. Bratislava.
Píchová, E. (1985): Komplexní zpracování fyzikálních vlastností hornin flyšového pásma a centrálněkarpatského paleogénu východního Slovenska. – MS Geofond. Bratislava.
Píchová, E. - Plička, M. - Mitevová, J. (1986): Fyzikální vlastnosti hornin na vrtu Šariš-1. – MS a.s. Geofyzika. Brno.
Plíva, G. et al. (1976): Reinterpretace refrakčně seizmických dat v oblasti východoslovenského flyše. – MS Geofond. Bratislava.
Plíva,G. et al. (1977): Reinterpretace refrakčně seizmických dat v oblasti východoslovenského flyše. – MS Geofond. Bratislava.
Pospíšil, L. (1983): Analýza a syntéza geologických a geofyzikálnych štruktúr pomocou údajov získaných prostriedkami DPZ. – MS Geofond. Bratislava.
Pospíšil, L. (1985): Příspěvek gravimetrie k interpretaci nelineární struktury Stropkov – Svidník. – Zem. Plyn Nafta, 30, 1, 67-75. Hodonín.
Pospíšil, L. - Filo, M. (1982): Niektoré problémy a výsledky interpretácie tiažových anomálií v širšom okolí humenskej štruktúry. – Miner. slov., 14, 4, 343-353. Spišská Nová Ves.
Pospíšil, L. - Nemčok, J. - Feranec, J. (1982): Analýza "nelineárnej štruktúry Svidník - Stropkov" identifikovanej interpretáciou kozmických snímok. – Miner. slov., 14, 6, 539-548. Spišská Nová Ves.
Rudinec, R. (1981): Záverečná správa hlbokého štruktúrneho vrtu Lipany-2. – MS archív MND záv. Michalovce.
Rudinec, R. (1986): Štruktúra Lipany a niektoré zaujímavé geologické a ropno-geologické výsledky. – Zem. Plyn Nafta, 31, 4, 521-527. Hodonín.
Rudinec, R. - Řeřicha, M. (1985): Záverečná správa vrtu Lipany-5. – MS archív MND záv. Michalovce.
Scheele, H. (1944): Bericht über magnetische Messungen in Gebiet der Ostslowakei. – MS archív a.s. Geofyzika. Brno.
Stráník, Z. (1965): Geologie magurského flyše Čerchovského pohoří a západní části Ondavské vrchoviny. – Zbor. geol. Vied, Západ. Karpaty, 3, 125-178. Bratislava.
Stránska, M. et al. (1986): Hustotná mapa hornín Západných Karpát na území ČSSR. Záverečná správa. – MS Geofond. Bratislava.
Šutor, A. - Čekan, V. (1965): Regionální gravimetrický a geomagnetický průzkum v oblasti východního Slovenska. – Sbor. geol. Věd, užitá Geofyz., 4, 35-57. Praha.
Uhmann, J. (1974): Výzkum hlubinné stavby v neogenní předhlubni a ve flyšovém pásmu Karpat. – MS Geofond. Bratislava.
Uhmann, J. et al. (1977): Hustoty, porózita a magnetická susceptibilita hornin v oblasti Hanušoviec, Stropkova, Medzilaboriec, Papina a Humenného. – MS Geofond. Bratislava.
Váca, F. et al. (1971): Detailní tíhový průzkum, lokalita "šambronský chrbát". – MS Geofond. Bratislava.
Wojas, A. (1977): Refrakčno-seizmický prieskum vo východoslovenskom flyši. Záverečná správa. – MS Geofond. Bratislava.

Geofyzikální průzkum na uhlovodíky v centrálněkarpatském paleogénu a flyšovém pásmu východního Slovenska

(Resumé anglického textu)

Milan Mořkovský - Josef Novák - Regina Lukášová

Předloženo 20.října 1988

Již první výsledky reflexně seizmických měření provedené metodou RNP v oblasti východoslovenského flyše signalizovaly mimořádně obtížné seizmogeologické podmínky (Jurga-Cidlinský 1961). Jak se ukázalo později, jsou podmíněny zejména složitou vrásovo-příkrovovou stavbou území a značnou mocností flyšových komplexů. Vznikají velmi intenzívní poruchové vlny a současně dochází k silnému útlumu užitečných odražených vln. Proto nejsou registrovány reflexy od reliéfu flyšového podkladu. Následná reflexně seizmická měření s analogovou registrací a zejména pozdější seizmická měření SRB potvrdila výše uvedené poznatky o nepříznivých seizmogeologických podmínkách východoslovenského flyše.

Seizmická měření SRB provedená v centrálněkarpatském paleogénu ukázala, že v této oblasti jsou podmínky pro seizmický průzkum – oproti flyšovým Karpatům – příznivější. Na základě interpretace seizmického materiálu je možno, i když místy ne zcela jednoznačně, sledovat reliéf karbonátů v podloží sedimentů paleogénu a také přesmykovou stavbu jak mezozoika, tak zejména paleogénu. Možnost odlišení sedimentů centrálněkarpatského paleogénu od pelitů keuperu na základě časových řezů SRB je ovšem malá. Na základě těchto relativně příznivých výsledků a také v souvislosti s příznivým hodnocením perspektiv naftoplynonosnosti přibradlové oblasti byla v širším okolí Lipan proměřena poměrně hustá síť seizmických profilů SRB, která v této oblasti umožnila konstrukci strukturního schématu zakrytého reliéfu dolomitů Centrálních Karpat v podloží paleogénu.

Ve flyšovém pásmu byly větší objemy reflexně seizmických prací v modifikaci SRB realizovány zejména v oblasti Smilna a v okolí Zboje.

V tomto článku předkládáme nejzávažnější výsledky zpracování a interpretace seizmických materiálů SRB, získané ve studované oblasti. Největší pozornost byla věnována širšímu okolí Lipan. Kromě reflexní seizmiky bylo využito i výsledků tíhových a magnetických měření, měření fyzikálních vlastností hornin, refrakční seizmiky, vrtní refrakce, seizmokarotážních měření a výsledků akustické i elektrické karotáže i výsledků dalších geofyzikálních metod.

Gravimetrie

Za první prakticky využitelná tíhová měření lze považovat až gravimetrické práce počínaje rokem 1954. Jednalo se o regionální tíhová měření s hustotou jednoho měřicího bodu na 2–3 km^2. Detailní tíhový průzkum s hustotou 3–6 měřicích bodů na km^2 je v

zájmovém území prováděn od roku 1970. Jeho dílčích výsledků v území mezi Šambronem–Lipany využili Čekan-Mořkovský (1982) k sestavení map reziduálních anomálií tíhového pole. Ukázalo se, že mapa reziduálních anomálií tíhového pole s poloměrem vystředění 2 km zobrazuje litologické změny hornin centrálněkarpatského paleogénu. Mapa reziduálních anomálií s poloměrem vystředění 2–16 km naopak zřejmě charakterizuje (jak ukazují výsledky reflexní seizmiky) reliéf karbonátů Centrálních Karpat. Výsledky tíhových měření byly souborně zpracovány zejména Menčíkem (1957), Čekanem-Šutorem (1960), Ibrmajerem-Doležalem-Mottlovou (1959), Ibrmajerem-Doležalem (1962) a Ibrmajerem (1963, 1978). Vzhledem ke komplikovaným strukturně tektonickým poměrům východoslovenského flyše a jeho podkladu, i přes řadu řešených problémů, je interpretace tíhových dat stále velmi složitou.

Magnetometrie

Jak ukázalo regionální magnetické měření s hustotou jednoho měřicího bodu na 2 až 3 km^2 provedené v letech 1955–1957, je charakter geomagnetického pole monotónní (± 20 nT). To nepochybně souvisí s malou susceptibilitou flyšových komplexů i jejich podloží, resp. s jejich malou diferenční susceptibilitou. Uvážíme-li, že měření bylo konáno se střední chybou ± 4 nT, je zřejmé, že interpretace geomagnetického pole je problematická. Naměřený materiál souborně zpracovali Ibrmajer-Doležal-Mottlová (1959), Šutor-Čekan (1965), resp. Šutor in Kadlečík et al. (1977).

Fyzikální vlastnosti hornin

Fyzikální vlastnosti hornin byly měřeny na hlubinných vrtech PU-1 Šambron, MLS-1 Humenné, Zboj-1, Lipany-1,2,3,4,5, Hanušovce-1, Smilno-1, Šariš-1, resp. Prešov-1 (příl. 1). Komplexně zpracovala fyzikální vlastnosti hornin v zájmové oblasti Píchová (1985).

Údaje o fyzikálních vlastnostech hornin jsou významné ze dvou hledisek. První hledisko souvisí s využitím těchto dat při hodnocení výsledků geofyzikálních metod. Zvláštní význam mají údaje o hustotách hornin při interpretaci tíhových měření v oblastech postižených tangenciální tektonikou. Ondra-Hanák (1989) zjistili celkově vyšší hustoty hornin bradlového pásma včetně křídových komplexů a paleogenních obalů – pročských vrstev – zejména oproti krynické jednotce a i oproti přilehlému centrálněkarpatskému paleogénu. Z výsledků detailních tíhových měření vyplývá, že zejména svrchnokřídové a rovněž i paleogenní obaly bradlového pásma v úseku Plavče–Lubotína až po příčný pavlovský zlom vyvolávají souvislou kladnou anomálii. Zvýraznění této tíhové anomálie zřetelně souvisí s výchozy púchovských slínů a můžeme je sledovat z okolí Mošurova podél jižního okraje bradlového pásma až po pavlovský zlom. Východně od tohoto zlomu, spolu s vyznívání púchovských slínů a nástupem flyšového vývoje svrchní křídy, tíhový projev bradlového pásma zaniká. Je pravděpodobné, že se tam i snižuje hustota pročských vrstev.

Druhé hledisko se týká obecného posuzování problémů ropoplynonadějnosti území. Analýza fyzikálních vlastností hornin, zejména hustoty a porózity, prokázala vysoký stupeň kompakce hornin zejména centrálněkarpatského paleogénu, a to jak podle

výsledků měření na povrchově odebraných vzorcích, tak i na jádrech hlubinných vrtů. Husák et al. (1986) ze stupně kompakce vyvozují původní mocnost šambronských vrstev 5–6 km. Oproti autorům se domníváme, že kromě diageneze hrálo významnou roli i tektonické zhutnění. Výsledkem komplikovaného vývoje jsou velmi nízké primární porózity hornin. V centrálněkarpatském paleogénu, bradlovém pásmu i flyšových Karpatech převažují hodnoty porózity do 1 % (Píchová 1985). Je tedy zřejmé, že s výjimkou karbonátových hornin je nutno z hlediska kolektorských vlastností uvažovat pouze se sekundární porózitou.

Letecké a družicové metody

Letecký magnetometrický a radiometrický průzkum v měřítku 1:200 000 je popsán ve zprávě Mašína et al. (1960). Naměřené magnetické pole je v zájmovém území vcelku monotónní. Detailním leteckým měřením v měřítku 1:25 000, kterým byl zastižen zejména jižní okraj zájmového území, byla zjištěna významnější anomálie pouze v širším okolí Radatic. Gnojek (1987) ji považuje za projev bazického tělesa. Při radiometrickém průzkumu bylo naměřeno pole bez výraznějších anomálií.

Metodami dálkového průzkumu země byla zjištěna kruhová struktura v prostoru Svidník-Stropkov. Její vznik vysvětlují Pospíšil-Nemčok-Feranec (1982), resp. Pospíšil (1983, 1985) buď její přítomností na systému hlubinných tektonických linií, nebo jako oblast kolizní zóny odlišných podložních bloků.

Refrakční seizmika

Celková délka refrakčně seizmických profilů proměřených v zájmové oblasti činí 826 km (příl. 1). Výsledky měření jsou zveřejněny v příslušných zprávách a jsou také obsahem komplexních hodnocení zejména Plívy et al. (1976, 1977) a Kadlečíka et al. (1977).

Všechna zpracování refrakčních měření ve flyši narážela na potíže podmíněné seizmogeologickými podmínkami složité vrásovo-příkrovové stavby flyšových Karpat.

Z celkového hodnocení podkladů refrakční seizmiky vzhledem k dosaženým vrtným a geofyzikálním výsledkům jak na našem, tak i polském a sovětském území vyplynul názor, že za podklad flyšových komplexů by bylo možno považovat refrakční rozhraní o hraniční rychlosti vyšší než 6000 m/s (Kadlečík et al. 1977). Tento názor však nepotvrdil vrt Smilno-1, který v hloubce udávaného rozhraní (5000 m) zastihl bazální polohy černého flyše. Uvedená rozporná zjištění vedla k zastavení refrakčně seizmických prací jak na našem, tak i na polském a sovětském území flyšových Karpat.

Věrohodnějších výsledků se dosáhlo refrakční seizmikou v centrálněkarpatském paleogénu, kde údaje vrtu Lipany-4 nejsou v rozporu s udávanou hloubkou refrakčního rozhraní a kde je i obecný souhlas s výsledky reflexní seizmiky.

Vrtně refrakční měření

Metoda vrtní refrakce byla aplikována na hlubinných vrtech MLS-1 Humenné a Lipany-1 (příl. 1).

Výsledky získané na vrtu Lipany-1 prokázaly značné anomality v šíření lomených vln,

ze kterých i při tehdejším jen omezeném stavu poznatků o hluboké stavbě vyplývalo, že se nejedná o projevy téhož rychlostního rozhraní. Z těchto důvodů byly další práce zastaveny. Získané údaje nasvědčovaly přítomnosti většího množství rozhraní, jež nebylo možno blíže identifikovat. Až z výsledků současného zpracování vyplynulo, že tato rozhraní odpovídají jednak reliéfu dolomitů v podloží centrálněkarpatského paleogénu, jednak tektonickým plochám – přesmykům – v centrálněkarpatském paleogénu, event. v bradlovém pásmu. Jejich vzájemné oddělení z materiálů vrtní refrakce není možné.

Seizmokarotážní měření

Seizmokarotáž byla v zájmovém území realizována na 11 hlubinných vrtech (Lipany-1, 2 a 3, Šariš-1, PU-1 Šambron, Plavnica-1, Hanušovce-1, Smilno-1, Zboj-1, MLS-1 Humenné, resp. Prešov-1, viz příl. 1). Získané údaje daly konkrétní představu o rychlostech elastických vln v pracovní oblasti a umožnily, zejména v centrálněkarpatském paleogénu, věrohodný převod časových údajů do hloubkového měřítka.

Reflexní seizmický průzkum do roku 1971

První reflexně seizmická měření ve východoslovenském flyši oscilografickou seizmickou aparaturou byla uskutečněna v letech 1959-1960 v okolí Adidovců a Stropkova. V letech 1970-1971 bylo provedeno ve v. části flyše měření analogovou seizmickou aparaturou RX 24 S II. Seizmické údaje získané v analogové formě byly později převedeny do digitální formy pomocí počítače EMR ADVANCE 6070. Reflexní seizmická metoda přinesla v uvedeném období obtížně interpretovatelný materiál. Situace profilů je znázorněna v příl. 1.

Reflexní seizmika v modifikaci SRB

Od roku 1972 byl reflexně seizmický průzkum zájmové oblasti realizován v modifikaci společného reflexního bodu (SRB). Do roku 1984 včetně bylo touto metodou proměřeno 50 profilů o celkové délce 477 km; kromě profilů zahrnutých do předloženého zpracování, tj. do roku 1984 včetně, jsou v příl. 1 a 2 zakresleny i profily SRB z let 1985–1986, tedy 64 profilů o celkové délce 669 km.

Terénní seizmické práce byly realizovány odpalovou technologií, nejčastěji středovým roztažením, zpočátku 6násobným, od roku 1976 12násobným překrytím. Vzdálenost středů seskupení geofonů byla 50 m . Registrace odražených elastických vln byla zajištěna digitální seizmickou aparaturou SN 328,SN 338A nebo DFS IV. Do roku 1975 se jednalo o 24kanálové, později o 48kanálové seizmické aparatury. Vzorkovcí interval byl 2 ms.Zdrojem elastických vln byly nálože průmyslových trhavin o hmotnosti 20–30 kg, odpalované z vrtaných sond hlubokých převážně 25–30 m. Metodika terénních prací byla určena zejména na základě parametrických měření.

Do roku 1978 byla naměřená seizmická data zpracovávána na digitální seizmické centrále EMR 6070 řady ADVANCE, vybavené zapisovací jednotkou TNR 91. Seizmické programy umožňovaly standardní zpracování. Migrace seizmických vln byla

prováděna pomocí vážené difrakční sumace. Od roku 1979 je v n.p. Geofyzika, Brno, v provozu počítač RDS 500, doplněný procesorem APOLLO a řízený programovým systémem GEOMAX (registrovaná ochranná značka firmy CGG). Oproti systému EMR má GEOMAX podstatně širší programové možnosti. Má např. automatický způsob výpočtu reziduálních statických korekcí. Významná je i možnost měření a zpracování seizmických dat na křivočarých profilech technikou Slalom line (registrovaná ochranná značka firmy CGG). Migrace seizmických vln je realizována pomocí vlnových rovnic (program WEMIG).

Jak ukázalo zhodnocení Kadlečíka et al. (1977) i další práce zejména v okolí Smilna v letech 1981 a 1984, nepřináší metoda SRB v intenzívně zvrásněném flyši významnější výsledky. Při pracích detailnějšího charakteru je možno v seizmických řezech vyčlenit některé mladší přesmykové linie s plošším úklonem. Ty bývají prakticky jedinými souvislejšími odraznými elementy. Nejsou registrovány reflexy, jež by bylo možno s větší mírou pravděpodobnosti spojovat s reliéfem flyšového podkladu.

V centrálněkarpatském paleogénu je možno reflexní seizmikou sledovat reliéf dolomitů mezozoika a přesmykovou stavbu jak mezozoika, tak zejména paleogénu. Jedná se převážně o poeocenní, pravděpodobně staroštýrské zpětné přesmyky od SV k JZ, které vtiskly stavbě centrálněkarpatského paleogénu, bradlového pásma i krynické jednotky významné rysy. Leško-Chmelík-Fusán (1980) tyto tektonické linie podél vnitřního okraje bradlového pásma nazývají lipanskými přesmyky. Jejich ověření v terénu a řešení dalších problémů spojených s mladou přesmykovou tektonikou vyžaduje úzkou spolupráci s mapérskými specialisty studovaného území.

Převod seizmických dat z časového oboru do hloubkového měřítka byl realizován pomocí grafů závislosti $2t_o(H)$. Byly zkonstruovány pro každý seizmický profil na základě geologických modelů a údajů seizmokarotážních měření. Příklad zjednodušené závislosti $2t_o(H)$ pro profil 42/82 je zakreslen v příl. 3. Rychlostní poměry mohly být nejdetailněji vysledovány v širším okolí Lipan, kde byla provedena seizmokarotážní měření na vrtech PU-1 Šambron, Plavnica-1, Šariš-1 a Lipany-1, 2 a 3. Při určení rozsahu působnosti těchto rychlostních závislostí bylo využito zejména údajů podpovrchových rychlostí (příl. 2). Závislosti středních rychlostí na hloubce podle seizmokarotážních údajů vrtů situovaných v zájmovém území jsou uvedeny na obr. 1.

Výsledkem zpracování a interpretace seizmických dat jsou časové a hloubkové seizmické řezy s geologickou interpretací. Jejich ukázky jsou uvedeny na příl. 3 a obr. 2, 3, 4 a 5.

Hlavním grafickým výstupem interpretace časových a hloubkových seizmických řezů SRB je časová mapa a strukturní schéma zakrytého reliéfu dolomitů triasu v podloží centrálněkarpatského paleogénu (obr. 6, příl. 4). V zájmovém území povrch dolomitů triasu vesměs generelně klesá k S až SV. Tento trend je přerušen výrazným hřbetem s osou j. Šambron–Bajerovce–Krásna Lúka–s.Krivany–Lipany–Červená Voda–Šarišské Sokolovce. Závažným momentem předložené koncepce je interpretace plynulého pokračování podkladu centrálněkarpatského paleogénu k SV za bradlové pásmo (ve smyslu názorů Nemčoka 1961, 1978), které lze s různou mírou věrohodnosti sledovat až pod vrcholové části Čergova. Lze se domnívat, že tíhová anomálie Bajerovce-Krásna Lúka je kulminující zónou reliéfu dolomitů.

Vysvětlivky k obrázkům a přílohám

1. Závislost středních rychlostí na hloubce podle výsledků seizmokarotážních měření. 1 - Hanušovce-1; 2 - MLS-1 Humenné; 3 - Lipany-1; 4 - Lipany-2; 5 - Lipany-3; 6 - Plavnica-1; 7 - Smilno-1; 8 - PU-1 Šambron; 9 - Šariš-1; 10 - Zboj-1.
2. Seizmický profil 19/76, časový řez s geologickou interpretací (12násobné překrytí, vzdálenost bodů příjmu 50 m; časově proměnná filtrace a dekonvoluce, zvýraznění koherence vlnového pole, vlnová migrace). 1 - centrálněkarpatský paleogén; 2 - peliticko-karbonátový vývoj vyššího mezozoika (alb-keuper); 3 - dolomity středního triasu (event. pestré břidlice a křemence spodního triasu); 4 - krystalinikum; LP - lipanské přesmyky.
3. Seizmický profil 22/78, časový řez s geologickou interpretací (12násobné překrytí, vzdálenost bodů příjmu 50 m; časově proměnná filtrace a dekonvoluce, zvýraznění koherence vlnového pole, vlnová migrace). 1 - centrálněkarpatský paleogén; 3 - dolomity středního triasu; 5 - povrchový výchoz bradlového pásma; LP - lipanské přesmyky.
4. Seizmický profil 26/79, časový řez s geologickou interpretací (12 - násobné překrytí, vzdálenost bodů příjmu 50 m; časově proměnná filtrace a dekonvoluce, zvýraznění koherence vlnového pole, vlnová migrace). 1 - centrálněkarpatský paleogén; 3 - dolomity středního triasu; 5 - povrchový výchoz bradlového pásma.
5. Seizmický profil 20/78-20A/78-20B/80, hloubkový řez s geologickou interpretací. 1 - odrazové elementy na profilech 20/78 a 20B/78 odpovídající reflexům : a - velmi výrazným , b - výrazným, c - nevýrazným; 2 - odrazové elementy na profilu 20A/78 odpovídající reflexům: a - výrazným, b - nevýrazným; 3 - úklony vrstev zjištěné na vrtu Šariš - 1;4 - stratigrafické hranice; 5 - zlomy; 6 - pískovcové souvrství centrálněkarpatského paleogénu; 7 - centrálněkarpatský paleogén (průběh jeho báze je zvýrazněn šikmým šrafováním); 8 - alb-lias; 9 - spodní lias-keuper (peliticko karbonátový vývoj vyššího mezozoika): a - spodní lias, b - keuper; 10 - střední trias (dolomity s anhydritovými polohami); 11 - spodní trias (pestré břidlice werfenu, křemence); 12 - krystalinikum: a - granodiority, b - ruly, LP - lipanské přesmyky.
6. Časová mapa reliéfu dolomitů triasu. 1 - bradlové pásmo; 2 - reflexně seizmické profily SRB; 3 - hlubinné vrty; 4 - zlomy; 5 - izochrony dvojnásobného času po 1,0 s; 6 - dtto, po 0,1 s; 7 - dtto, po 0,05 s.

Příl. 1. Geofyzikální prozkoumanost centrálněkarpatského paleogénu a flyšového pásma východního Slovenska (do roku 1986). 1 - bradlové pásmo; 2 - předterciérní komplexy; 3 - centrálněkarpatský paleogén a flyš; 4 - neogenní sedimenty; 5 - neogenní vulkanity; 6 - reflexně seizmické profily SRB (silně jsou zakresleny profily 19/76, 22/78, 26/79, 20/78-20A/78-20B/80 a 42/82, ilustrované na obr. 2, 3, 4, 5 a příl. 3); 7 - seizmická parametrická měření (od roku 1972); 8 - reflexně seizmické profily (jednoduché překrytí - oscilografická registrace, regulovaný směrový příjem - RNP, hlubinné seizmické sondování - HSS); 9 - refrakčně seizmické profily; 10 - vrtně refrakční profily; 11 - vrty, na jejichž jádrech byly měřeny fyzikální vlastnosti; 12 - vrty, na nichž bylo provedeno seizmokarotážní měření, resp. vertikální seizmické profilování;13 - vrty s provedeným vrtně refrakčním měřením. Vrty: Han - Hanušovce, MLS-1 Hu - Humenné, Lip - Lipany, Pl - Plavnica, Smi - Smilno, PU-1 Sam - Šambron, Sar - Šariš, Zj - Zboj.

Příl. 2. Schéma podpovrchových rychlostí a oblastí působnosti rychlostních křivek zjištěných seizmokarotážním měřením na vrtech PU-1 Šambron, Šariš-1 a Lipany-1, 2 a 3. 1 - bradlové pásmo; 2 - předterciérní komplexy; 3 - centrálněkarpatský paleogén a flyš; 4 - neogenní sedimenty; 5 - neogenní vulkanity; 6 - vrty, na nichž bylo provedeno seizmokarotážní měření; 7 - reflexně seizmické profily SRB. Podpovrchové rychlosti v rozmezí: 8 - 2500-3000 m/s, 9 - 3000-3300 m/s, 10 - 3300-3600 m/s, 11 - 3600-3900 m/s, 12 - 3900-4200 m/s, 13 - 4200-4600 m/s. Oblast použití rychlostní křivky podle seizmokarotážního měření na vrtu: 14 - PU-1 Šambron, 15 - Šariš-1, 16 - Lipany-1, 2 a 3.

Příl. 3. Seizmický profil 42/82 (část). Nahoře: časový řez s geologickou interpretací (12násobné překrytí, vzdálenost bodů příjmu 50 m; časově proměnná filtrace a dekonvoluce, zvýraznění koherence vlnového pole, vlnová migrace). Dole: hloubkový řez s geologickou interpretací a schematickým znázorněním závislosti dvojnásobku času na hloubce. Tato závislost vychází zejména z výsledků seizmokarotážních měření na vrtech Lipany-1, 2 a 3. 1 - centrálněkarpatský paleogén; 2 - dolomity středního triasu; LP - lipanské přesmyky.

Příl. 4. Strukturní schéma reliéfu dolomitů triasu. 1 - reflexně seizmické profily SRB; 2 - bradlové pásmo; 3 - hlubinné vrty, které ověřily reliéf dolomitů triasu; 4 - hlubinné vrty, které skončily v centrálněkarpatském paleogénu; 5 - zlomy; 6 - izolinie vertikálových hloubek reliéfu dolomitů triasu po 500 m, vztažené k nulové hladině; 7 - dtto, po 100 m.

Sborník geologických věd	Užitá geofyzika 25	Pages 49–66	8 figs.	– tab.	– pl.	Praha 1992 ISBN 80-7075-110-X ISSN 0036-5319

Velocity distribution modelling on building site of the nuclear power plant of North Moravia - A case history

Modelování rychlostního rozložení na lokalitě jaderné elektrárny Severní Morava

Vladimír Dvořák[1] - Petr Firbas[1] - Zuzana Skácelová[1]

Received July 1, 1988

1 : 50,000
15-34, 15-43
25-12, 25-21

Microearthquake monitoring
Velocity modelling
Interpretation

Dvořák, V. - Firbas, P. - Skácelová, Z. (1992): Velocity distribution modelling on building site of the nuclear power plant of North Moravia - A case history. - Sbor. geol. Věd, užitá Geofyz., 25, 49–66. Praha.

Abstract: To determine local microearthquake hypocentres, detailed knowledge of local seismic velocity distribution is required. For this reason a seismic survey along several refraction profiles has been performed on the building site of the nuclear power plant of North Moravia. Refraction data (travel times) from these profiles has been interpreted using 2D inverse technique described in Firbas - Skorkovská (1986, 1988). Since this interactive program package has been used for the first time with real data, individual steps of computation are described in some detail in this paper. Resulting 2D velocity models for selected profiles are presented.

[1]*Institute of Physics of the Earth, Brno, Ječná 29a, 612 46 Brno*

Introduction

The seismic hazard assessment of a nuclear power plant site requires delineating of seismically active faults in its vicinity. An active fault can be revealed by determining local earthquake hypocentres using microearthquake networks (Lee - Stewart 1981). Local seismic velocity distribution must be known in detail for accurate and reliable location of microearthquake hypocentres. If the number of stations in the network as well as the number of the earthquakes recorded is high enough, then the velocity distribution can be computed simultaneously with the hypocenter parameters utilizing data from local earthquakes. In Crosson (1976a, b) a method for such a simultaneous inversion is described for 1D layered velocity model. The problem of 3D velocity

distribution estimation from teleseismic data is solved e.g. in Aki - Lee (1976). Perhaps the most straightforward approach is to determine the 3D velocity distribution inverting travel-times from controlled blasts.

The microearthquake network on the site of the nuclear power plant of North Moravia (Cidlinský et al. 1986) consists of five three-component stations only, which seems to be insufficient for the simultaneous inversion of hypocentre parameters and the 3D velocity distribution. Therefore an additional seismic measurement had to be performed to determine the velocity distribution. Seismic refraction method has been used along eight profiles (see Fig. 1). Since the geological structure of the site is rather complex, strong lateral velocity variations have been expected.

The inverse kinematic problem for laterally inhomogeneous (2D) structures can be solved by the method of "trial and error". This method is efficient in the case when the used computer program is written as an interactive one. This idea was materialized in the interactive program package 2-DIM (2-D Interactive Modelling) described in Firbas - Skorkovská (1986).

In 2-DIM package a simplified method of solving the direct kinematic problem is used. The approach used goes back to ideas presented in Aric - Gutdeutch - Sailer (1980) and makes use of ray tracing ideas developed by Červený and Pšenčík (1981). In the approach of Firbas and Skorkovská (1986, 1988) the x-z plane in which the velocity distribution is to be approximated is automatically divided into a set of triangles fully covering the model. At a point inside a triangle the velocity value is given by a linear combination of

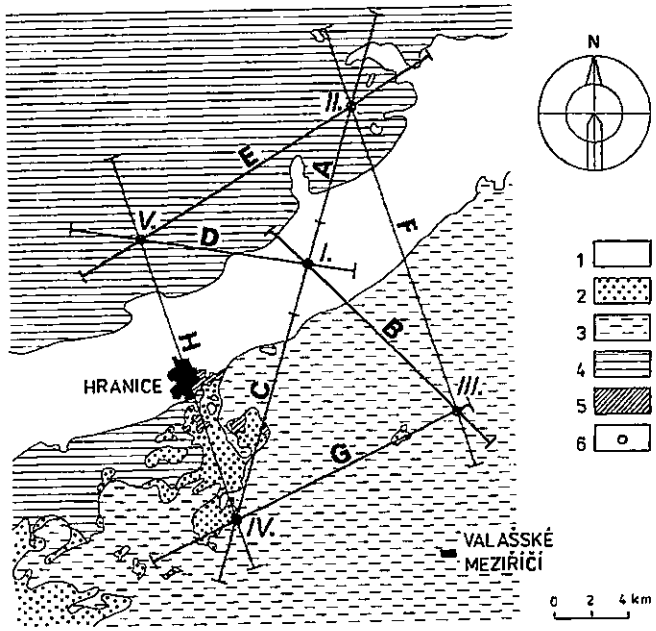

1. Geological map of the site with the situation of seismic profiles and microearthquake network stations.
1 – Neogene (Badenian); 2 – Neogene (Carpathian); 3 – Paleogene (flysh); 4 – Culm; 5 – Devonian; 6 – a three-component station of the microearthquake network.

model. At a point inside a triangle the velocity value is given by a linear combination of the velocity values at the corners of the triangle. Consequently, the velocity gradient inside any triangle is constant and the raypath inside each triangle is represented by a part of a circle. In such a case the direct kinematic problem can be solved analytically. The computation of raypaths and travel times is simple and fast.

In this paper we will describe the first application of 2-DIM interactive program package to real field data. Therefore the computational procedure is being followed step-by-step including the data preparation stage. The possibilities offered by the program are described from the point of view of an interpreter, not a programmer. The authors' description of the program (Firbas - Skorkovská 1986, 1988) is extended wherever we feel it could be useful for an interpreter. The resulting velocity models for selected profiles are presented to demonstrate the possibilities of the program package and the algorithm used.

Data acquisition

At the stage of field measurements eight refraction profiles (named A to H) were surveyed on the site. Their layout together with the simplified geological map is shown in Fig. 1. Every profile connects two stations of the microearthquake network so that these could have been directly used as profile registration points. The remaining 3 "off-profile" stations of the microearthquake network were registrating as well during the profile measurements and so they have supplied us with additional "3D information".

Each of the five stations of the microearthquake network is equipped with a three-component geophone set fixed in a 6 m deep borehole. Three independent channels are available for the data transmission from any station to the recording center. The three signals from the three-component geophone are digitized, preprocessed and coded in the station encoder. Then they are transmitted by radio to the central recording station of the microearthquake network.

The two "profile stations" of the network were temporarily reconfigured. Only the Z-component of the three-component borehole geophone was used for registration and the two remaining telemetry channels were used for the transmission of the data from two "satellite geophones", i.e. geophones which were situated on the measured profile in a distance of about 2–3 km from the borehole and which were connected to the station encoder by a cable. Then the data from all three geophones (Z-component of the borehole geophone and two satellite geophones) were transmitted to the recording centre. The result of the above described reconfiguration was that three recording points with 2–3 km spacing were available instead of one single point.

By the reconfiguration of two "profile stations" of the microearthquake network 6 reception points were available. These points were supplemented by a standard seismic prospection equipment situated at a suitable location near the middle of the profile. In this case 10–14 geophones with 100 m spacing were used. To enlarge the number of reception points, two pieces of special equipment (one-channel, real-time station with analog registration) were used at every profile.

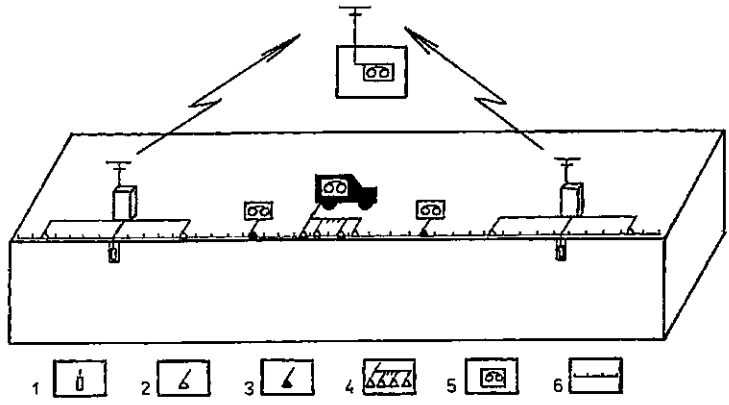

2. Typical profile geometry. 1 – a three-component borehole geophone; 2 – a "satellite" geophone; 3 – the geophone of supporting one-channel equipment;4 – the spread of the prospection seismic equipment; 5 – a registration device; 6 – shot points.

The position of each geophone was surveyed with high precision (few meters). As the position of all geophones mentioned was kept fixed during the period of profile measurements, no additional repositioning errors could enter the subsequent data processing. To ensure good lateral resolution of the velocity model, shot points with relatively small spacing (0.5 to 1 km) were used. Typical profile geometry is outlined in Fig. 2.

The absolute shot time was measured at each shot point with a special equipment and the operation of seismic prospection equipment was started automatically by a radio shot command as it is usual in reflection surveys. The network registration could have been done in trigger mode, but for security sake the tape recorder was forced to register all data well in advance of the planned shot time (15 to 30 s). The recording continued for approximately 1 minute to cover all useful seismic waves. The connection between the shot point and the network central station was maintained by radio. The detailed description of field measurements can be found in Cidlinský et al. 1986. The above described way of refraction measurement (utilizing fixed positions of all receivers on a profile during the survey) enabled us to shorten the measurement period substantially in comparison with standard methodology when a seismic spread is moved along the profile and shots from individual shot points have to be repeated to get the profile wave field. Further advantage of such a methodology was that the off-profile three-component stations of the microearthquake network formed additional measuring points which acquired additional data which could serve for a 3D velocity model study. The more dense grid of shot points used (in comparison with a sparse grid in standard refraction survey) allows to perform an energy attenuation study of the locality (needed e.g. for microearthquake energy estimation) and last but not least it allows to calibrate the network both kinematically and dynamically.

Travel time curves

For each seismic profile, records have been organized according to the common point of reception. Travel time curves (TTCs) have been formed after seismic waves were correlated and their onset times determined. For this purpose mainly the picking mode of an available interactive visualization program was used. The data from microearthquake network stations and seismic prospection equipment were converted to a common computer format to enable correlation and onset picking with the same accuracy. The magnetic records from the supporting one-channel analog stations were visualized, the onset times were picked on the analog records and the corresponding TTCs were formed. It became obvious, that refracted P-waves were the only wave type which could be reliably correlated over large range of epicentral distances. These waves formed the first arrival in each seismic record. Refracted S-wave could be identified at most records but the accuracy of its onset time reading was usually much worse than that of P arrivals and had not therefore been used in the current interpretation. Although essential effort was made, reflected waves were not reliably correlated. It is well known that for layered media the first arrival TTC consists of several branches representing P waves refracted in various layers. As the area under study was supposed to have a complex structure with several layers laterally limited in space, the separation of the first arrival "compound" TTC without good preliminary knowledge of the velocity structure was not possible. This assumption about "compoundness" of the first arrival TTC was verified in the course of the interpretational process and helped to avoid mistakes in wave type identification. So the created "compound" TTC was divided into separate segments corresponding to individual refracted waves only after some first stage of interactive interpretation.

Corrections of travel times

The procedure described above gives the "raw" travel times which depend on a number of factors, namely:

1) global velocity distribution along the profile,
2) local velocity distribution at the shot point,
3) local velocity distribution at the point of reception,
4) error of shot time reading,
5) error of onset time reading, and
6) transmission delay in the recording equipment.

ad 1) The dependence of travel times upon the velocity distribution is the basic relation for the problem at hand. By the inversion of this relation the velocity distribution (strictly spoken only the model of the velocity distribution) can be derived. The other relations (points 2–6) are treated as small disturbances to this one and are to be removed from the data by corrections.

ad 2 & 3) These factors include the local deviations of real velocity distribution from that represented in the model. The decision about which changes in velocity distribution

can be represented in the model and which are to be treated as the local deviations depends on the resolution power of the particular field measurement. In our case the velocity distribution below the weathering zone was included in the model while the influence of this weathering layer was removed by corrections. As the resulting TTCs were organized according to the common point of reception, it is obvious, that the corresponding reception point corrections shifts the TTC as a whole while the shot point corrections will smooth it. The shot point corrections were computed from the known charge depth and from the estimated velocity below the weathering zone. By such a procedure the accuracy better than 10 ms was achieved for the shot point corrections. Receiver point corrections could have been computed from the weathering layer parameters (thickness, velocity). However, as the receiver point correction and the correction for the registration equipment, delay act simultaneously, they were both treated as a single correction (see point 6 below).

ad 4) The error in shot time reading was less than 5 ms and could therefore be neglected.

ad 5) The survey was planned in such a way as to ensure that the first onset on individual traces could be read with accuracy of about 10 ms.To achieve this, test measurements were performed on the site to find an optimum charge weight for proper signal to noise ratio.The accuracy of 10 ms could not be improved substantially due to sampling frequency used by the recording equipment. The microearthquake network equipment operated with the sampling frequency of 125 Hz while the seismic prospection station used the sampling frequency of 250 Hz.

ad 6) As different types of registration equipment were used at various reception points, the resulting TTCs were shifted with respect to each other. Because the exact values of transmission delays of all equipment were difficult to measure, the appropriate corrections have been derived from the data. By a minimization procedure we have found the set of time shifts which gives the best agreement for all the reciprocal times on all TTCs. This procedure also contained the reception point corrections and a very good fit of reciprocal times was achieved. The maximum misfit of times at reciprocal points was in the range of the required accuracy, namely 10 ms.

Travel time curves created by the above described procedures were used as input data for further interpretation by the interactive modelling program package.

Starting velocity model

The starting model creation was the first step of our interpretation procedure. Program package can deal with velocity models consisting of layers separated by piecewise linear interfaces. The maximum number of layers is 10. It implies that max. 11 interfaces can be considered, the first of them being the relief and the last the bottom of the model.

The shape of each interface is defined by its intersections with vertical grid lines. Their number can be up to 20. The first and the last grid lines form left and right boundary of the model. The position of an interface between grid lines is determined by linear interpolation. Interfaces must not intersect but the coincidence of neighbouring inter-

faces is possible in any interval. In such a way rather complex structures can be easily modelled.

The velocity distribution is described differently for the first layer and for the others. It is well known that the first (uppermost) layer is often the most complicated one. This fact is respected by 2-DIM and a relatively complicated velocity distribution can be defined within the first layer. The velocity values are specified in a rectangular grid defined by vertical and horizontal grid lines. The vertical lines coincide with the lines used for the definition of interfaces. The spacings of both horizontal and vertical grid lines are arbitrary. The grid must cover the first layer completely. The first layer is limited by the first and the second interfaces. The velocity along these interfaces could be either interpolated from the values at grid points or given explicitly by the interpreter. In the case when the velocity along the first (or the second) interface are given explicitly, the values at grid points above (or below) the interface are ignored. After the velocity along the interfaces has been specified, the first layer is automatically decomposed into a set of triangles. The velocity at any point inside the first layer is then computed by linear interpolation.

The velocity distribution within the second and further (lower) layers is described in a more simple way. The values of velocity are given at the intersections of vertical grid lines with both interfaces limiting the layer. As each inner interface separates two layers and the velocity values are given for both the upper and the lower interfaces of any layer, two independent values can be specified for the velocity at any point of the interface. If these two velocities are different, the interface represents a first order velocity discontinuity at this point. If these velocities are equal, the interface corresponds to a velocity discontinuity of the second order.

The velocity at a general point inside any layer is computed by the linear interpolation method (Aric - Gutdeutsch - Sailer 1980, Firbas - Skorkovská 1986, 1988).

Within 2-DIM program package the module MODEL handles all the work with models. It maintains the catalogue of existing models, creates new models and updates the old ones. It is designed in a very user-friendly way enabling the interpreter to create a new model quickly and conveniently. For example it is not necessary to insert the velocity values at all grid points within the first layer, the omitted values are automatically filled in by linear interpolation from the specified ones. The velocity distribution along a vertical grid line can be also given by a constant gradient. If the velocity is constant along an interface,it can be entered as a single value. Every entered value can be easily changed either immediately or after finishing some block of input operations.

When preparing starting models we used information about the geological structure of the site and the results of previous geophysical (mainly seismic) measurements in the investigated area (i.e. Cidlinský et al. 1986). Having gained some experience we used two types of interfaces in models, namely the interfaces of the first order and the velocity isolines. Any interface between two geological units was represented as the first order interface in the velocity model. In addition, several interfaces of second order were introduced which did not represent any geological surface. The velocity was kept constant along the second order interfaces, i.e. they represented velocity isolines. This approach enabled us to describe the velocity distribution within a geological layer in a

more detailed way by dividing it into several fictitious layers with different velocity gradient. Isolines corresponding to the same velocity values were used for all profile models. These isolines were later used for the transformation of the set of 2-D velocity models into one composite 3-D model (not described in this paper).

It is specific for our situation that the first layer of the model corresponds to the Neogene sedimentary basin on almost all profiles (see Fig. 1). This basin is relatively shallow and narrow in the directions of the profiles. Having in mind the limited resolution power of the field measurements, we cannot make full use of the more detailed velocity description offered by the program for the first layer. On the E-profile, where this sedimentary basin is not present, the model could be represented as only one (the first) layer and the velocity distribution could have been described by a grid. However, for the reason of comparability, the way of modelling utilizing interfaces and isolines was used for all profiles.

The input of travel time data is also supervised by the module MODEL. Each TTC is characterized by its "shot point position" (which is in fact the point of reception position in our case where the roles of sources and receivers are exchanged).

Each point on the time-distance curve is specified by its x-coordinate and the corresponding travel time. When entering individual points of a TTC the interpreter may add the shot point position with zero travel time for the reason of the graphic output.

Ray computation

Module RAY is the main part of the whole program package 2-DIM. It performs the 2-D initial-value ray tracing in the specified model and allows the interpreter to compare the computed travel times with the field data and to update the model so as to improve the fit of the computed and the experimental travel times. Since much attention is paid to the description of RAY in Firbas - Skorkovská (1986),only some notes useful from the point of view of an interpreter will be presented here.

The picture of ray diagram and TTCs can be plotted on the graphic monitor or on the four-colour plotter. The latter possibility proved to be the more convenient one and was therefore preferred throughout the interpretation procedure. To improve the resolution of the TTC pictures the reduction velocity 6 km/s or 8 km/s was frequently used.

There are two parameters entered for each ray to be computed, i.e. the shot point position and the initial angle. The program checks whether the input coordinates of the shot point fall within the limits of the model. When the z-coordinate of the source above the first interface is entered, the program automatically places the shot point on this interface. This very useful feature enables the interpreter to specify the shot point on the Earth's surface without exact knowledge of its z-coordinate.

When the shot point position and the initial angle for a ray have been determined,computation starts. The path of the ray within the model can be followed on the plotter directly in the course of the ray computation. The true raypath within one triangle, which is a part of a circle, is replaced by a straight line for plotting purposes only. This simplification speeds up the plotting of rays but sometimes (mainly when the ray touches

an interface with strong velocity contrast) the interpreter may lose some useful information, namely how close the ray has approached the critical angle for this interface.

The behaviour of the computed ray at the interfaces can be either specified beforehand by a code or the ray can be controlled interactively, i.e. at every interface the interpreter decides whether the ray should continue across the interface as a refracted one or whether it should reflect. When only the refracted rays are of interest, this can be specified beforehand and the program does not stop at interfaces. The interpreter can also break the computation of any ray, whenever he decides that it is not the one he wants. If a ray cannot fulfill the requirements of the code (i.e. if it cannot reach the surface) the program informs about the reason of this failure, which is often the impact of the ray at the bottom or at the left or right boundary of the model. The use of the ray code is described in detail in Firbas - Skorkovská (1986, 1988). When a ray has successfully terminated, i.e. when it has reached the surface, the computed travel time is plotted (against the x-coordinate of the endpoint) into the prepared TTC plot.

It is the interpreter's responsibility to select the initial angles of rays in such a way that their end points would cover all the range of the experimental TTC. It is well known that several rays with quite different initial angles can exist which end at the same point on the surface. These rays can correspond to various branches of refracted waves or they can also represent the waves reflected at the interfaces inside the model. When the travel times of those rays differ substantially, there is no problem to choose the ray which corresponds to the wave branch whose travel times have been recorded in the field. When the travel times of several rays with the same endpoint are close to each other, the ray with minimum travel time should be selected for further interpretation because very often it is the one the onset time of which has been picked on the field records.

Sometimes finding the initial angle for which the corresponding ray ends within a desired range of epicentral distances might be rather difficult. It is well known that the epicentral distance is a very sensitive function of initial angle in the situation when the corresponding rays strike some interface with strong velocity contrast under the angle slightly less than critical. Although we often know that the initial angle resulting in the demanded epicentral distance exists and, moreover, we also know the interval within which the angle falls, still a rather time consuming procedure is required to find it. We therefore expect to supplement the program with a simple routine able to find the ray which ends in the point specified. In such a way only the successful rays would be plotted. This improvement would speed up the useful ray finding procedure and relieve the interpreter of some portion of routine work. As an automatic two-point ray tracing in 2-D structures is a complicated procedure, the simple routine which we expect to implement should handle only those specific cases when the interpreter is sure about the existence and about the initial angle limits of the desired ray.

Model updating

Having obtained a set of computed travel times the interpreter can proceed to the most important and the most difficult part of the interpretation procedure. He has to compare

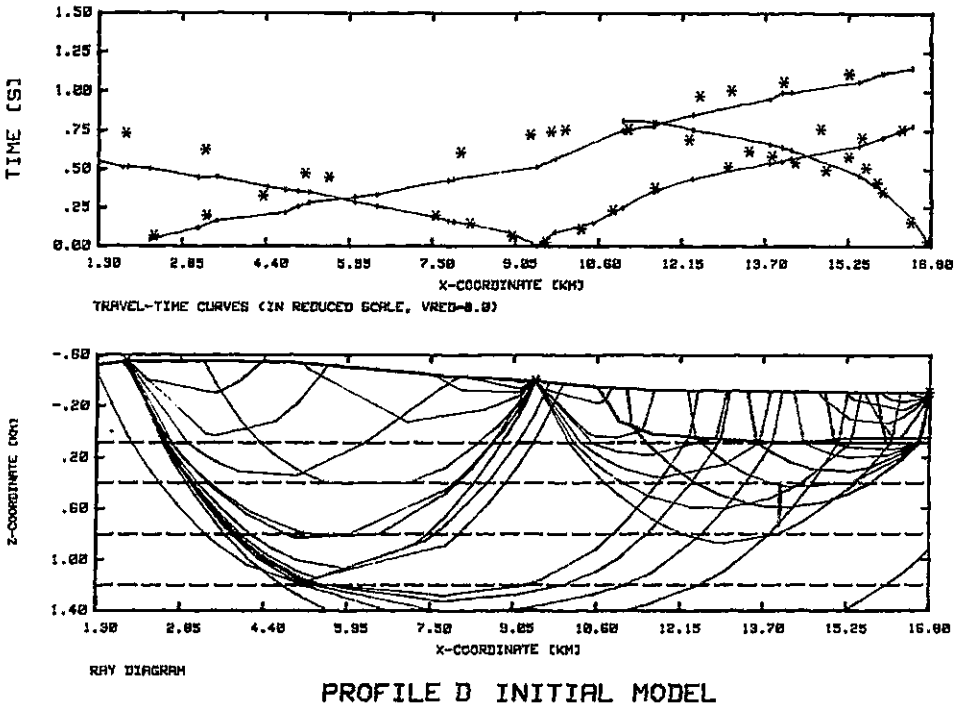

3. Computational procedure. Ray diagram, experimental TTCs (I) and computed travel times (*) for the initial velocity model at the profile D. First order interfaces ——, isolines —·.

the computed travel times with the experimental TTCs, to consider the misfits and subsequently to try to improve the velocity model.

An experimental travel time curve is given as a set of discrete points in the (x, t) plane. Since it is very difficult to find the ray terminating exactly at the point where the experimental travel time is available, an interpretation method for the experimental TTCs is needed. The most simple of such methods, i.e. the linear interpolation, is performed by the plotting routine, so that the resulting experimental travel time plot is piecewise linear. This approximation is quite sufficient in most cases, so that the lines connecting the data points can be considered the part of the TTC and the computed travel times can be fitted to them. Some caution is needed when the data points are sparse or the relief between the endpoints varies strongly.

Nevertheless, there are parts of the TTCs where the linear interpolation of travel times fails completely. As mentioned above, experimental TTC may not represent a single seismic wave, but at each receiver position the wave with the shortest travel time is

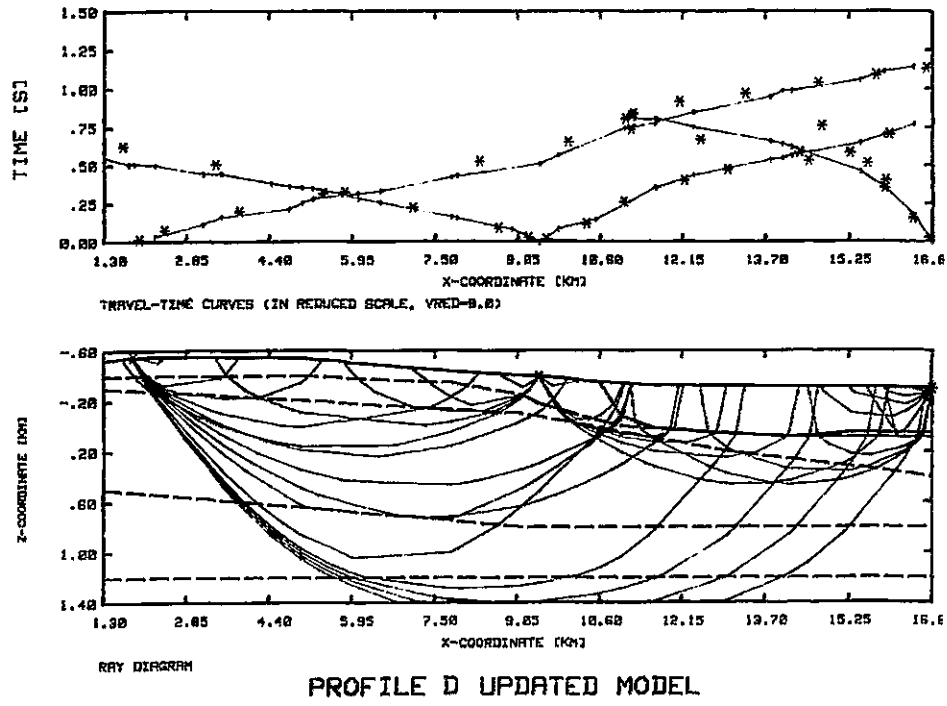

4. Computational procedure. Ray diagram, experimental TTCs (I) and computed travel times (*) for the updated velocity model at the profile D (after first iteration). First order interfaces —, isolines - -.

represented. Thus there is a possibility that the two subsequent TTC points correspond to different waves (or TTC branches) and the straight line interpolated between them must not be taken as a part of the TTC. Such connecting line has no physical meaning and the computed travel-times must not be fitted to it. The difficulties described above can be expected wherever the slope of an experimental TTC changes substantially. The interpreter should reveal such cases and be extremely careful when fitting the computed travel-times at those epicentral distances.

By making some changes in the velocity model the interpreter can improve the fit of the computed and the experimental travel times. After obtaining some experience this procedure is fairly straightforward and fast.

In this case the best way to obtain the velocity model consistent with the field data was (in consent with Firbas - Skorkovská 1986, 1988) to fit the travel times in smaller epicentral distances first. By this method the shallow parts of the velocity model were modified first and they usually need not be corrected in latter stages of the model

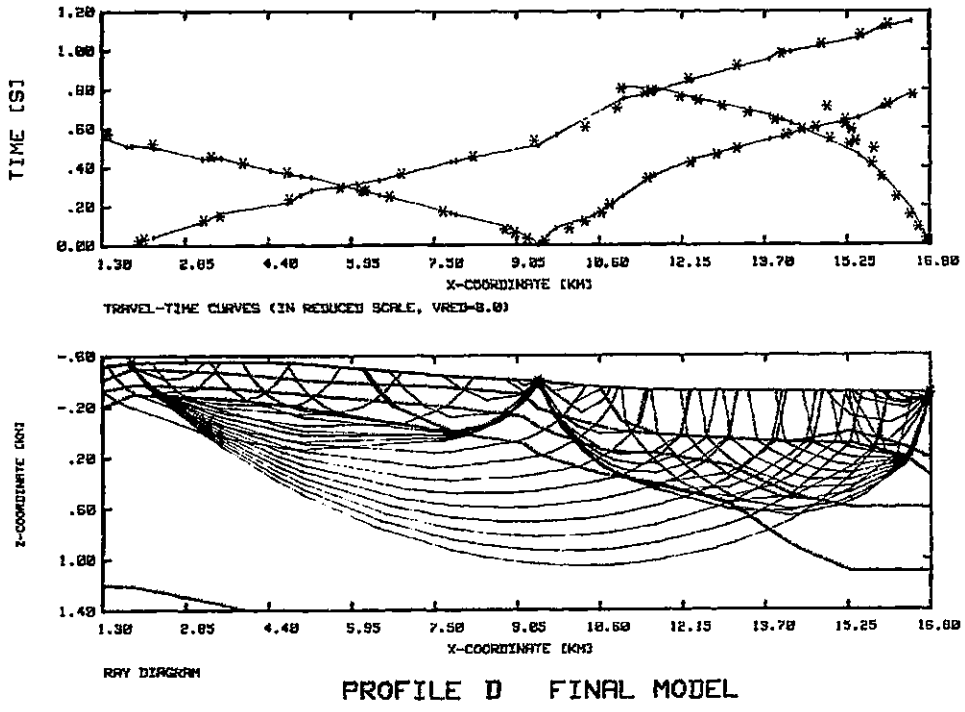

5. Computational procedure. Ray diagram, experimental TTCs (I) and computed travel times (*) for the final velocity model at the profile D (after 9 iterations). First order interfaces —, isolines - -.

improvement procedure. The iteration procedure was stopped when the fit better than 20 ms was achieved for most experimental TTC points. In most cases we were able to get a satisfactory fit in less than ten iterations.

In Figs. 3–5 the development of the velocity model at the D-profile is illustrated. Fig. 3 shows the initial model. In Fig. 4 the updated model after the first iteration and in Fig. 5 the final velocity model after the 9th iteration is presented. Only three travel time curves are plotted in each picture, nevertheless all experimental TTCs were respected in the procedure of improving the model. The experimental travel times are marked by vertical bars while the computed times by asterisks. As can be clearly seen, the fit of travel times is much better after the first iteration (Fig. 4) than for the initial model (Fig. 3). For the final velocity model very good fit was obtained (Fig. 5).

To demonstrate the complexity of the models obtained we present the final models for the profiles E, F and H at Figs. 6 to 8, where the interfaces of the first order and the

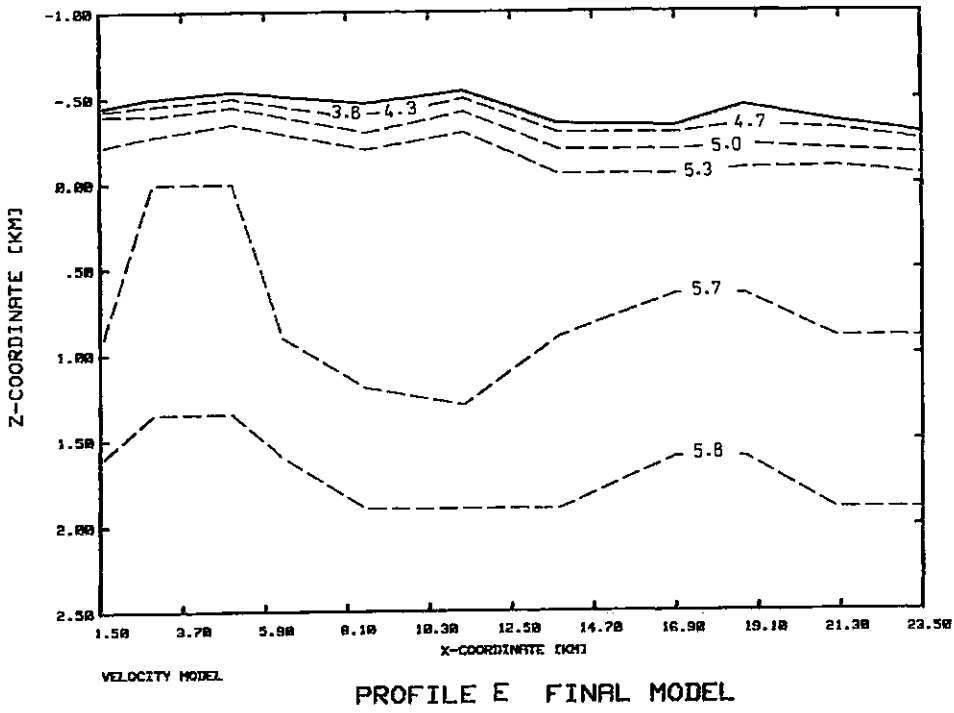

6. Example of the resulting 2D velocity model for profile E.

interfaces of the second order (velocity isolines) are plotted by the solid and the dashed line respectively.

Conclusions

The method described in Firbas - Skorkovská (1986, 1988) was used to derive 2-D laterally inhomogeneous velocity models based on the seismic field measurement performed on the building site of the nuclear power plant of North Moravia. The interactive program system 2-DIM developed by the authors of the above mentioned papers was used here for the first time with field data.

During the process of computation some important features of the program system became obvious:

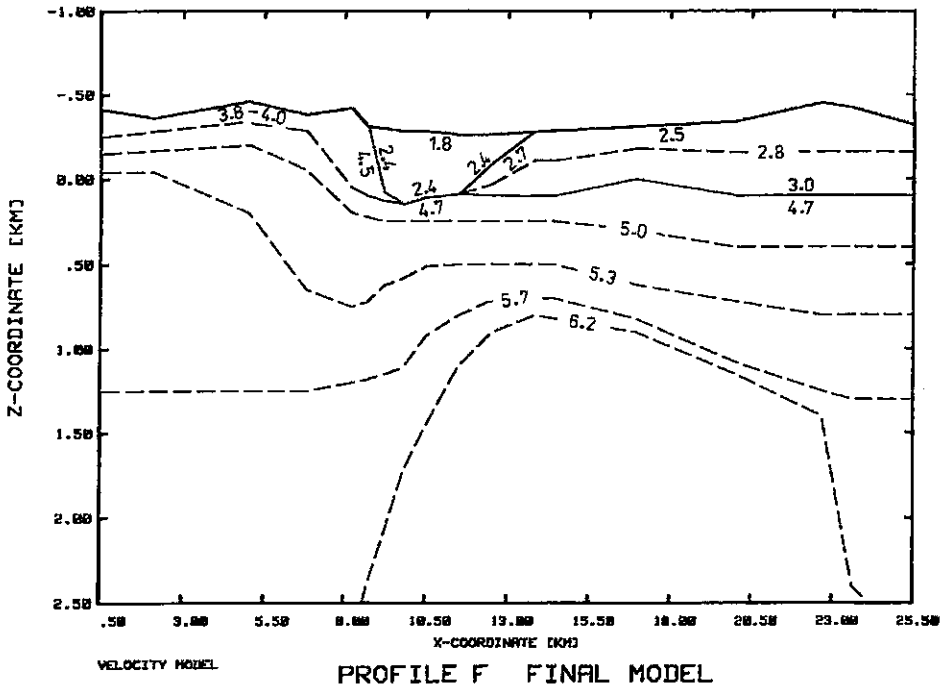

7. Example of the resulting 2D velocity model for profile F.

a) rather complicated laterally inhomogeneous velocity structures can be approximated with a satisfactory degree of accuracy and the corresponding velocity models can be constructed easily,

b) input field data (travel times) can be entered rather conveniently,

c) the calculation of rays is fast enough, and

d) the composed plots (ray diagrams combined with both experimental and computed travel times) supply the interpreter with all the information necessary for fast and successful model updating, so the acceptable fit of travel times can be obtained in a relatively low number of iterations.

K tisku doporučil I. Pšenčík
Přeložil V. Dvořák

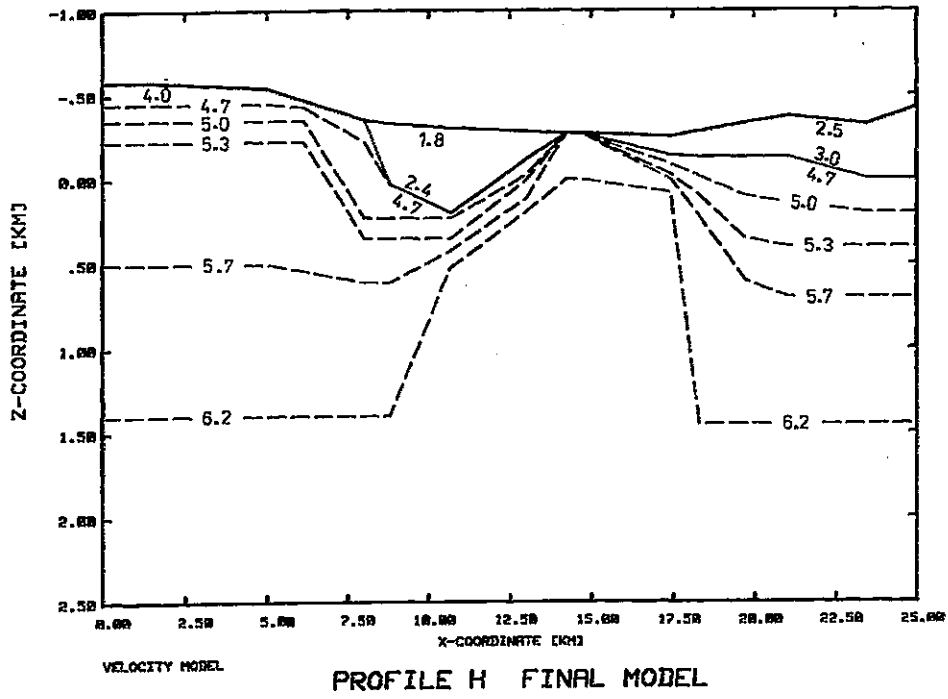

8. Example of the resulting 2D velocity model for profile H.

References

Aki, K. - Lee, W.H.K. (1976): Determination of three-dimensional velocity anomalies under a seismic array using first P arrival times from local earthquakes. Part I. A homogeneous initial model. – J. geophys. Res., 81, 4381–4399. Washington.

Aki, K. - Richards, P. (1980): Quantitative seismology, theory and methods. – Freeman. San Francisco.

Aric, K. - Gutdeutsch, R. - Sailer, S. (1980): Computation of travel times and rays in a medium of two-dimensional velocity structure. – Pure appl. Geophys., 118, Birkhäuser Verlag. Basel.

Cidlinský, K. et al. (1984): Závěrečná zpráva dílčího úkolu reflexně-seismického průzkumu lokality JE Blahutovice. – MS Geofyzika. Brno.

Cidlinský, K. et al. (1986): Geofizičeskaja razvedka punkta strojitelstva atomnoj elektrostancii Severnaja Moravija. Zaključitelnyj otčet po detalnomu sejsmičeskomu rajonirovaniju. – MS Geofyzika. Brno.

Crosson, R.S. (1976a): Crustal structure modelling of earthquake data. Part 1. Simultaneous least squares estimation of hypocenter and velocity parameters. – J. geophys. Res., 91, 3036–3046.Washington.

Crosson, R.S. (1976b): Crustal structure modelling of earthquake data. Part 2. Velocity structures of the Puget Sound region, Washington. – J. geophys. Res., vol. 81, 3047–3053. Washington.

Červený, V. - Pšenčík, I. (1981): 2 D seismic ray package. Research report.– MS Institute of Geophysics. Charles University. Praha.

Dvořák, V. - Kochová, H. - Kolejka, V. - Pavelka, L. (1986): Zaključitelnyj otčet po častičnomu zadaniju "Detalnaja sejsmorazvedka MOV v modifikacii OGT". – MS Geofyzika. Brno.

Filková, V. (1984): Blahutovice JE. Seismokarotážní měření na hlubinném vrtu Blahutovice-1. – MS Geofyzika. Brno.

Firbas, P. - Skorkovská, M. (1986): Velocity distribution modelling in laterally heterogeneous media (program for a desk-top computer). – Sbor. geol. Věd, užitá Geofyz., 20, 139–153. Praha.

Firbas, P. - Skorkovská, M. (1988): Interactive program for kinematic problems in laterally heterogeneous media. – Sbor. geol. Věd, užitá Geofyz., 24, 51–69. Praha.

Lee, W.H.K. - Stewart, S.W. (1981): Principles and applications of microearthquake networks. In B. Salzman (ed.): Advances in geophysics. Supplement 2.– Academic Press. New York.

Synek, V. - Jančovič, L. (1981): JE Blahutovice, inženýrskogeologický průzkum. – MS Geofyzika. Brno.

Šafránek, V. (1980): Zpráva o seismickém měření na projektovaném staveništi JE Blahutovice. – MS Geofyzika.Brno.

Modelování rychlostního rozložení na lokalitě jaderné elektrárny Severní Morava

(Resumé anglického textu)

Vladimír Dvořák - Petr Firbas - Zuzana Skácelová

Předloženo 1. července 1988

V současné době stále narůstá pozornost věnovaná sledování seizmicity lokalit velkých staveb, zejména jaderných elektráren. Pomocí citlivých seizmologických měření je statisticky sledováno časoprostorové rozložení ohnisek místních zemětřesení a na základě těchto dat je vyhodnocováno případné seizmické ohrožení lokality.

Pro přesné a spolehlivé určení ohniska zaregistrovaného seizmického jevu je nezbytná dobrá znalost rychlostního modelu dané lokality. Při sestavování se vychází ze znalostí o geologické stavbě území a z výsledků předcházejících geofyzikálních (především seizmických) měření. Při nedostatku těchto dat je nutno pro sestavení spolehlivého třírozměrného rychlostního modelu provést a vyhodnotit speciální měření.

Na lokalitě jaderné elektrárny Severní Morava bylo proměřeno celkem osm refrakčních profilů. Protože geologická stavba zájmového území je dosti složitá, bylo nutno očekávat, že výsledné rychlostní modely budou silně laterálně nehomogenní. Obrácená kinematická úloha seizmiky v dvourozměrném laterálně nehomogenním prostředí je složitý problém, k jehož řešení je vypracováno množství metod. Zvolili jsme řešení pomocí počítačového modelování s využitím programového systému 2-DIM (2D-Interactive Modelling), vytvořeného v s.p. Geofyzika Brno. Pro sestavení 2D-rychlostního modelu pro zpracovávaný profil se používá tzv. metoda „trial and error", kde je pro zvolený počáteční model řešena přímá kinematická seizmická úloha, tj. jsou spočteny teoretické hodochrony, které jsou porovnány s hodochronami naměřenými. Na základě tohoto srovnání je změněn model a jsou pro něj spočteny nové teoretické hodochrony. Tímto postupem lze již po několika iteracích dojít k dobré shodě teoretických a naměřených hodochron.

V článku je podán podrobný popis programového systému 2-DIM z hlediska uživatele, protože jde o jeho první použití na reálná data. Postup výpočtu je sledován krok za krokem včetně přípravy dat. Pozornost je věnována některým nedostatkům, které se v systému vyskytují. Aby byly demonstrovány možnosti programového systému a použitého algoritmu, jsou předkládány výsledné 2D-rychlostní modely pro tři vybrané profily.

Vysvětlivky k obrázkům

1. Geologická mapa oblasti se situací seizmických profilů a stanic sítě detailního seizmického rajónování (DSR).
   1 – neogén (baden); 2 – neogén (karpat); 3 – paleogén (flyš); 4 – kulm; 5 – devon; 6 – třísložková stanice sítě DSR.

2. Typické uspořádání profilu.
   1 – třísložkový geofon ve vrtu; 2 – „satelitní" geofon; 3 – geofon podpůrné jednokanálové aparatury; 4 – roztažení prospekční seizmické aparatury; 5 – registrační zařízení; 6 – body odpalu.
3. Postup výpočtu. Paprskový diagram, naměřené hodochrony (I) a vypočtené časy šíření (*) pro startovací rychlostní model na profilu D. Rozhraní prvního řádu ——, izolinie - - - -.
4. Postup výpočtu. Paprskový diagram, naměřené hodochrony (I) a vypočtené časy šíření (*) pro zlepšený rychlostní model na profilu D (po první iteraci). Rozhraní prvního řádu ——, izolinie - - - -.
5. Postup výpočtu. Paprskový diagram, naměřené hodochrony (I) a vypočtené časy šíření (*) pro konečný rychlostní model na profilu D (po 9 iteracích). Rozhraní prvního řádu ——, izolinie - - - -.
6. Příklad výsledného 2D-rychlostního modelu pro profil E.
7. Příklad výsledného 2D-rychlostního modelu pro profil F.
8. Příklad výsledného 2D-rychlostního modelu pro profil H.

Sborník geologických věd	Užitá geofyzika 25	Pages 67 – 81	8 figs.	– tab.	– pl.	Praha 1992 ISBN 80-7075-110-X ISSN 0036-5319

Geodynamic analysis of the Nízke Tatry Mountains based on geophysical and remote sensed data

Geodynamická analýza Nízkych Tatier na základe DPZ a geofyziky

Soňa Halmešová[1] - Rudolf Holzer[2] - Darina Marušiaková[1] - Lubomil Pospíšil[3]

Received December 20, 1989

Remote sensed data
Geophysical data
Interpretation

Halmešová, S. - Holzer, R. - Marušiaková, D. - Pospíšil, L. (1992): Geodynamic analysis of the Nízke Tatry Mountains based on geophysical and remote sensed data. – Sbor. geol. Věd, užitá Geofyz., 25, 67-81. Praha.

Abstract: Satellite images revealed an extensive deformation on the southern slopes of the Nízke Tatry Mts. range. This deformation can be ascribed to a group of gravity nappes. Geological survey, however, neither confirmed nor negated its existence. Therefore, a detailed analysis of aerial images was carried out on the scale of 1:35,000. Analytical interpretation led to the construction of a special morphotectonic and geodynamic scheme of the area, supported by the various geophysical data.

[1]*Geofyzika, a.s., Bratislava, Geologická 18, 825 52 Bratislava*
[2]*Katedra inžinierskej geológie prírodovedeckej fakulty Univerzity Komenského, Mlynská dolina, 842 15 Bratislava*
[3]*Geofyzika, a.s., Brno, Ječná 29a, 612 46 Brno*

Introduction

The complex analysis showed that during the Tertiary the southwestern part of the Nízke Tatry Mts. presumably had the character of a horst whose relative fast uplifts had been caused by active deformations within the fundament (Fig. 1). Complicated faults or fracture systems of great diversity were found, many of them of the strike-slip character. Also expressive dissection of the relief, the chaotic arrangement of levelled surfaces and numerous geodynamic features outline the intricate geological environment and complicated Late Alpine development of the whole structure.

Methodology

In the interpretation of images we proceeded in the following methodological steps:
– evaluation of the tectonics of the area, with regard to orders of faults, fault zones, fracture zones, etc. and to the analysis of the drainage system,
– analysis of the morphological features, reflecting the peculiarities of the geotectonical development of the area (the relief forms, levelled surfaces, etc.),
– distinction of geodynamic processes and other geodynamic phenomena,
– re-evaluation of the previous and recent findings concerning the geological-tectonic development,
– evaluation of the latest geophysical and structural-geological data, correlation of data yielded by the individual research methods applied, and
– compilation of data, construction of maps and cross-sections.

The purpose of the chosen methodological process was to realize a complex analysis of the geological environment with emphasis on its properties and behaviour. Results of analytical processing of stereoscopic models, regional geological and geophysical surveys and other studies were synthetized into an organic set of information on the study area.

Analysis of morphological features

Geomorphological research in the area (Škvarček 1973, Škvarček pers. com., Košťálik 1971) showed the heterogenous nature of the relief leading to expressive difference in elevations of levelled surfaces in midmontaneous and river systems. The morphological analysis realized on the stereoscopical model confirmed this relief destruction into various individualized blocks and strips, their heights extraordinarily differentiated. As

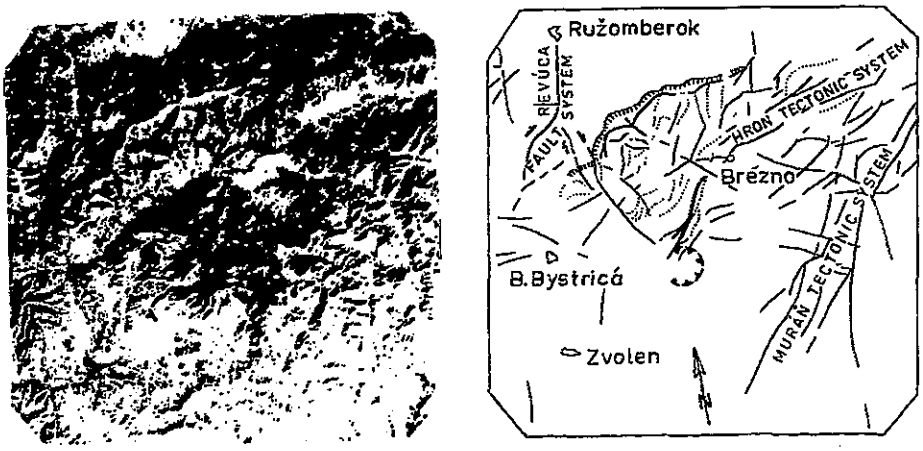

1. Area of the southern slopes of the Nízke Tatry Mts. (part of the LANDSAT image and its interpretation).

it is indicated by contemporary investigations these are results of various, not yet strictly distinguished movements and of the selective exogenetic destruction of rocks. Neither the extensive gravity movement on the southern slopes of the Nízke Tatry Mts. can be excluded. This assumption is supported by the height differentiation of the midmontaneous levelled surfaces (in absolute values from 850 to 1,400 m a.s.l.) and of the river terrace system (100 to 300 m relatively above the Hron River valley). Due to the extreme morphological conditions it was possible only to range following groups of levelled surfaces:

1. less than 700 m a.s.l.,
2. 700 to 1,000 m a.s.l.,
3. 1,000 to 1,300 m a.s.l., and
4. more than 1,300 m a.s.l.

Analysis of fault and fracture systems of the rock mass

Three basic stages of the Alpine cycle are decisiv in the tectonic development of the Nízke Tatry Mts. (Andrusov 1958, Maheľ 1986).

1. Upper Permian to Middle Cretaceous (Paleo Alpine), closed by the folding of the central West Carpathians and by thrusting of the Mesozoic nappes in the Upper Cretaceous.
2. Lower Cretaceous to Miocene (Meso Alpine) closed by folding of the outer Flysch Belt and thrusting of flysch nappes in the Lower Miocene.
3. Lower Miocene (Badenian) to Quaternary (Late Alpine) – neotectonic, with volcanic activity, horizontal and vertical movements leading to the contemporary mosaic configuration of the West Carpathians to ridges and depressions. The movements have been taking place up to the present time and have manifested themselves by seismic activity (Pospíšil et al. 1985, Schenk et al. 1979).

The late Alpine movements resulted in the general uplift of the West Carpathians with expressive differentiation of movements of individual blocks along transcurrent faults, mainly of the NE-SW direction. This movement in the principal direction of horizontal stresses from the south resulted in the motion of the eastern part of the West Carpathians to the north and northeast.

Two areas with different uplifting-subsiding tendencies were distinguished in the study region:

1. The subsiding Hron River valley from the ENE to WSW following the post-Paleogene megasynclinal depression and the adjoining depressions. The Mesozoic folds have the character of subhorizontal thrusts making sharp angles with post-Paleogene faults causing the subsidence of the Hron River valley.

2. The elevation area of the Nízke Tatry and Veľká Fatra Mts. and the northern part of the Vepor Mts. with an uplifting tendency where the key role in forming the fracture tectonics was played by recent differential movements at the Late Alpine evolution stage.

It was impossible to find out on the satellite images which linear elements belong to older evolution stages and which to the Late Alpine development stage. According to

the development and diversity of the geomorphological features it can be assumed that the majority of fault and structural-tectonic features are from the latest evolution stage or are results of several stages. For instance, the linear Hron River valley is presumably based on one ancient fault in partial segments documented by linear, steep and sporadically facetted slopes. The facets in valleys were taken as a criterion for interpretation of faults (e.g. numerous facets along the northern part of the Korytnice River valley indicating the Revúca fault line).

The fault and fracture zones are best characterized by the configuration of the drainage system. It can be assumed that the river follows the lines or zones of tectonic or lithological "weakening". In this way the principal directions of prevailingly linear tectonic zones, dislocations and shorter fault-fracture elements were distinguished (Fig. 2):

1. NE-SW, ENE-WSW systems (western branch of the Revúca fault zone, the Hron River valley and the system of lines in the east of the area). In this direction runs the Hron lineament (Pospíšil et al. 1986) interpreted as a transcurrent fault with a large dextral strike-slip.

2. NW-SE, NNW-SSE (the eastern branch of the Revúca fault zone and transverse faults between Lučatín and Brusno, in the East the Rohozná and Čierny Hron River fault).

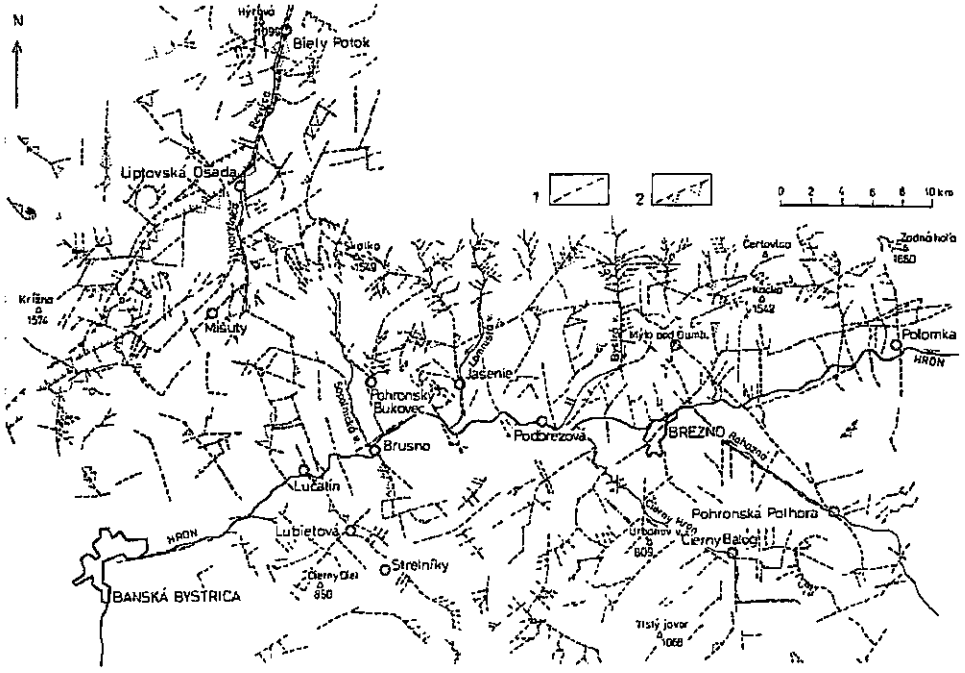

2. Tectonic analysis of the southern slopes of the Nízké Tatry Mts. from aerial images. 1 – fault fractures, 2 – faceted slopes.

3. N-S faults forming important valleys in this direction on southern slopes of the Nízke Tatry Mts. as well as the northern part of Revúca fault system.

All the tectono-structural features are indicated by the forms of valleys, abrupt changes of drainage system, spring lines, erosional features, morphological structures, etc.

Analysis of geodynamic processes

Important secondary factors, demonstrating the dynamics of the geological environment, and of all exogenetic processes, are geodynamic phenomens.

The following factors were in the focus of the interest:

1. slope deformations (creep, slide and fall gravity deformations, taluses, block disintegration and block fields),
2. erosion elements (gully and sheet erosion, erosion edges),
3. surface karst phenomena (sinkholes, areal and linear surface karst elements),
4. forming of proluvia (young alluvial cones), and
5. weathering.

Slope deformations. The relatively new results of tectonics, engineering-geological and geophysical investigations show that numerous structures at the Earth's surface so far related to the dynamics and mechanism of tectonic (plicative and disjunctive) movements are actually connected with gravitational tectonics. In the Veľká Fatra Mts. such deformations are represented on top ridges in the vicinity of elevation points Zvolen Mt. (1,402 m a.s.l.), Chabenec Mt. (1,955 m a.s.l.), Krížna Mt. (1,574 m a.s.l.), etc. (Nemčok 1982).

Along the mountain ridges they form a linear succession and may represent a boundary of the active root area of an extensive gravity deformation.

The slides could be well identified on the Veľká Fatra Mts. slopes (Turecká valley), on the Nízke Tatry Mts. slopes (S of the village Dolná Lehota, Prašivá Mts., Kozí chrbát Mt, etc.), but namely on the slopes of intramontanous basins, e.g. near Lubietová village (Fig. 3). Their direct connection with the significant tectonic Revúca zone cannot be excluded.

Erosion phenomena. Two types of erosion can by encountered in the area of interest: gully erosion and sheet erosion. Due to a large uplift of the mountain, an intensive drowncutting of water flows took place and created a variable erosion relief with various types of the water system. At the present time the size of the erosion downcutting and its extension depend on the gradual disintegration of the rocks and on climatic changes.

In places of tectonic or lithological weakening mainly on the steep slopes a considerable progress of back erosion can be observed (Fig. 3). Scours, deep ravines and gorges, and also flat closures of mountain valleys in the top parts of the ridges are formed. In the greater part of the area, back erosion has modelled the top parts into sharply-cut shapes and thus disintegrated ancient structural planes.

Karst phenomena. Karstification is scarce in the area of interest due to the relatively rare occurrence of soluble karst carbonate rocks. Its surface elements can be encountered only in the south-western part near the village Poníky and Nemecká where the sinkholes

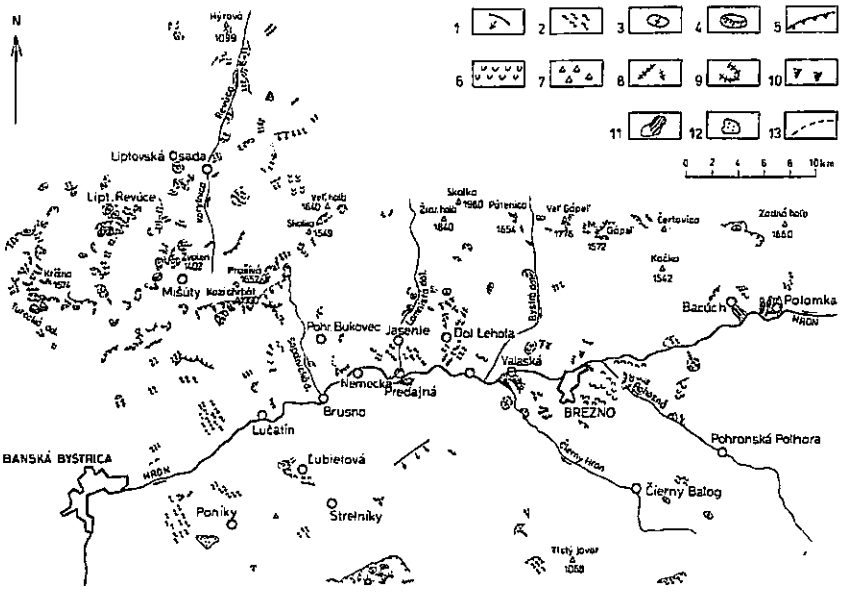

3. Analysis of geodynamical phenomena. 1 – slope deformations generally, 2 – talus creep, 3 – block rifts, block fields, 4 – individual blocks, 5 – scarps, 6 – landslides, 7 – alluvial fan, 8 – gully erosion, 9 – erosion edge, 10 – sheet erosion, 11 – proluvial cones, 12 – sinkholes, 13 – karst valleys (after Varga - Lada 1988).

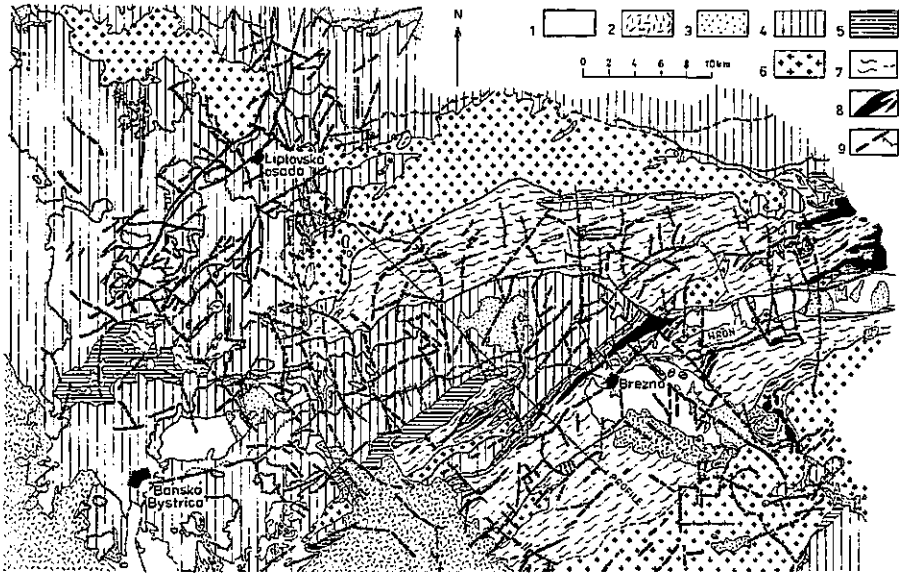

4. Geological scheme of main fault and fracture systems. 1 – neogene, 2 – neovolcanic products, 3 – Paleogene, 4 – Mesozoic complexes, 5 – Paleozoic and crystalline complexes, 6 – granitoids, 7 – metamorphites, 8 – amphibolites, 9 – known and interpreted faults.

form small groups of greater or smaller depressions. Linear arrangement indicating occurrences and systems of tectonic lines cannot be observed (Fig. 3).

Other phenomena. Among the best identified phenomena belong proluvial cones. On images they are clearly visible by the tributaries of the Hron River.

The most intensive products of weathering in the diversified relief remodelled by erosion and denudation activity were transported away.

Correlation of remote sensing, regional geological and geophysical data

The position of fault zones, fault lines and other structural features manifested by means of remote sensing, corresponds to regional geological and geophysical data in the study area is in a good agreement. First of all, the stereoscopic interpretation of various images produces much more continuous picture (and complex results) than geological or other maps on different scales. Evidently, the interpretation criteria allow an identification of faults also in the places where they have not been the corfirmed by field mapping. All the identified faults are mostly wide zones of the highest inhomogenity rate in terms of secondary lithological changes, fragmentation or blockiness. They are all very expressive in the morphology. In this connection of greatest significance is the confirmation of extraordinarily manifested tectonic zone, corresponding partly to the Revúca fault system. First of all the interpreted branching into the two separate systems (Fig. 4) was of significance. One of them, N-S or NNE-SSW system, progresses along the Revúca River valley and indicates the continuation of important regional tectonic

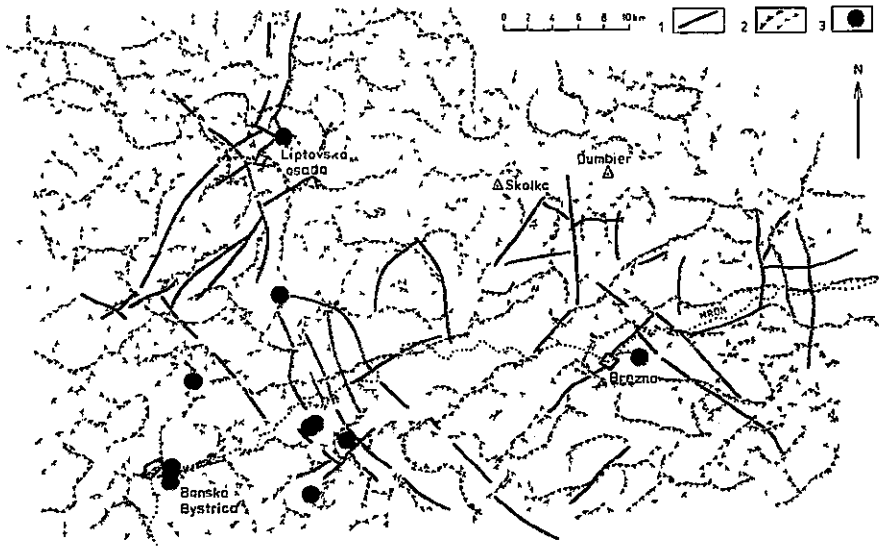

5. Map of vertical density boundaries and earthquake foci. 1 – interpreted fault, 2 – vertical density boundary, 3 – earthquake focus.

boundary – so called Považansko-Ihráčsky fault system. The second branch in the direction NNW-SSW could mark the indication of the west border of the Nízke Tatry Mts. gravity deformation. The analysis of satellite, aerial and radar images confirmed a great relief diversity, frequent changes in its morphological forms, development of gravity elements on slopes, etc. within the entire Revúca system.

The map of vertical density boundary (Fig. 5) was based on the gravity data which demonstrate the diversity and frequent tectonic delimination of structural blocks. the interpreted tectonic lines often coincide with density boundaries or with places of discrupted correlation. The loss of correlation can be observed along the entire lenght of the Revúca fault zone, Hron lineament etc. Geophysical data focussed our interest to the disruption of the NW-SE branch of the Revúca system. This not exactly limited wide zone is deformed there and along about 5 km it is bending to the WNW-ESE direction. It may be the crossing point of several tectonic faults with variable orientations.

The tectonic predisposition of the Hron River between Banská Bystrica and Brezno where two distinct NW-SE and NE-SW striking faults have been interpreted, can be supported by an intensive gravity gradient. Many of interpreted structural and tectonical boundaries, e.g. Mýto-Tisovec fault zone, Čertovica line have been confirmed by geoelectric, magnetometric and gravity data.

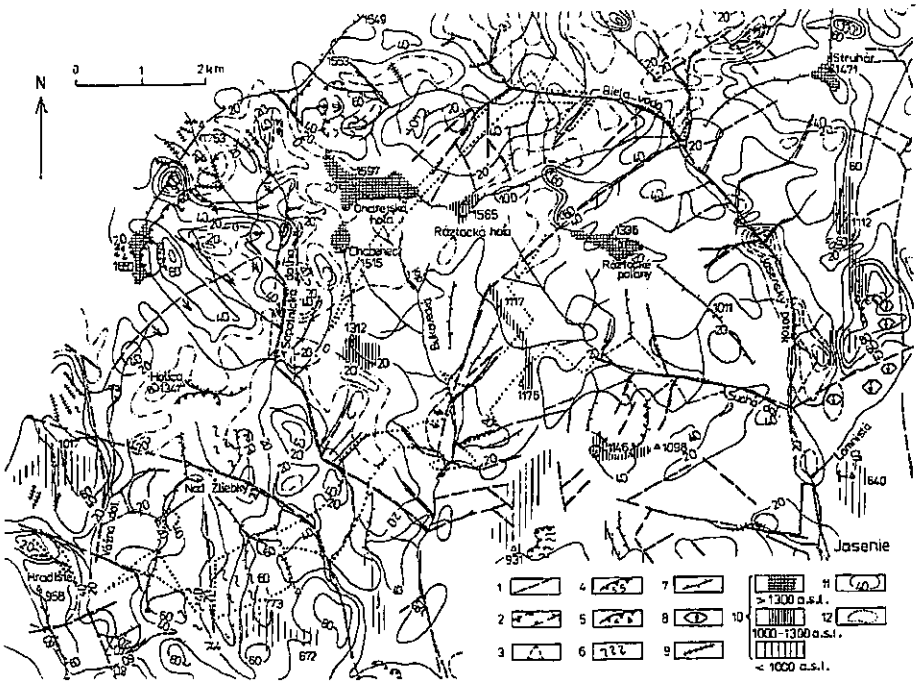

6. Relationship between the zone of the induced polarization anomalies and interpreted faults. 1 – faults and fractures, 2 – zones of interpreted faults, 3 – faces, 4 – creep deformations, 5 – alluvial fan, 6 – slope deformation generally, 7 – horsts, 8 – block rifts, block fields, 9 – erosion edges, 10 – midmountaneous leveled surfaces (850–1,400 m a.s.l.), 11 – magnetic anomaly (+40 nt), 12 – induced polarization anomaly.

The broader surroundings of the south slopes in the middle-west part of the mountain has been the focus of investigations for ore prospecting. Geophysical measurements and aerial photographs yielded a detail picture of the tectonics of the area. Mapping of the so called "productive zone" showed equal values of resistivity and polarizability to those of the immediate surroundings of the existing deposit (Vybíral et al. 1986). The zone of the anomalous induced polarization values strikes from the NE to SW and it is evidently bounded by fault zones (Fig. 6). Tectonic lines interpreted on the images disturb this zone in form of shifts and disruptions so that it proves the particular interest from the viewpoint of tectonics, geological structure and mineralization in this area.

Obtained geophysical data from various methodological stages cannot be fully illustrated in the geological cross-sections, but only in a schematic section (Fig. 7). It is because of an unclarity in the geological interpretation of the Nízke Tatry Mts. structure itself. Moreover, new seismic and magnetoteluric data on transcarpathian profile 21 (Tomek et al. 1989; Varga - Lada 1988) provide a picture completely different from the one so far assumed. In that way the new proofs and criteria for verification of the so called "gravity nàppe" and the Hron lineament (Klinec et al. 1985, Pospíšil et al. 1986) do not exclude the influence of Late Alpine tectonics.

In geomagnetic data, the most expressive anomaly is the Mýto-Tisovec fault zone accompanied with Tertiary volcanites and the Revúca fault zone which probably served as the cahnnel way for volcanic products.

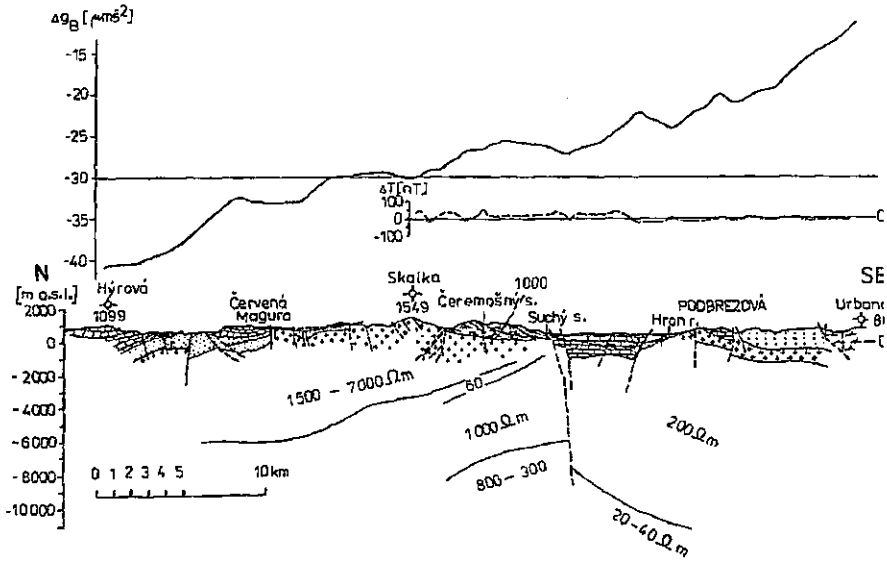

7. Geological cross section over the Nízke Tatry Mts. with results of geophysical investigations. Δg_B – gravity curve, ΔT – magnetic anomalies curve, resistivity values interpreted from the magnetotelluric curves.

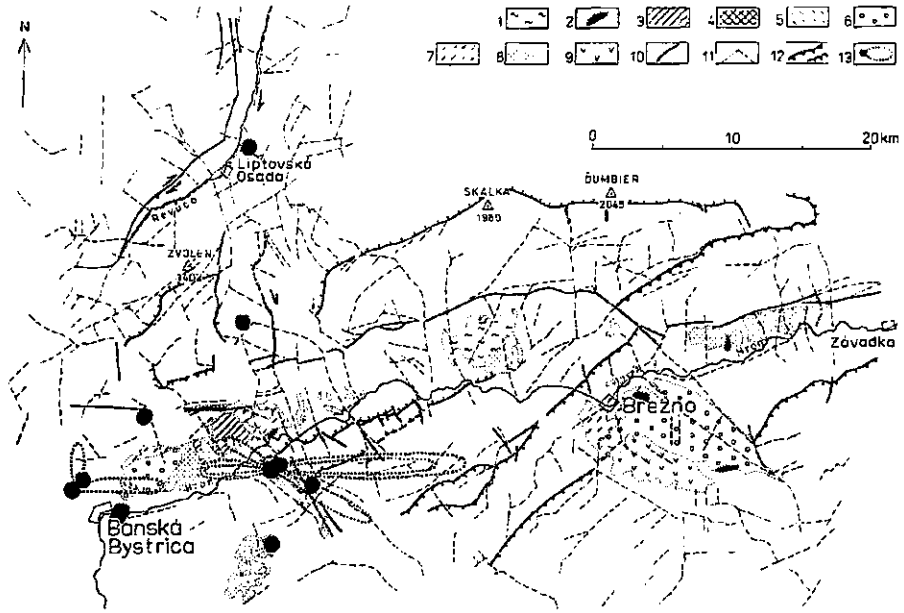

8. Dynamics of the Revúca fault system. 1 – the Vajsková conglomerates, 2 – sediments of mottled series (pre-Lutetian), 3 – dolomitic conglomerate facies, 4 – sediments of the Podkonice series, 5 – sandstone - conglomerate facies, 6 – claystone lithofacies, 7 – regressive facies of Oligocene, 8 – gravel (Pliocene), 9 – neovolcanics, 10 – known faults, 11 – interpreted faults and fractures, 12 – overthrusts, 13 – earthquake epicenters.

Seismotectonics of the area

The data on the occurrence of strong earthquakes (Brouček 1987; Procházková - Kárník 1978; Schenková - Kárník 1988) in Central Slovakia (Fig. 8) mostly come from an earlier period so that the positions of some shock epicentres around the Revúca fault system might be inaccurate. Nevertheless, it can be shown that except for the earthquakes confined to the Verona-Semmering-Váh lineament in the West Carpathians (Schenk et al. 1985; Buday et al: 1986), great part of the earthquakes in Central Slovakia are confined to the surroundings of the Hron and Revúca fault systems.

The earthquakes originating in Central Slovakia are bound to the area of broader surroundings of the town Banská Bystrica. To a certain extent, their occurrence can be correlated with the region of the intersection of the Revúca fault system and the Hron tectonic zone. The most interesting, and in fact unclarified, is the strong shock of June 5, 1443 (8^{o}–9^{o}MSK), which caused serious damage in a large area. In contemporary writings a shock felt in Hungary, Moravia, Poland, Bohemia and in Austria is mentioned. From the fragmentary information available, its position cannot be determined with sufficient accuracy, however: its location was most probably in the broader neighbourhood of Banská Bystrica (Kárník et al. 1948). The depth of this earthquake is estimated at 25 km. Its origin could be bound to the Hron tectonic zone, for even some other

earthquakes (1855, 1862) of an intensity of 6°–6.5° MSK are found in this zone between Banská Bystrica and Ľubietová. The focal depths of the earthquakes of this region vary within a range of 4–12 km.

The earthquake occurrences (Figs. 5, 8) can be associated with the weakened places of the Hron and Myjava-subTatra tectonic zones, among which the Revúca fault system passes or rather parallel zone lying 20–30 km west of the Revúca zone.

Even though we know 18 earthquake shocks in the area under investigation, the paucity of direct recordings did not allow us to determine the fault plane solution for any of them.The latest earthquakes, from June and November 1989, have not been processed yet. Nevertheless, the available seismological material enabled us to determine the directions of decreased seismic energy (Fig. 8, Schenk et al. 1989). We made use of the isoseismal maps known for some of the mentioned shocks, all of them being in the south part of the area investigated. The radius differences of the isoseismals characterize a different degree of seismic energy attenuation with distance; positive values correspond to the direction of lower attenuation, i.e. to the direction of the structure-tectonic elements. The performed analysis shows that in the valley of the Hron river, EW or actually ENE-WSW directions prevail. Their coincidence with the hron tectonic zone direction is very good (Pospíšil et al. 1986).

In addition to the data on earthquake occurrence, we utilized the results of gravity and magnetic measurements of this area (Obernauer 1980) and the correlations of seismological data with the course of photolineations determined from satellite images (Pospíšil et al. 1985). It appears that contrary to the previous interpretations, we can include into the dextral transcurrent system evan its broader surroundings, i.e. even the tectonic zone that bounds the crystalline basement of the Veľká Fatra Mts. in the east side. According to gravity data, the zone continues to the southwest as far as the western margin of "the Staré Hory tectonic window" (Andrusov 1965). All the interpreted disturbances are manifest in the gravity field by sharp gradients, which segment them into a series of narrow elongated positive zones corresponding to incised mesozoic carbonate complexes (young grabens).

It is understandable that an analysis of the fault movement activity cannot account for the entire time-and-space development of the study area. The character of faults, hawever, suggests the probable force conditions that must have existed in a given area under the origin of the boundary system. A paleogeographic analysis of the Tertiary development of the area revealed an uplift tendency of the Low Tatra region with respect to its surroundings until the Pliocene period (Klinec et al. 1985). The cyclic character (pulsations) of the uplift seams to have had a rapid course in the last period, which was apparently evoked by the horizontal movements of the Carpathian blocks along the faults of NE-WS and ENE-WSW direction (Janků et al. 1984; Pospíšil et al. 1985, 1989). Those faults are buried and seated under Tertiary sediments in the crystalline basement. On the surface, only fragments of these faults can be seen (e.g. Strážovské vrchy Mts., the Vysoké Tatry, Vepor part of Slovenské Rudohorie Mts., Vienna basin etc.). The Revúca fault system, which has a dextral character of movement, connects Hron and Myjava-subTatra tectonic systems of a higher order and can thus be regarded as a second order system of wrench faults.

The configuration of the faults of Revúca disturbance system indicates that the origin of the 2nd-order faults must have been sided by a tectonic predisposition of the area that increased the depth reach of these boundaries. This is also evidenced by the rise of intermedial magmas along these faults to the surface (volcano Poľana). The liveness of these faults is also confirmed by the present knowledge of the earthquake occurrence in the area under study. Present earthquake activity is known from the Revúca reiver valley and its south continuation.

Conclusions

The purpose of contemporary studies on the southern and southwestern slopes of the Nízke Tatry Mts. and Veľká Fatra Mts. was to verify the important tectonic boundaries and deformation structures interpreted on satellite images.

The interpretation results of serial photographs and radar images were included in analytical maps of tectonic, geodynamic and morphostructural features on the scale of 1:50,000. This analysis showed their great heterogeneity rate in the area of interest. The relief diversity is most probably due to the movements of Late Alpine active blocks, but the theory of a large gravity deformation can by no means be excluded. The geodynamic phenomena analysis and their relation to the tectonic features confirmes the intensivedestruction of the "gravity nappe" area. Beside these conclusions also the continuity of the Revúca fault system, its branching, further the Mýto-Tisovec tectonic zone and the proof of the existence of the so called Hron lineament was of great significance.

Despite the analyzed data we cannot draw the final decisive conclusion of the development and destruction of the south slopes of the mountain. The explanation of that problem is closely connected with an analysis of the development of the broader area and with more detail analytical and complex data.

K tisku doporučil O. Fusán
Přeložil L. Pospíšil

References

Andrusov, D. (1958): Geology of Czechoslovak Carpathians. – Veda, 392 p. Bratislava (in Slovak).

Brouček, I. (1987): Catalogue of earthquakes for Slovakia. – Geoph. Inst. Slovak Acad. Sci. MS Bratislava.

Buday, T.-Pospíšil, L.-Šutora, A. (1986): Geological meaning of some boundaries in Western Slovakia and Eastern Moravia interpreted from satellite images. – Miner. slov., 18, 6, 481–499. Bratislava.

Bujnovský, A. (1979): Geological profile and structure elements of nappes in the NW part of the Low Tatra and Revúca Fault Zone. In M. Mahel'(ed.): Tectonic profiles through the West Carpathians. – Geol. Inst. Dionýza Štúra, 85–89. Bratislava.

Janků, J.-Pospíšil, L.-Vass, D. (1984): Contribution of remote sensing to knowledge of the Western Carpathian structure. – Miner. slov., 16, 2, 121–137. Bratislava (in Slovak).

Klinec, A.-Pospíšil, L.-Pulec, M.-Feranec, J.-Stankoviansky, M. (1985): An identification of the gravity nappe in the Nízke Tatry by means of satellite images. – Miner. slov., 17, 6, 485–499. Bratislava.

Koštálik, J. (1971): Geomorphological conditions of Brezno basin. – Geogr. čas., 23, 2, 102–106. Bratislava (in Slovak).

Kubiny, D. (1962): Geological position of the Stare Hory Crystalline Complex. – Geol. Práce, Zoš., 62, 26–38. Bratislava (in Slovak).

Maheľ, M. (1986): Geological structure of the Czechoslovak West Carpathians. Paleo–Alpine units. – Veda, 503 p. Bratislava (in Slovak).
Nemčok, A. (1982): Landslides in Slovak Carpathians. – Veda, 319 p. Bratislava (in Slovak).
Obernauer, D. (1980): Geophysical research of the western part of the Slovenské rudohorie Mts. and the Eastern part of the Low Tatra. – Faculty of Natural Science, PhD Thesis, 115 p. Bratislava (in Slovak).
Pospíšil, L.- Vass, D. (1984): Influence of the structure of the lithosphere on the formation and development of intramontane and back molasse basins of the Carpathian Mts. – Geophys. Transaction, 30, 355–371.
Pospíšil, L.-Nemčok, J.-Graniczny, M.-Doktor, S. (1985): A contribution of remote sensing methods to the identification of faults with a strike-slip movement in West Carpathians. – Miner. slov., 18, 5, 385–402. Bratislava.
Pospíšil, L.-Schenk, V.-Schenková, Z. (1985): Relation between seismoactive zones and remote sensing data in the West Carpathians. – Proc. 3rd Intern. Symp. Analysis of Seismicity and Seismic Risk, Liblice, vol. 1, 256–263. Praha.
Pospíšil, L.-Halmešová, S.-Marušiaková, D. (1986): An analysis and synthesis of geological and geophysical structures using the remote sensing data. – MS Geofyzika, 112 p. Bratislava (in Slovak).
Pospíšil, L.-Bezák, V.-Nemčok, J.-Feranec, J.-Vass, D.-Obernauer, D. (1989): The Muráň tectonic system as example of horizontal displacement in the West Carpathians. – Miner. slov., 21, 4, 305–322. Bratislava.
Procházková, D.-Kárník, V. (1978): Atlas of isoseismal maps for Central and Eastern Europe. – Geophys. Inst.,Čs. akad. věd, 134 p. Praha.
Schenk, V.-Schenková, Z.-Pospíšil, L. (1989): Fault system dynamics and seismic activity - examples from the Bohemian Massif and the Western Carpathians. – Geophys. Transactions, 35, 1–2, 101–116. Budapest.
Schenk, V.-Schenková, Z.-Pospíšil, L.-Zeman, A. (1985): Seismotectonic model of the upper part of the Earth's crust of Czechoslovakia. – Stud. geophys. geod., 30, 321–330. Praha.
Schenková, Z.-Schenk, V.-Kárník, V. (1979): Earthquake epicentres in Central and Eastern Europe. – Stud. geophys. geod., 23, 197–203. Praha.
Schenková, Z.-Kárník, V. (1988): Catalogue of earthquakes for Central and Eastern Europe. – Geophys. Inst. Czechosl. Acad. Sci. Praha.
Škvarček, A. (1973): An outline of the Quaternary evolution of the mountaineous part of the Hron River valley. – Geogr. čas., 25, 2, 112–120. Bratislava (in Slovak).
Tomek, Č.-Dvořáková, L.-Ibrmajer, I.-Kordb, T.-Biely, A.-Lexa, J.-Zbořil, A. (1989): Crustal structures of the West Carpathians on the deep reflection seismic line 2T. – Miner. slov., 21, 1, 3–26. Bratislava (in Czech).
Varga, G.-Lada, F. (1988): Magnetotelluric measurement on the profile 2T. – MS ELGI Budapest – Geofyzika Brno, 29 p. (in Czech).
Vybíral, V. (1986): The Nízke Tatry Mts., Sb-south. Res. rep. 1981–1985, 121 p. Geofyzika Bratislava (in Slovak).

Geodynamická analýza Nízkych Tatier na základe DPZ a geofyziky

(Résumé anglického textu)

Soňa Halmešová - Rudolf Holzer - Darina Marušiaková - Lubomil Pospíšil

Predložené 20. decembra 1989

Pohorie Nízkych Tatier patrí z hľadiska vývoja Centrálnych Západných Karpát ku kľúčovým územiam. Na základe štúdia kozmických snímok bola na južných svahoch Nízkych Tatier interpretovaná rozsiahla deformácia zatriedená do skupiny gravitačných príkrovov. Ďalšie výskumy však jej existenciu plne nepotvrdili. Preto sa prikročilo k podrobnej analýze leteckých snímok v mierke 1:35 000, predovšetkým s dôrazom na štruktúrno-tektonické, morfologické a geodynamické fenomény tohto hypotetického modelu, doplnenej o interpretáciu výsledkov geofyzikálneho prieskumu.

Komplexná analýza územia ukázala, že počas terciéru mala jz. strana Nízkych Tatier pravdepodobne povahu hráste, ktorej zdvihy boli podmieňované aktívnymi poruchami vo fundamente. Boli zistené komplikované a rádovo veľmi rôznorodé zlomové poruchy, zlomy alebo puklinové systémy, z ktorých mali mnohé charakter horizontálnych posunov. Rovnako aj mimoriadna disekcia reliéfu, chaotické usporiadanie úrovní zarovnávania a množstvo geodynamických javov načrtáva značnú komplikovanosť stavu geologického prostredia a neotektonického vývoja celej štruktúry.

Relatívne rýchly výzdvih pohoria dokázaný paleogeografickou analýzou bol pravdepodobne spôsobený pravostrannými pohybmi karpatských blokov pozdĺž zlomov I. rádu smeru VSV-ZJZ. Revúcky zlomový systém, ktorý vykazuje tiež pravostranný pohyb, je aktívny od hlavných fáz alpínskeho vrásnenia až podnes. Tento systém zlomov II. rádu (smer S-J) je považovaný za nejdôležitejšie rozhranie pre vznik študovanej gravitačnej deformácie.

Ako ukazujú doterajšie výsledky diaľkového prieskumu a geologicko-geofyzikálneho výskumu, možno predpokladať úzku súvislosť medzi výskytom ložísk rúd (W, Au, Sb) a uvedenými hlboko zasahujúcimi tektonickými poruchami.

V nemenšej miere získané poznatky možno uplatniť tiež pri inžiniersko-geologickom hodnotení základných zložiek geologického prostredia a riešení seizmotektonických problémov.

Vysvetlivky k obrázkom

1. Južné svahy Nízkych Tatier (výrez zo snímku LANDSAT a interpretácia).
2. Tektonická analýza j. svahov Nízkych Tatier podľa družicových snímkov. 1 – zlomová štruktúra, 2 – facetový svah.
3. Analýza geodynamických javov. 1 – sklonové deformácie, 2 – osypový tok, 3 – blokové rifty, 4– individuálne bloky, 5 – príkre srázy, 6 – zosuvy, 7 – aluviálne kužele, 8 – erózna rokľa, 9 – erózna hranica, 10 – plošná erózia, 11 – proluviálny kužel, 12 – krasové javy (Varga - Lada 1988).
4. Schéma hlavných zlomových systémov. 1 – neogén, 2 – neovulkanity, 3 – paleogén, 4 – mezozoický

komplex, 5 – komplexy paleozoika a kryštalinika, 6 – granitoid, 7 – metamorfity, 8 – amfibolity, 9 – známe a interpretované zlomy.

5. Mapa vertikálnych hustotných rozhraní a zemetrasných ohnísk. 1 – interpretovaný zlom, 2 – vertikálne hustotné rozhranie, 3 – ohnisko zemetrasenia.

6. Vzťah medzi zónou anomálie vyzvanej polarizácie a interpretovanou tektonikou. 1 – zlomy, 2 – interpretované zlomy, 3 – svahy, 4 – sufové deformácie, 5 – aluviálne kužele, 6 – svahové deformácie, 7 – hráste, 8 – rifty a bloky, 9 – erózna hranica, 10 – medzihorie vo výške 850–1400 m n.m., 11 – magnetická anomália (+ 40 nT), 12 – anomália IP.

7. Geologický rez Nízkych Tatier a geofyzikálna data. Δg_B – Bouguerova tiažová anomália, ΔT – anomália totálneho vektoru geomagnetického poľa, odporové krívky z magnetotelurických meraní.

8. Dynamika revúckeho zlomového systému. 1 – konglomeráty Vajskovej, 2 – pestrá séria (pre–lutenian), 3 – fácia dolomitických konglomerátov, 4 – sedimentárna séria Podkonice, 5 – fácia piesčitých konglomerátov, 6 – ílovcová litofácia, 7 – transgresívny oligocén, 8 – pliocénny štrk, 9 – neovulkanity, 10 – zlomy, 11 – interpretované zlomy, 12 – príkrovy, 13 – ohnisko zemetrasenia.

Sborník geologických věd	Užitá geofyzika 25	Pages 83–90	5 figs.	– tab.	– pl.	Praha 1992 ISBN 80-7075-110-X ISSN 0036-5319

Influence of position of measuring electrodes on registration of the self-potentials

Vliv polohy měřících elektrod na registraci vlastních potenciálů

František Ryšavý[1]

Received April 3, 1990

Well-logging
Self-potentials

Ryšavý, F. (1992): Influence of position of measuring electrodes on registration of the self-potentials. – Sbor. geol. Věd, užitá Geofyz., 25, 83–90. Praha.

Abstract: The self-potential method (SP), as one of the main well-logging methods up to now permanently used, has never been considered from the view of position of a measuring tool. Every measuring tool can be fixed only and only in one of two possible positions. The tool must be either lie on the axis of the borehole or pressed on a wall of the borehole. An influence of technical and geological parameters is given due to the so-called characteristic function which differs for each of the above mentioned positions of the measuring tool. In recent time the level of electric noise is increasing and that is why the SP potential is negatively influenced by that noise. It seemed to be better to consider again the SP lateral which had been early preferred, but later, geophysicists have lost their interest because interpretation of this method was complicated and not exactly explained. Now, the SP lateral described after the electric field theory can undertake a role of the SP potential. In the past the characteristic function of the SP potential, when the tool is centralized, was described. However, the characteristic function of the tool pressed on a wall of the borehole has never been derived. Because of this we were not able to appreciate an influence of the measuring tool in either of the mentioned positions and to compare it.

Any characteristic functions of the SP lateral for both of the above positions were not derived and therefore no comparison of both measuring lateral systems was possible. The aim of this paper is to define all characteristic functions of both the SP potential and SP lateral. Only in this way we can calculate an influence of all the mentioned systems.

But simultaneously it means we are able to use corrections for bed thickness, bed diameter and in the case of the SP lateral also a correction for base of the tool. Since we are interested in the self potential situated on a wall of the borehole, we can compute this potential not only from the SP potential but also from the SP lateral due to its exactly defined characteristic function.

[1]*KaC, a. s., Hodonín, Vídeňská 22, 695 30 Hodonín*

Introduction

From the experience with registration of the self-potentials in their natural environment we know that using of a correction for the momentary position of the measuring

electrodes in a borehole is nearly impossible. The electrodes oscillate in the borehole within registration and they move between two extreme positions there.

The tool can be placed on the borehole axis, which is the first position or to touch a wall of the borehole, which is the second position.

Theory

If we accept the condition to fix the measuring tool within registration in the first or the second position, we can ensure constant conditions of registration in one of the above positions. These conditions will be, of course, for each position different. They become evident by means of different form of a so-called characteristic function, which is the function describing an influence of the bed thickness and the borehole diameter on a registration of the self-potentials.

We shall distinguish between the characteristic function of centralized tool in the borehole axis and the characteristic function of pressed tool on the wall of the borehole.The first case was described by Dachnov (1967) who dealt with the theory of the SP potential. The SP lateral has been resolved by Marušiak (1956), who had used known approach of Dachnov (1947). The second case, in the meantime, has not been concerned.

The SP potential U_{SP} registered by measuring tool lying in a mud is defined by the formula

$$U_{SP} = \eta \,.\, E_{SP} \tag{1}$$

where η is factor of the electric current transmission.

Factor η depends on such physical factors as the specific resistance of an invasion zone, the specific resistance of mud and the specific resistance of adjacent rocks. This function is given by following equation (2)

$$\eta = 2 \,.\, \frac{R_m \,.\, R_i + R_m \,.\, R_S}{R_m \,.\, R_i + R_m \,.\, R_s + R_i \,.\, R_s} \tag{2}$$

where R_i is the specific resistance of an invasion zone [Ω m],

R_m the specific resistance of mud [Ω m], and

R_s the specific resistance of adjacent rocks [Ω m].

We have not taken notice to factor E_{SP} up to now. Let us pay an attention to it, too. We can write it in the following form.

$$E_{SP} = \varepsilon_{SP} \,.\, f\left(\frac{z}{d}, \frac{h}{d}\right) \tag{3}$$

where z is a distance between centre of the bed and the point of observing [cm], d the borehole diameter [cm], and h thickness of the bed [cm].

The factor ε_{SP} holds the Nernst's formula. But the second term – function – is a mentioned characteristic function of the SP potential expressing an influence of the measuring tool position. For the SP lateral is accepted the formula (4):

$$\Delta U_{SP} = \eta \,.\, \Delta E_{SP}. \tag{4}$$

And for $\Delta\ E_{SP}$ we can write then that

$$\Delta E_{SP} = \varepsilon_{SP} \,.\, f\left(\frac{z}{d}, \frac{h}{d}, \frac{L}{d}\right), \tag{5}$$

where L is base of the lateral tool e.g. a distance between both centres of M and N electrodes [cm].

The above function is called the characteristic function of the SP lateral. The characteristic function of both the SP potential and the SP lateral has different form for a different position of the measuring tool.

If we have the SP potential tool centralized in the borehole axis, we shall use formula (6) defined by Dachnov (1967).

$$f(\bar{z}, \bar{h}) = \frac{1}{2}\left[\frac{(2\bar{z}+\bar{h})}{\sqrt{(2\bar{z}+\bar{h})^2+1}} - \frac{(2\bar{z}-\bar{h})^2}{\sqrt{(2\bar{z}+\bar{h})^2+1}}\right]. \tag{6}$$

If the SP potential tool is pressed on the wall of the borehole, we may use the formula derived after information about the space angle (see Dachnov 1967).

$$f(\bar{z},\bar{h}) = \frac{1}{\pi} \,.\, \left[\frac{(2\bar{z}+\bar{h})}{\sqrt{(2\bar{z}+\bar{h})^2+4}} \,.\, K\left(\frac{2}{\sqrt{(2\bar{z}+\bar{h})^2+4}}\right) - \frac{(2\bar{z}-\bar{h})}{\sqrt{(2\bar{z}-\bar{h})^2+4}} \,.\, K\left(\frac{2}{\sqrt{(2\bar{z}-\bar{h})^2+4}}\right)\right] \tag{7}$$

where K ( ) is the complete elliptical integral of the first type.

For the SP lateral tool we are using similar formulas. If the SP lateral tool is centralized in the borehole axis, we shall write new equation (8) derived from (6).

$$f(\bar{z},\bar{L},\bar{h}) = \frac{1}{2} \,.\, \left[\frac{(2\bar{z}+\bar{L}+\bar{h})}{\sqrt{(2\bar{z}+\bar{L}+\bar{h})^2+1}} + \frac{(2\bar{z}-\bar{L}-\bar{h})^2}{\sqrt{(2\bar{z}+\bar{L}+\bar{h})^2+1}} - \right.$$
$$\left. - \frac{(2\bar{z}+\bar{L}-\bar{h})}{\sqrt{(2\bar{z}+\bar{L}-\bar{h})^2+1}} - \frac{(2\bar{z}-\bar{L}+\bar{h})}{\sqrt{(2\bar{z}-\bar{L}+\bar{h})^2+1}}\right]. \tag{8}$$

When the SP lateral tool is pressed on the wall of the borehole, we may use formula (9).

$$f(\bar{z},\bar{L},\bar{h}) = \frac{1}{\pi} \,.\, \left[\frac{(2\bar{z}+\bar{L}+\bar{h})}{\sqrt{(2\bar{z}+\bar{L}+\bar{h})^2+4}} \,.\, K\left(\frac{2}{\sqrt{(2\bar{z}+\bar{L}+\bar{h})^2+4}}\right) + \right.$$
$$+ \frac{(2\bar{z}+\bar{L}-\bar{h})}{\sqrt{(2\bar{z}+\bar{L}-\bar{h})^2+4}} \,.\, K\left(\frac{2}{\sqrt{(2\bar{z}-\bar{L}-\bar{h})^2+4}}\right) -$$
$$\left. - \frac{(2\bar{z}+\bar{L}-\bar{h})}{\sqrt{(2\bar{z}+\bar{L}+\bar{h})^2+4}} \,.\, K\left(\frac{2}{\sqrt{(2\bar{z}+\bar{L}-\bar{h})^2+4}}\right) -\right.$$

$$-\frac{(2\bar{z}-\bar{L}+\bar{h})}{\sqrt{(2\bar{z}-\bar{L}+\bar{h})^2+4}}\cdot K\left(\frac{2}{\sqrt{(2\bar{z}-\bar{L}+\bar{h})^2+4}}\right)\Bigg]. \tag{9}$$

Symbols $\bar{z}$, $\bar{L}$, $\bar{h}$ are normalized by the borehole diameter e.g. it holds that

$$\bar{z}=\frac{z}{d}, \tag{10}$$

$$\bar{h}=\frac{h}{d}, \tag{11}$$

$$\bar{L}=\frac{L}{d}. \tag{12}$$

Both potential characteristic functions are symmetrical after the bed centre. The lateral characteristic functions are asymmetrical after bed centre. Marušiak (1956) defined formula of the SP lateral by means of derivation the equation (6). The character of the lateral curves was similar like in our case, but the mathematical form was another. He studied only the centered lateral tool.

The characteristic function has two extreme positions – centered tool in the borehole axis and pressed tool on the wall of borehole. It was given by situation that the space angle of an observing point was not defined for a general position of this point but for each of the extreme positions as well. But in practice we need to use only the tool steady fixed in one of the above positions and therefore I did not define the general formula.

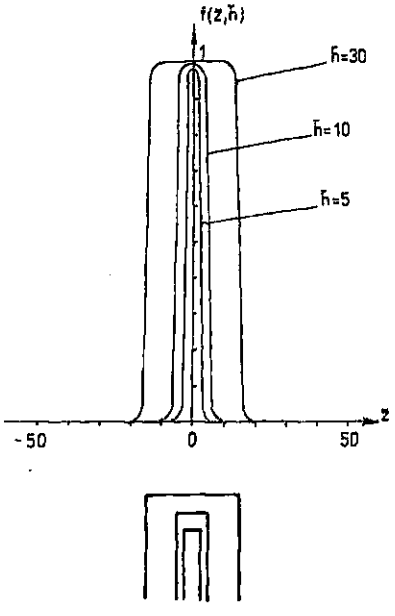

1. The SP potential curves of a measuring tool centralized in the borehole axis for beds of different thickness.

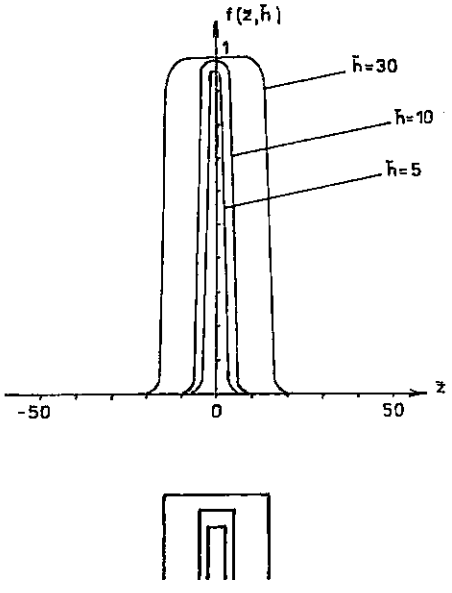

2. The SP potential curves of a measuring tool pressed on the wall of borehole for beds of different thickness.

Discussion

The results of mathematical analysis of all four events are completed by illustrations of the characteristic functions. On Fig. 1 and 2 there is the SP potential centered in the borehole axis and the SP potential pressed on a wall of the borehole. The graph of the characteristic function is made for several beds having different thickness. It is evident that bounds of the bed lay in points of inflection of the characteristic function and this holds for both centralized and pressed measuring systems. More, it is evident the thick beds of both above systems have almost identical characteristic function. But the thin beds are better characterized by centralized measuring tool having higher deflections of the characteristic function and this function has also higher steepness.

For the SP lateral tool is a similar situation. On Fig.3 and 4 there is the characteristic

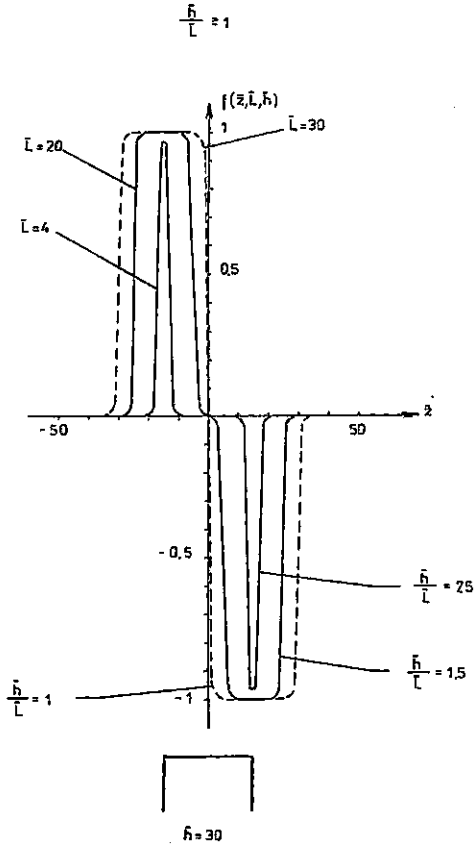

3. The SP lateral curves of a measuring tool centralized in the borehole axis for $h \geq L$

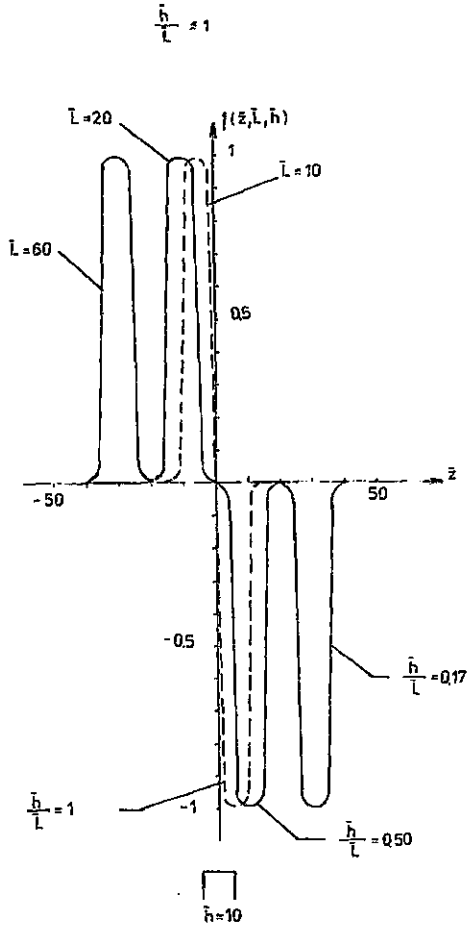

4. The SP lateral curves of a measuring tool centralized in the borehole axis for $h \leq L$.

function of the SP lateral illustrated. We must distinguish between events, when $h > L$ and $h \leq L$, because it has a fundamental significance for an evaluation of bed thickness. By comparison of curves we shall conclude that the characteristic function of thick beds is almost identical for both the centralized and pressed tool. However, the thin beds or a short spacing of the tool are better characterized by centralized tool.

A graph common for both mentioned lateral systems is drawn on Fig. 5. It is the technical characteristic curve transforming the apparent bed thickness into the real bed thickness. From illustration it is evident that in all events for $h < L$ it holds $h^* = L$. In contrary for $h > L$ it holds $h^* = h$. The event $h = L$ is common for both mentioned cases.

Pay a little attention to the SP lateral. Up to now there has it been held to determine the bed thickness only when $h > L$. But from the made analysis we can evaluate the bed thickness also at that case, when $h < L$. Even though the apparent bed thickness equals to base e.g. $h^* = L$, the real bed thickness is coded for a such event in latitude of positive and negative lateral deflection, which is determined by distance between both pair points of inflection. And just this fact we must use.

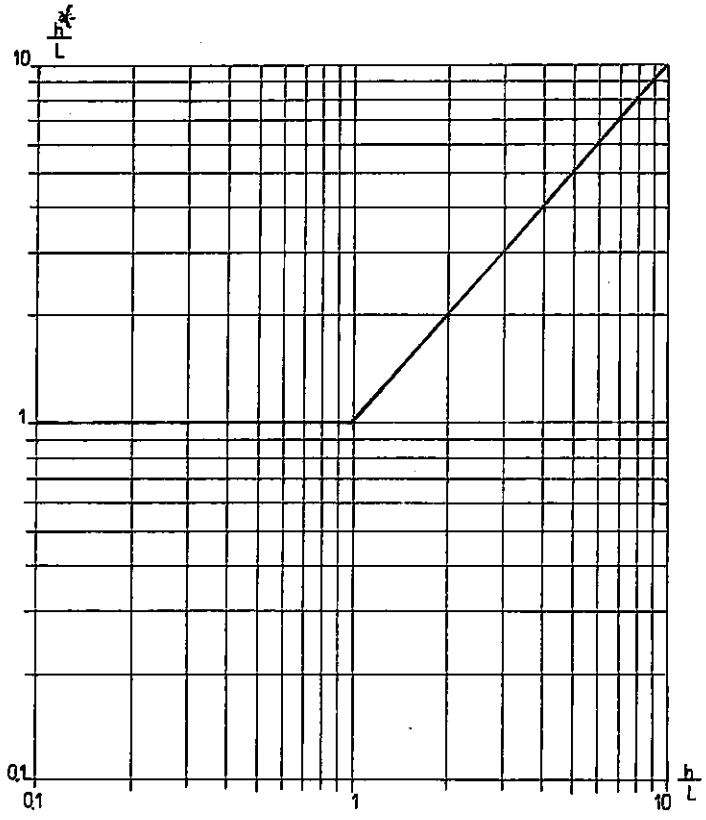

5. The transforming characteristic curve of the SP lateral from the apparent bed thickness into the real bed thickness.

Conclusions

Finally, we can summarize the procedure analysis to the following conclusions :

1. The bounds of beds are defined by position of inflection points for every beds in the case of the SP potential.

2. By comparison of pressed and centralized systems it is evident that for thick beds the both systems are equivalent but for thin beds the centralized system is giving more outstanding deflections. This holds both for the SP potential and the SP lateral.

3. For the SP lateral the bounds of beds are directly determined only if $h \geq L$. When $h < L$, for an evaluation we must use another method of interpretation, because the bed thickness is not defined by distance between maximum and minimum of deflections but by distance between the pair inflection points of positive and negative deflection.

4. As the potential is influenced by very large electric noise we can calculate now with the repeated evaluation of the SP lateral. The characteristic function can give for it all prerequisites.

For interpreters this method can have quite new significance, because they will be able to use corrections for the bed thickness, the borehole diameter and in the case of the SP lateral also a correction for base of the tool. Due to them it will be possible to compute factor ε_{SP} situated on the wall of the borehole, which has the direct significance for interpretation.

K tisku doporučil A. Těžký
Přeložil F. Ryšavý

References

Dachnov, V. N. (1947): Promyslovaja geofizika. – Gostoptechizdat. Moskva.

Dachnov, V. N. (1967): Elektritcheskije i magnitnyje metody issledovanija skvazin. – Nedra. Moskva.

Dachnov, V. N. (1985): Geofizitcheskije metody opredelenija kollektorskych svojstv i neftegazonasytchenija gornych porod. – Nedra. Moskva.

De Witte, L. (1950): Relations between resistivity and fluid contents of porous rocks. – Oil Gas J., 49, 16, Tulsa, Oklahoma.

Doll, H.G. (1950): The SP in shaly sands. – J. Petrol. Technol., 2, 7. Dallas, Texas.

Kozel, J. (1965): Difuzně adsorpční potenciály a jejich vztah ke kolektorským vlastnostem hornin. – MS Geofyzika, a.s., Brno.

Marušiak, I. (1956): Využitie krivky gradienta vlastných potenciálov pre určenie hraníc vrstiev. – Sborník prací Ústavu pro naftový výzkum, 31–33. SNTL. Praha.

Segesman, F. (1962): New SP correction charts. – Geophysics, 27, 6.

Těžký, A. (1961): Praktická použitelnost metod pro interpretaci elektrické karotáže v jílovitých pískích. – Užitá geofyzika, 1. Brno.

Tixier, M. F. (1949): Electric log analysis in the Rocky Mountains. – Oil Gas J., 48, 6. Tulsa. Oklahoma.

Vendelshtejn, B.J. (1966): Issledovanije razrezov neftjanych i gazovych skvazin metodom sobstvennych potencialov. – Nedra. Moskva.

Vliv polohy měřících elektrod na registraci vlastních potenciálů

(Résumé anglického textu)

František Ryšavý

Předloženo 3. dubna 1990

Vliv polohy měřících elektrod ve vrtu můžeme posoudit prostřednictvím tzv. charakteristické funkce, udávající váhové zastoupení vlivu průměru vrtu, mocnosti vrstvy a u gradientu SP navíc i báze sondy, což je vzdálenost středů obou měřících elektrod. Existují dva krajní případy polohy měřících elektrod hlubinné sondy :

- kdy je centrována v ose vrtu,
- kdy je přitlačována na stěnu vrtu.

Byly studovány charakteristické funkce pro obě polohy jak pro potenciál SP, tak i pro gradient SP. V předložené práci jsou tyto charakteristické funkce uvedeny. Následuje diskuse výsledků a analýza výsledných rovnic, doplněná řadou obrázků.

Na základě této diskuse je možno dojít k závěrům:

1. Hranice vrstvy u metody potenciálu SP jsou jednoznačně určeny polohou inflexních bodů křivky charakteristické funkce.

2. Z porovnání centrovaného a přitlačovaného měřicího systému vyplývá, že u mocných vrstev nevzniká takřka žádný rozdíl. U tenkých vrstev je centrovaný systém vhodnější, neboť dává strmější a výraznější výchylky. To platí jak pro potenciál, tak pro gradient.

3. Až dosud bylo možno u gradientu SP určovat ty vrstvy, jejichž mocnost byla větší než báze sondy gradientového systému. Práce ukazuje na možnost interpretace i těch vrstev, jejichž mocnost je menší než báze sondy gradientového systému. Vzdálenost mezi pozitivní a negativní výchylkou je v takovém případě rovna bázi sondy, avšak informace o mocnosti vrstvy je dána vzdáleností mezi párovými inflexními body pozitivní a negativní výchylky.

4. Pro interpretaci Nernstovy rovnice je potřebné znát parametr ε_{SP}. Pomocí charakteristické rovnice určíme tento parametr nejen podle potenciálu SP, ale i podle gradientu SP. V době, kdy dochází ke zvýšení úrovně elektrických šumů, je měření gradientu SP výhodnější, neboť výpočet parametrů ε_{SP} je potom přesnější.

Vysvětlivky k obrázkům

1. Křivky potenciálu SP měřicí sondy centrované v ose vrtu pro vrstvy rozdílné mocnosti.
2. Křivky potenciálu SP měřicí sondy přitlačované na stěnu vrtu pro vrstvy rozdílné mocnosti.
3. Křivky gradientu SP měřicí sondy centrované v ose vrtu, když platí $h \geq L$.
4. Křivky gradientu SP měřicí sondy centrované v ose vrtu, když platí $h \leq L$.
5. Transformační charakteristika gradientu SP mezi zdánlivou a skutečnou mocností vrstvy.

Sborník geologických věd	Užitá geofyzika 25	Pages 91–100	8 figs.	– tab.	– pl.	Praha 1992 ISBN 80-7075-110-X ISSN 0036-5319

Numerical modelling of electromagnetic induction in the Earth magnetic polarization

Numerické modelování pole elektromagnetické indukce při magnetické polarizaci

Julius Miecznik[1]-Przemyslaw Borzemski[1]

Received November 24, 1988

Numerical modelling
Magnetotelluric method

Miecznik, J. - Borzemski, P. (1992) : Numerical modelling of electromagnetic induction in the Earth magnetic polarization. – Sbor. geol. Věd, užitá Geofyz., 25, 91–100. Praha.

Abstract: The basis for interpretation of magnetotelluric observations is the knowledge of the distribution of electromagnetic field for two- and three-dimensional geoelectrical models. For some models analytical solutions are available while for others there are only numerical methods of solution of induction problem and, among them, particularly differential methods. For two-dimensional (2-D) models the cases of electric and magnetic polarization must be considered separately. In the paper algorithm for computation of electromagnetic field, induced with the plane wave, is given for two-dimensional model and magnetic polarization. Geometrical and physical parameters of the model are arbitrary. The results of the computations are given as the curves of magnetotelluric profiling and soundings. The computing program is written in Turbo C language for IBM PC-AT microcomputers.

[1]*Instytut geofizyki Akademii górniczo-hutniczej,A.Mickiewicza 30, Kraków,Polska*

Introduction

The effectivity of magnetotelluric methods is much increased with the knowledge of distribution of electromagnetic field for two- and three-dimensional geoelectrical models. The essence of the problem is the solution of the Helmholtz equation for the particular polarization of the plane wave as the field source. Analytical solutions are possible for the models having simple geometrical forms (Rikitake 1960). Such models include cylindrical or spherical body buried in a layered medium (Kaufmann-Keller 1981). The solution of the problem needs the relation of field presentation in rectangular coordinate system and in spherical or cylindrical systems. The effect is obtained by representing the plane wave as a sum of spherical or cylindrical waves. Analytical

solutions have limited range of application but, on the other hand, they allow to establish explicitly the relations between field characteristics and physical and geometrical parameters of the studied model. Accuracy of the analytical solutions may be determined in relatively simple way.

For the models with complex geometrical forms and arbitrary electrical conductivity, numerical methods are effective. Of these, differential methods are widely applied. There are several solutions in these methods. The most general case is when the node of approximating net lays on the contact of four different conductivities σ_1, σ_2, σ_3, σ_4 or corresponding wave numbers k_1, k_2, k_3, k_4. In the below . In the below given algorithm for electromagnetic field the method of the Varga approximation (1962) of the Helmholtz equation is used.

Differential methods may be used for arbitrary distribution of conductivity in geoelectrical model. The difficulties are related with the solution of large system of equations generated in the whole region. For electric and magnetic polarization of primary field,completely different boundary conditions are formulated for upper and lower border of the region.

In the paper the case of magnetic polarization is discussed.

Algorithm of electromagnetic field computation

Let us consider two-dimensional geoelectrical model in which the axis of homogeneity agrees with the axis of the Cartaesian x, y, z coordinate system ($+ z$ axis is directed vertically down). The primary field is the plane electromagnetic wave harmonically dependent on time t, i.e. exp. $(- i \omega t)$, where ω is frequency of field changes. Electric conductivity of the medium is the function of position, $\sigma = \sigma (x, z)$. Assuming that the field induced in the medium does not change along y-axis, electric polarization has the following components

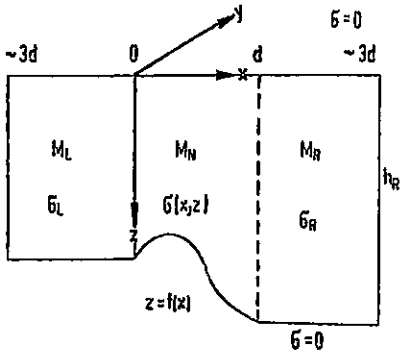

1. Two- dimensional geoelectrical model. x, y, z – rectangular coordinate system; d – width of inhomogeneity; M_N, M_L, M_R – inhomogeneous, left and right regions; σ_L, σ_R – electric conductivity; h_L, h_R – depth of high resistivity basement.

$$E^E (0, E_y, 0)$$

$$H^E (H_x, 0, H_z) \qquad (1)$$

and for magnetic polarization

$$E^H (E_x, 0, E_z)$$

$$H^H (0, H_y, 0) \qquad (2)$$

On the Earth's surface $E_z = 0$.

It may be easily proved that field components directed along the homogeneity axis satisfy the following differential equation

$$(\Delta 2 + k^2) E_y = 0 \qquad (3)$$

for electric polarization, and

$$\frac{\partial}{\partial x}\left(\frac{1}{\sigma}\frac{\partial H_y}{\partial x}\right)+\frac{\partial}{\partial z}\left(\frac{1}{\sigma}\frac{\partial H_y}{\partial z}\right)+i\,\omega\,\mu\,H_y=0 \tag{4}$$

for magnetic polarization.

In the above given equations Δz stands for two-dimensional Laplace operator and $K^2 = i\,\omega\,\mu\,\sigma$ is a wave number of the medium. It may be easily found that for σ = const, equation (4) becomes Helmholtz equation.

We divide the studied medium into three regions. The central region, M_N, has width d and is the region of inhomogeneity. The boundaries of the left, h_L, and right, h_R, regions are shifted from the boundaries of inhomogeneous region for such the distance that the distortion due to inhomogeneity can be neglected and one-dimensional model, depending only on z-coordinate, can be assumed on the boundaries. In the upper and lower parts of the region we assume the medium for that $\sigma = 0$ (Fig. 1). Onto the constructed region the net is superimposed whose nodes lie on the contact of four different conductivities $\sigma_1, \sigma_2, \sigma_3, \sigma_4$ (Fig. 2). We replace Helmholtz equation in the nodes of the net by differential approximation. It is much simplified if Helmholtz equation is integrated over the area S

$$\int_S \Delta 2A\,dS = -\int_S k^2 A\,dS \tag{6}$$

where A is an arbitrary amplitude of the field. The integral on left-hand side is transformed using Green's equation after Piskorek (1980)

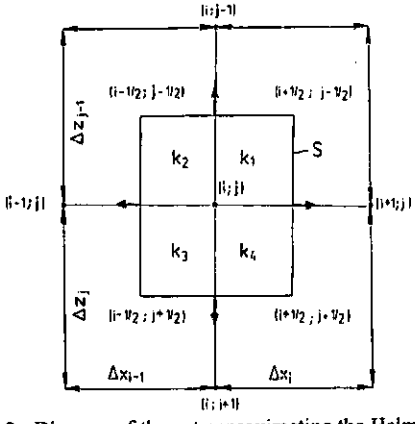

2. Diagram of the net approximating the Helmholtz equation. i,j – coordinates of the net node; Δx, Δz – net size, K_1, K_2, K_3, K_4 -wave number; S – area of the net.

$$\int_S \Delta 2A\,dS = \int_L \frac{\partial A}{\partial n}\,dL \tag{7}$$

L is the boundary of the region S, and n is its external normal.

The continuity of E_x and E_z components for magnetic polarization is the continuity of

$$\sigma^{-1}\frac{\partial H_y}{\partial z} \quad \text{and} \quad \sigma^{-1}\frac{\partial H_y}{\partial x},$$

respectively. Thus, equation (6) must have the form

$$\int_L k^{-2} \frac{\partial H_y}{\partial n} \, dL = -\int_S H_y \, dS \tag{8}$$

Substituting central differences for normal derivates and putting them into equation (8) and assuming that magnetic field inside the region S is constant and has the value of $H_y(i,j)$, we have

$$H_y(i,j) = C_{ij}^H \left[E_{ij}^H \, . \, H_y(i+1, j) + N_{ij}^H \, (i,j-1) + W_{ij}^H \, . \, H_y(i-1,j) + S_{ij}^H \, . \, H_y(i,j+1) \right] \tag{9}$$

where

$$E_{ij}^H = \frac{k_1^{-2} \, \Delta z_{j-1} + k_4^{-2} \, \Delta z_j}{2 \, \Delta x_i} \; ; \; N_{ij}^H = \frac{k_2^{-2} \, \Delta x_{i-1} + k_1^{-2} \, \Delta x_i}{2 \, \Delta z_{j-1}}$$

$$W_{ij}^H = \frac{k_2^{-2} \, \Delta z_{j-1} + k_3^{-2} \, \Delta z_j}{2 \, \Delta x_{i-1}} \; ; \; S_{ij}^H = \frac{k_3^{-2} \, \Delta x_{i-1} + k_4^{-2} \, \Delta x_i}{2 \, \Delta z_{j-1}}$$

$$C_{ij}^H = \left[E_{ij}^H + N_{ij}^H + W_{ij}^H + S_{ij}^H - \frac{1}{4} (\Delta x_i + \Delta x_{i-1}) \, (\Delta z_j + \Delta z_{j-1}) \right]^{-1} \tag{10}$$

The boundary conditions are relatively simply formulated for magnetic polarization.

On the upper boundary of the region, for $z = 0$, and having $E_z = 0$, from equation

$$(\nabla \times H)_z = \sigma E_z = 0$$

we get

$$H_y \, (x, 0) = \text{const.} \tag{11}$$

On the lower boundary, with insulating basement, we assume

$$H_y \, (x, z = f(x)) = 0 \tag{12}$$

On the left and right boundaries of the region we assume, as it was already mentioned, one-dimensional model. The component $H_y(z)$ must satisfy Helmholtz equation as well as conditions (11) and (12). Thus, we take

$$H_y(z) = C \, sh \, ik \, (h - z) \tag{13}$$

where C is an arbitrary constant.

In each internal node of the region we get the linear equation on account of unknown values of magnetic field. In the whole region, i x j linear equations are generated that can be written in matrix form

$$A \, . \, x = B \tag{14}$$

where A is an adjugate, five-diagonal matrix.

Matrix B is expressed in terms of coefficients E_{ij}^H, N_{ij}^H, W_{ij}^H, S_{ij}^H, and C_{ij}^H and field

values on the boundary of the region. Column vector x is the vector of searched field values $H_y(ij)$.
Electric field is calculated from equation

$$E_x = \frac{-1}{\sigma}\frac{\partial H_y}{\partial z} \tag{15}$$

The z-coordinate derivate of magnetic field intensity is computed numerically. Then, for electric and magnetic field, we compute apparent resistivity and phase shift according to relation

$$\rho_T = \frac{1}{\omega\mu}\left|\frac{E_x}{H_y}\right|^2 \quad ; \quad \varphi_T = |Arg|\,\frac{E_x}{H_y} \tag{16}$$

Theoretically, the most reasonable method of solution of the equation system (14) is Gauss-Seidel method, but in practice, it proved to be too slow. Thus, system of equations (14) is solved using the overrelaxation method which gives the expected results in the problem. Before iteration process, the system (14) must be conditioned in relation to diagonal element A_{ii}. After the operation, iteration loop has the form

$$\Delta H_y^n(i,j) = -\alpha\left[H_y^n(i,j) + E_{ij}\,H_y^n(i+1,j) + N_{ij}\,H_y^n(i,j-1) + W_{ij}\,H_y^n(i-1,j) + S_{ij}\,H_y^n(i,j+1)\right]$$

$$H_y^{n+1}(i,j) = H_y^n(i,j) + \Delta H_y^n(i,j) \tag{17}$$

where n is the number of iteration, and α is the parameter of overrelaxation.The error of successive iteration is defined as

$$\varepsilon^n = \sum_{}^{N_x-2}\sum_{}^{N_z-2} |\Delta H_y^n(i,j)| \tag{18}$$

The iteration process is stopped when $\varepsilon^n < 10^{-6}$. The proper choice of the overrelaxation parameter α is essential for optimization of parameter and speed of computations. The applied method of solution of the linear equations system enables the computations starting from the value $\lambda_1/h_1 = 5$, where $\lambda_1 = (10^7\ \rho_1\ T)^{1/2}$ is the wavelength in the medium with resistivity ρ_1, and T is the period of field variations. Below this boundary wave-length, the system of equations is improperly conditioned and the process becomes divergent. In the range of short waves the initial value of overrelaxation parameter must be carefully chosen. For longer waves, the value of α practically does not depend on the wave length and the previously computed value of overrelaxation parameter may be taken as the starting value in computation of the field value shorter wave.

The program is written in Turbo C language for microcomputer IBM PC. The actual version of the program allows using the nets $N_x \times N_z \le 7200$ (N_x and N_z – numbers of nodes in a net). The speed of computation is comparable to the speed of programs in FORTRAN.

Results of computations

The geoelectric cross-section, taken into computations, is shown in Fig. 3. Morphology of high-resistivity basement with resistivity ρ_3 is created by horst of width d_2 and trough of width d_3. Between the Earth's surface and the basement there is a horizontal layer with thickness H and resistivity ρ_2. Resistivity of the environment is ρ_1. The variable parameters of the model are: d_3/d_2 and ρ_2/ρ_1. The remaining parameters are constant and have the values: $h_1 = h_2 = 7.94$ unit; $h_3 = H = 1/2$. h_4; $h_4 = 1/2.h_1$.

Such geoelectric model enables to analyse the reproducibility of morphology of high resistivity basement and the problem of screening of electromagnetic field with the intermediate layer.

Electromagnetic response of the imposed geoelectric model is presented as the plots of apparent resistivity versus position, for given wave length (profiling) and as the curves of magnetotelluric soundings in points A, B, C, D (see Fig. 3).

If $\rho_2 = \rho_1$ i. e. there is no intermediate layer in geoelectric cross-section, then electromagnetic field changes are related mainly to the changes of morphology of high resistivity basement. The rate of its reproducibility for various wave lengths is shown in Fig. 4. In the range of low frequencies, impedance is inversely proportional to the longitudinal conductance of the overburden and, hence, all elevations of high resistivity basement are reflected in the field image.

The rate of reproducibility of basement depressions depends on the ratio of their widths to the length of electromagnetic wave and to the width of the surrounding elevations. In the case of narrow depressions, the structure is flown round by electromagnetic field and the depressions cannot be registered. This is shown in Fig. 5.

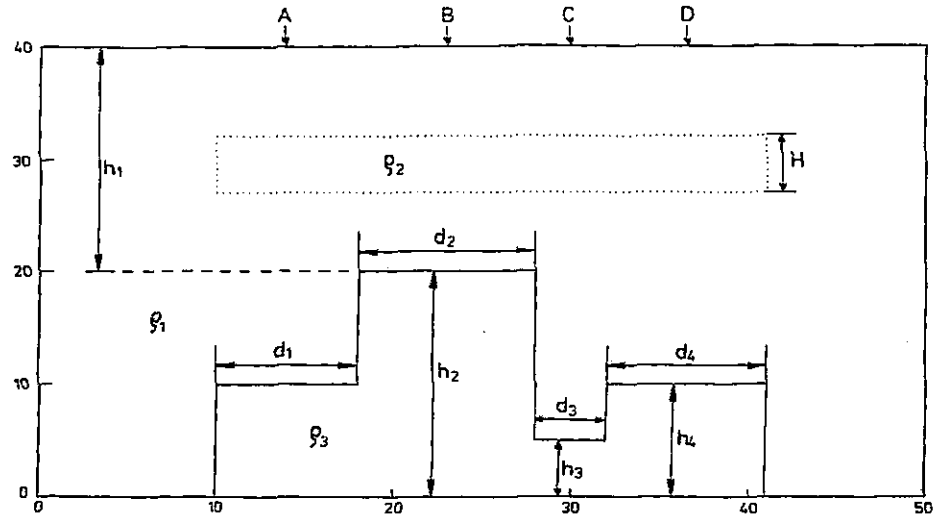

3. Geoelectrical cross-section used in computations. 10, 20, 30 – number of net nodes; A, B,C, D – sounding sites.

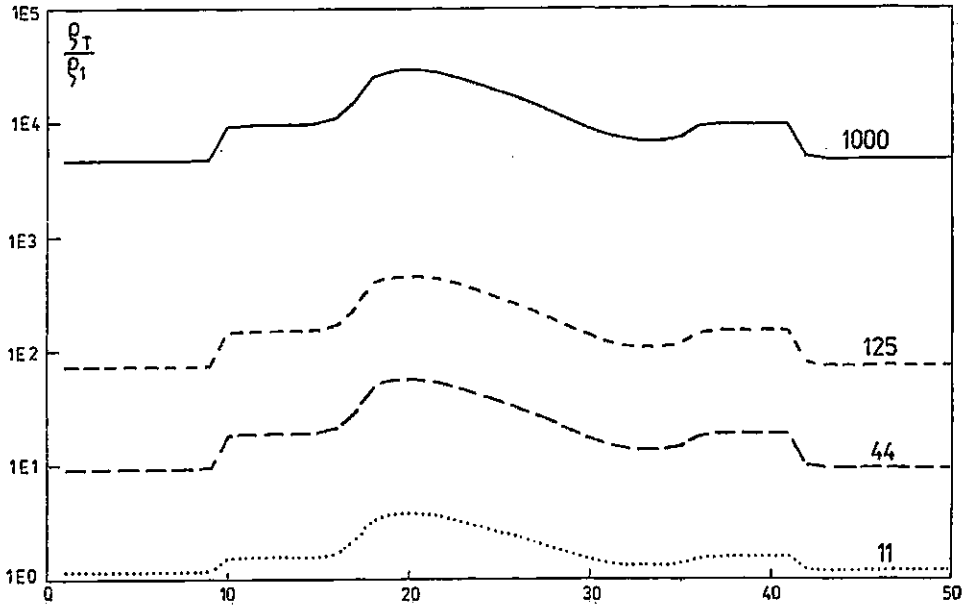

4. Magnetotelluric profiling curves. $d_3/d_2 - 2.39$, $\rho_2 = \rho_1$, parameter of the curves –relative electromagnetic wave length.

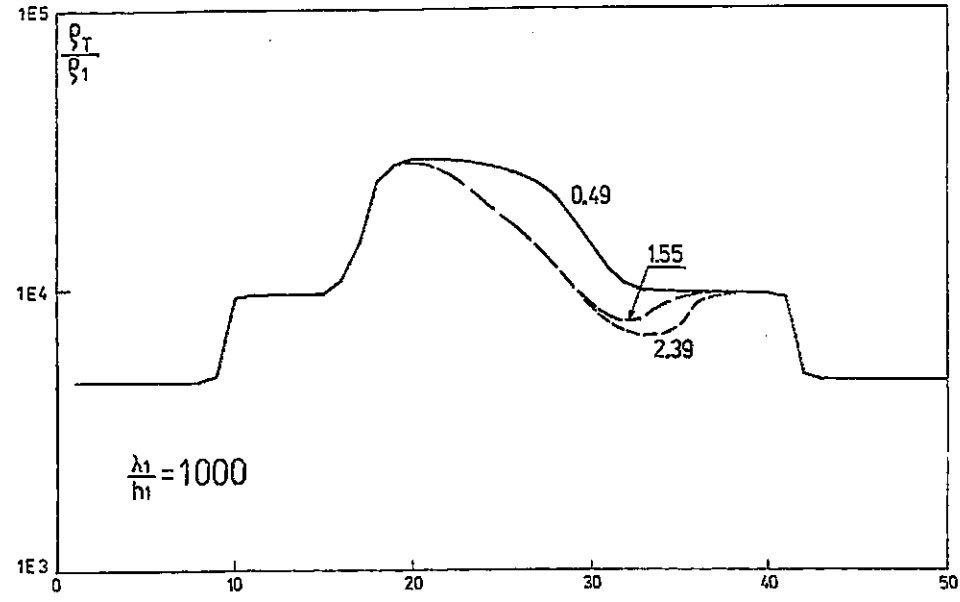

5. Magnetotelluric profiling curves. $\lambda_1/h_1 = 1000$; parameter of the curves – d_3/d_2; $\rho_2/\rho_1 = 1$.

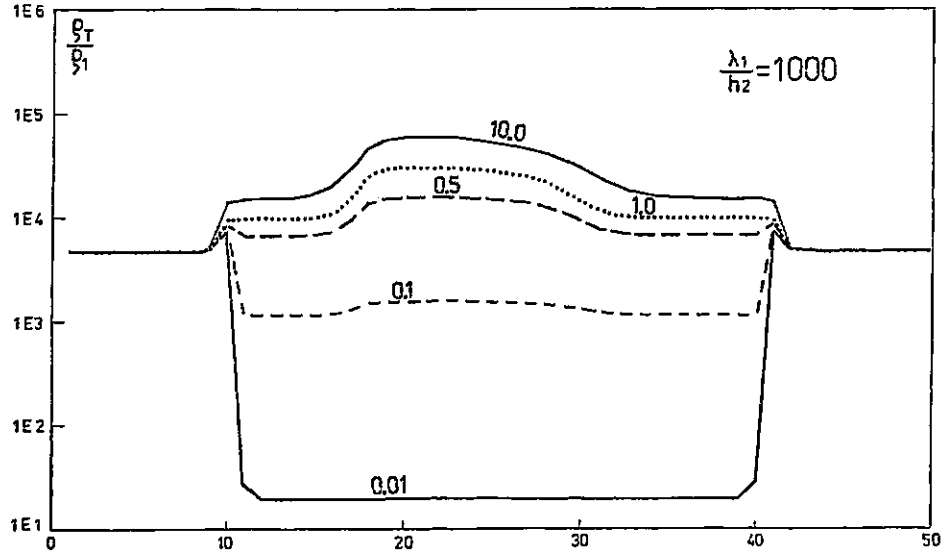

6. Magnetotelluric profiling curves. λ_1/h_1 =1000; parameter of the curves – ρ_2/ρ_1 .

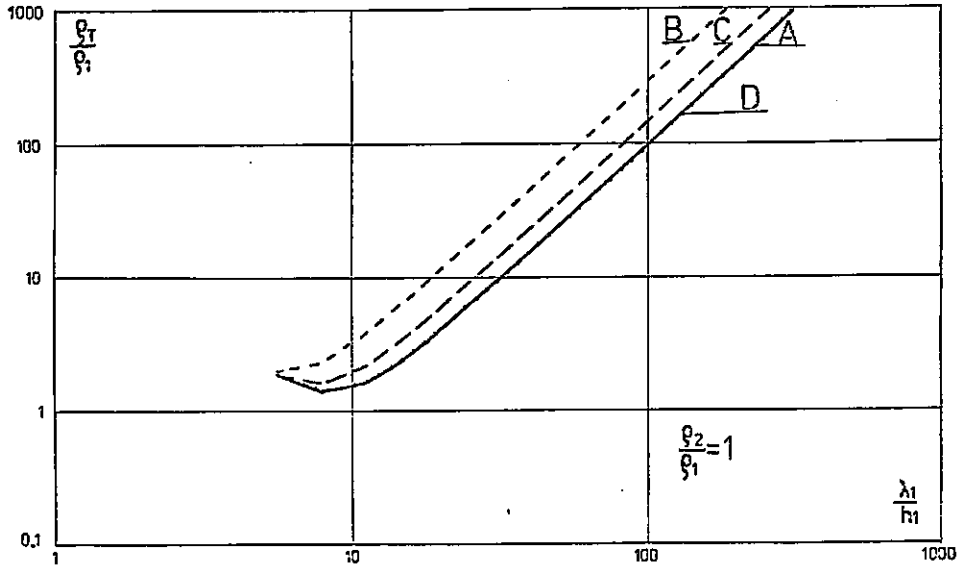

7. Amplitude magnetotelluric sounding curves. ρ_2/ρ_1 = 1; A, B, C, D – sounding sites.

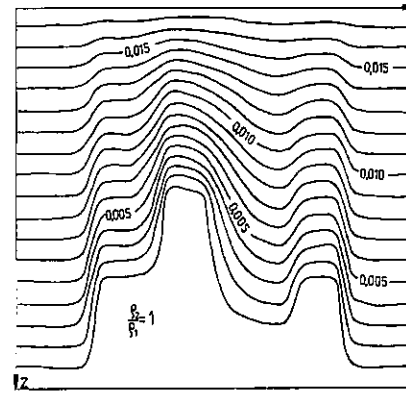

8. The changes of magnetic field intensity. $\rho_2 = \rho_1$; 0.005 – value of isoline of magnetic field intensity; x, z – coordinates of rectangular system.

Low resistivity intermediate layer acts as electromagnetic screen which damps the effects from the basement. The rate of screening depends, of course,on the ratio of layer resistivity to environment resistivity, what is shown in Fig. 6. The presence of high resistivity layer in geoelectric cross-section (particularly for low frequencies) does not lead to significant distortion of the image of high resistivity basement (see Fig. 6).

The sounding curves, computed for various points of the profile, generally behave similarly as in the case of one-dimensional model. The shape of the curves depends mainly on resistivity changes in vertical plane in the sounding point. Right, low resistivity asymptotes of amplitude sounding curves, reflect, first of all, the value of longitudinal conductance of the overburden in the sounding point. The rule does not apply to the sounding sites lying over narrow depressions of high resistivity basement, because of the above mentioned effect of electromagnetic field flowing around the structure (Fig. 7).

The changes of magnetic field amplitude in vertical plane x z are presented in Fig. 8, for geoelectric model without intermediate layer. On lower and upper boundary of the region, magnetic field satisfies the imposed boundary conditions. It is seen from the field image that in the regions where high resistivity horizon lies horizontally, magnetic field for low frequencies changes with depth approximately linearly.

The effect may be possibly used to develop the direct method of computing the depth of high resistivity basement.

K tisku doporučil J.Gruntorád
Přeložil P. Borzemski

References

Kaufman, A. - Keller, G.(1981): The magnetotelluric Sounding Method.– Elsevier. Amsterdam-London-New York.
Piskorek, A. (1980): Rovnanie calkove.- Wyd. Nauk. – Techn., Warszawa.
Rikitake, T. (1960): Electromagnetism and the Earth interior. – Elsevier. Amsterdam-London-New York.
Varga, R.S. (1962): Matrix iterative analysis. – Prentice Hall.

Numerické modelování pole elektromagnetické indukce při magnetické polarizaci

(Resumé anglického textu)

Julius Miecznik - Przemyslaw Borzemski

Předloženo 24. listopadu 1988

Základem pro interpretaci magnetotelurických měření je znalost rozdělení elektromagnetického pole pro dvou- a třírozměrné geoelektrické modely. Pro některé modely je známo analytické řešení, zatímco pro jiné známe pouze diferenciální postupy řešení problému indukce. V případě dvourozměrných modelů musí být elektrická a magnetická polarizace uvažována odděleně. V práci je podrobněji popsán algoritmus pro výpočet elektromagnetického pole, vyvolaného rovinnou vlnou pro případ dvourozměrného modelu a magnetické polarizace. Rozměry a fyzikální parametry modelu jsou volitelné. Výsledkem výpočtu jsou teoretické křivky pro magnetotelurické profilování a sondování. Program byl napsán v jazyce Turbo C pro osobní počítač IBM AT.

Vysvětlivky k obrázkům

1. Dvourozměrný geoelektrický model. x, y, z – pravoúhlý souřadnicový systém; d – šířka nehomogenity; M_N, M_L, M_R - nehomogenní, levostranná a pravostranná oblast; σ_L, σ_R – elektrická vodivost; h_L, h_R - hloubka vysokoodporového podloží.
2. Diagram aproximace Helmholtzovy rovnice. i,j – souřadnice síťových uzlů; Δx, Δz – velikost sítě; k_1, k_2, k_3, k_4 – vlnové číslo; S – plocha sítě.
3. Geoelektrický řez, použitý při výpočtu. 10, 20, 30 – body uzlů sítě; A, B, C, D – umístění sond.
4. Křivky magnetotelurického profilování. d_3/d_2 – 2,39; $\rho_2 = \rho_1$; parametr křivek – relativní délka elektromagnetické vlny.
5. Křivky magnetotelurického profilování. $\lambda_1/h_1 = 1000$; parametr křivek – d_3/d_2; $\rho_2/\rho_1 = 1$.
6. Křivky magnetotelurického profilování. $\lambda_1/h_1 = 1000$; parametr křivek – ρ_2/ρ_1.
7. Křivky amplitud magnetotelurického sondování. $\rho_2/\rho_1 = 1$; A, B, C, D – umístění sond.
8. Změny intenzity magnetického pole. $\rho_2 = \rho_1$; 0,005 – hodnota izolinie intenzity magnetického pole; x, z – souřadnice pravoúhlého systému.

Sborník geologických věd	Užitá geofyzika 25	Pages 101-116	12 figs.	1 tab.	– pl.	Praha 1992 ISBN 80-7075-110-X ISSN 0036-5319

Methodology of geophysical investigations in the area of the Jeseníky Mts.

Metodika geofyzikálních výzkumů v oblasti Jeseníků

Jan Gruntorád[1]-Miloš Karous[1]-Jaroslav Kněz[1]-Vladimír Vacek[1]

Received June 16, 1988

1:50,000
15-11, 12, 13, 14
15-31, 32, 33, 34

Geophysical methods
Mathematical statistics
Jeseník Mts.

Gruntorád, J. - Karous, M. - Kněz, J. - Vacek, V. (1992): Methodology of geophysical investigations in the area of the Jeseníky Mts. – Sbor. geol. Věd, užitá Geofyz., 25, 101–116. Praha.

Abstract: Within the framework of methodology of geophysical investigations in the area of the Jeseníky Mts. mathematical statistics was applied in evaluation of this area. The methods of resultant information content, of discrimination functions, and factor analysis were used. Geoelectric methods, namely the induced polarization method and the transient method were modified in order to achieve large depths of investigation. The procedure for constructing vertical sections of apparent resistivities and chargeabilities was proposed. It was shown that the actual distributions of resistivity and chargeability are best presented by deep vertical sections of standardized resistivities and chargeabilitis in a newly devised way which is described here.

[1]*Přírodovědecká fakulta Univerzity Karlovy, Albertov 6, 128 43 Praha 2*

Introduction

The geological investigation conducted in the Jeseníky Mts. in the years 1975 – 85 were oriented towards resolving actual geological problems. On a smaller scale, also methodological research was carried out to develop the method of mathematical statistics for prediction purposes, an introduction of geoelectric methods with larger depth of investigation, and also new methods of geoelectric data processing.

Delimitation of prospective areas by mathematical statistics methods

Ore prospecting, using geophysical and geochemical methods, is not easy and requires a complex approach. But also the sequence of individual survey phases and the closest possible link with geological data must be taken into consideration. These principles were observed in the course of prospecting in the Jeseníky Mts. There, in the first phase, the survey by gravity, airborne, and geoelectric methods was applied on the scale of 1:25,000 for the purposes of regional hydrogeochemical and lithogeochemical investigation. In the next phase, a complex of geophysical methods was employed in prospective area in a regular network of profiles, on the scale of 1:10,000.

The choice of areas for the expensive complex survey on the scale of 1:10,000 is a very responsible task because it directly influences the success and cost of the prospecting. Owing to methods of mathematical statistics, individual types of geophysical and geochemical fields (indications) can be objectively evaluated and the information contained in them evaluated and summed up in one resultant parameter. Depending on the knowledge of deposits and geology of the investigated area, a larger or smaller number of positive and negative standards can be introduced. Thus an important methodological principle will be observed – the link between geophysical, geochemical fields, and data on the deposits and geology of the area.

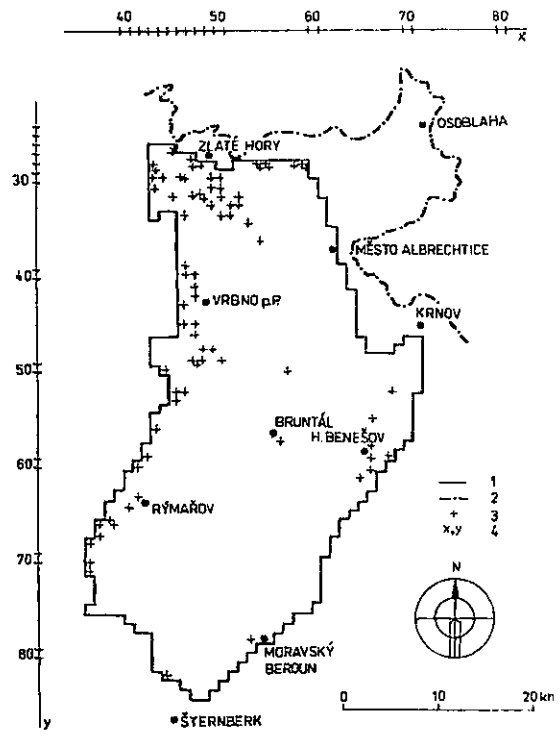

1. Penetration of planes of followed phenomena. 1 – boundaries of the studied area; 2 – state border with Poland; 3 – positive etalon; 4 – coordinates of kilometer square net.

The following methods of mathematical statistics were used for making the deposit prognosis for the Jeseníky Mts.: the method of resultant information content, the method of discrimination functions, and the method of factor analysis.

The investigated area is built of Devonian rocks of the Rejvíz, Vrbno, and Šternberk-Horní Benešov series, of the Culm of the Nízký Jeseník Mts., of neovolcanites, and Quaternary and Neogene sediments. The Variscan hydrothermal Cu-Pb-Zn deposits are the most significant of all ore deposits. The study area is delimited by the intersection of planes (Fig. 1) on which the observed

geophysical indications were detected, i.e. 1– magnetic field (Δ T), 2 – magnetic field pattern, 3 – residual gravity anomaly of zero order,4 – residual gravity anomaly of the third order, 5 – pattern of residual anomalies of zero order, 6 – pattern of residual anomalies of the third order, 7 – residual isostatic anomalies of the third order, 8 – spontaneous polarization field, 9 – spontaneous polarization field pattern, 10 – topofactor; hydrochemical indications: 11 – relative contents of Cu, 12 – of Pb, 13 – of Zn; physical properties of rocks: 14 – porosity, 15 – mineralogical density. The values of geophysical indications were read from a square kilometre grid in 1,200 elementary areas.

According to the method of resultant information content the information contained in each indication is given by the distribution of its positive and negative standards. If no negative standards are specified, the distribution of indications in the whole area can be used instead. The information content of each indication was tested using the Kolmogorov-Smirnov test.

$$D = \max_j \left| F_j^+ - F_j^- \right|$$

where F_j^+ and F_j^- represented relative cumulative frequency of the j^{th} gradation of indication values on positive and negative standards or on positive standards but in the whole area. The mutual dependences of individual indications were evaluated through a correlation matrix.

The resultant information content was obtained by the equations:

$$I_P = \sum_{m=1}^{s} \frac{P(A_{mi}^+)}{P(A_{mi}^-)}, \text{ or } I_L = \sum_{m=1}^{s} \log \frac{P(A_{mi}^+)}{P(A_{mi}^-)}$$

where $P(A_{mi}^+)$ or $P(A_{mi}^-)$ represent the probability of the i^{th} gradation of the m^{th} indication on positive or negative standards, s represents the number of indications from which the parameter is calculated. The probability is expressed by relative frequency. I_P or I_L is calculated for each elementary area on the basis of indication values in that area, and the resulting map is constructed.

The display of results of statistical processing of regional geophysical and geochemical data is variable. The quality of the resulting prediction map depends on the number of indications included and on the manner of calculating the information content which can be, according to the formula chosen, either proportional or logarithmic. Out of the thirty resulting maps, the map of proportional resultant information content of indications 2, 3, 7, 8, and 10 is presented as an example in Fig. 2.

The Zlaté Hory ore district and its broad surroundings, especially the prolongation of the Zlaté Hory ore structure in the SE direction under the Culm sediments are the most conspicuous in the prediction map. Well indicated is also the adjoining part of the Rejvíz series and the whole Devonian Vrbno group stretching in the direction of the towns of Vrbno, Karlova Studánka, Rýmařov, Horní Město to the Upper Moravian depression. Also the Devonian Šternberk-Horní Benešov belt, the deposit of Horní Benešov, and all

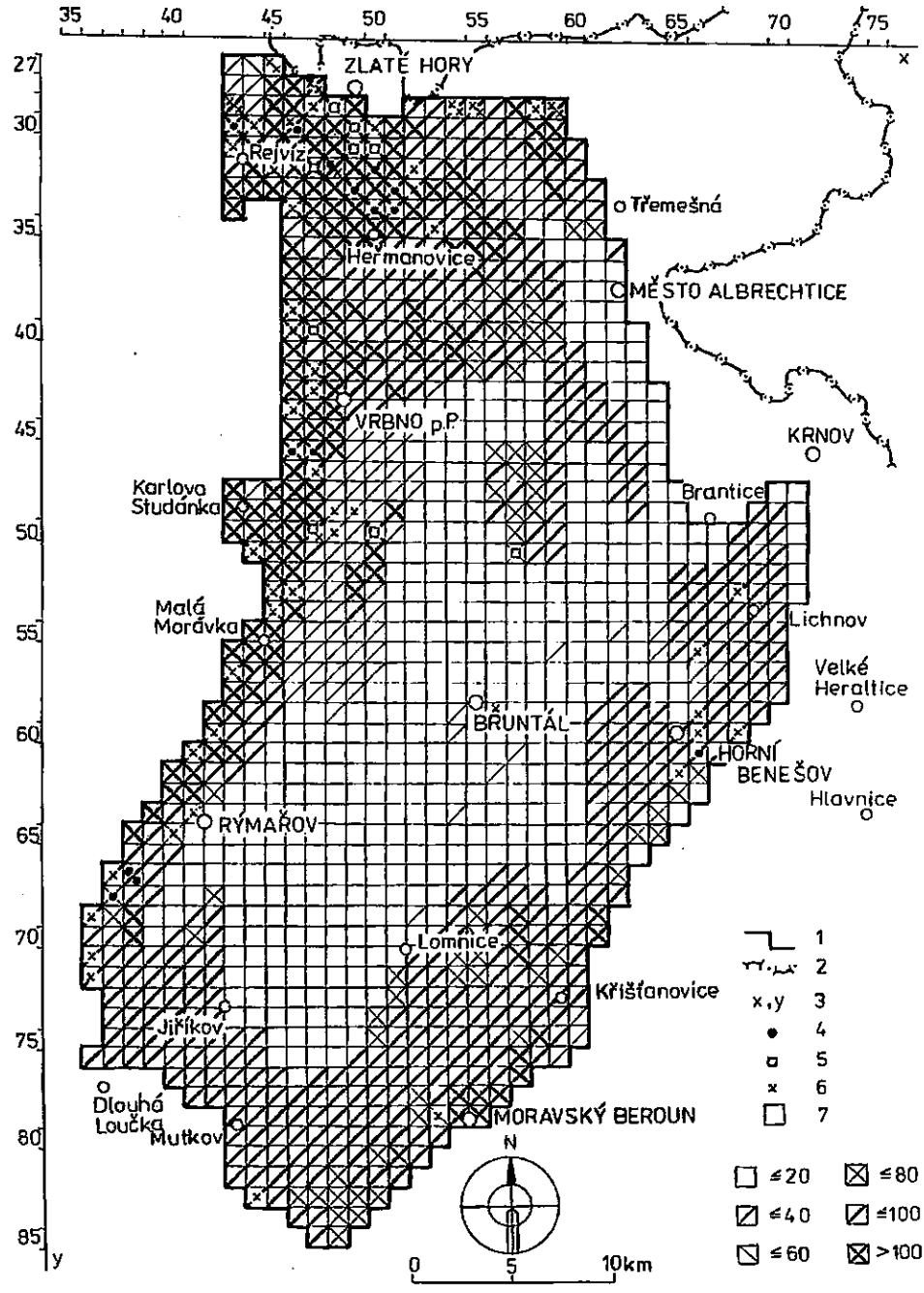

2. Map of summary ratio informativeness of indications 2, 3, 7, 8 and 10. 1 – boundaries of the studied area; 2 – state border with Poland; 3 – coordinate of kilometre square net; 4 – deposit; 5 – ore occurrence; 6 – ore indications; 7 – values of summary informativeness.

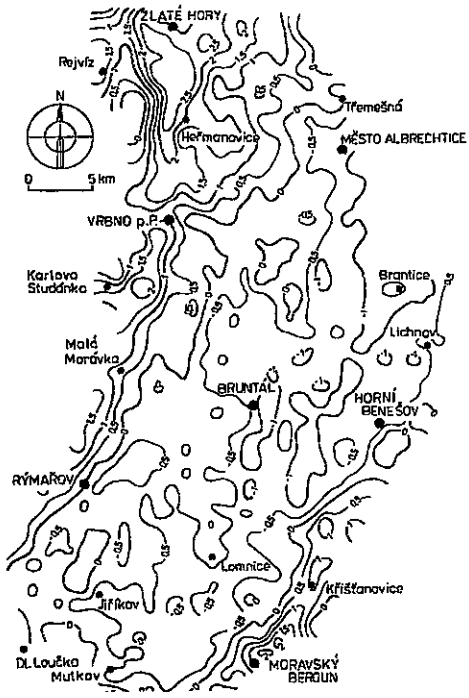

3. Map of isolines of physicochemical factor.

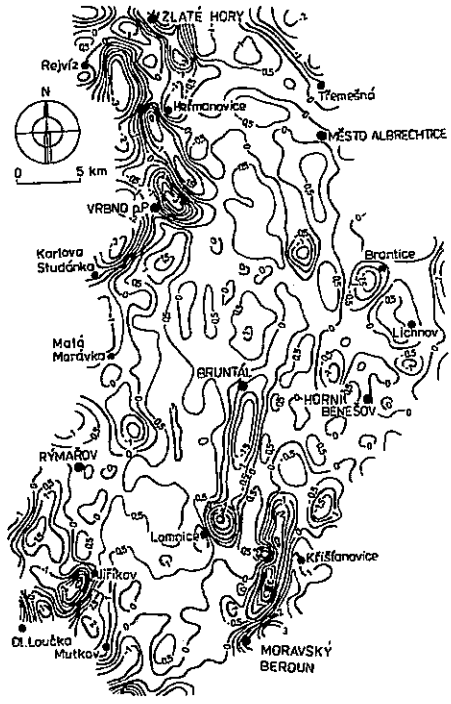

4. Map of isolines of structural tectonic factor.

ore occurrences found in the places with high resultant information content show positive indications. Less conspicuous are the indications west of Třemešná, south of the town of Albrechtice and between the municipalities of Bruntál, Lomnice and Mutkov. These indications are distributed along the boundary between the Andělská Hora and Horní Benešov Culm series. In these places an elevation of the Devonian can be anticipated beneath the Culm.

The results obtained by the method of discrimination functions are similar, the future prospect of individual areas is not, however, graded.

The method of factor analysis was applied on the same basis as the method of resultant information content. Its task is to study the inner structure of covariance matrix obtained from the set of m indications characterizing a certain phenomenon, in this case the geological structure and prospects of the investigated area as to the polymetallic ore deposits. The individual indications are usually statistically interconnected. Some indications can significantly contribute to resolving the problem under study while the remaining ones do not contribute to it at all. It is advisable to reduce the number m of the variables (indications) so that a smaller number p of new variables $(p < m)$ contained as much information from the original non-reduced variables as possible. At the same time it can be assumed that the new variables (factors) gather the initial indications in such a way that they always characterize a certain aspect of the investigated phenomenon.

This assumption is clearly confirmed in contour maps of the resultant factors in Figs. 3 and 4. The factor in Fig. 3 can be regarded as a physical- chemical factor closely related to ore mineralization because a prevailing influence of the spontaneous polarization (electrochemical) method is obvious. The factor in Fig. 4 detects a structural-tectonic situation. Methods reflecting the geological structure (residual gravity anomalies of the third order, Δ T field) contribute to its value most.

The map of contours of the factor in Fig. 3 delimits the area prospective for ores. The results are in agreement with the map of proportioned information content (Fig. 2). However, the delimination of prospective areas is more detailed and the contour pattern is clearer.

Methodology of frequency domain IP measurements

The induced polarization method (IP) is the most important geoelectric method in direct ore prospecting. This is why it was used in all field geophysical investigations in the Jeseníky Mts. The methodological research was focused on the application of frequency domain IP measurements and on the development of modification with great depth of investigation.

The frequency domain IP measurements were carried out using the Canadian device IPRF-2 Scintrex operating at frequencies 0.1, 0.3, 1, and 3 Hz. The correct function of the instrument was verified by laboratory model measurements and by comparative measurements at the Rejvíz-Bleskovec locality. During the following phases frequency domain measurements were carried out in the Jeseníky Mts. at the Zámecký vrch, Vidly, Bleskovec, and Zlaté Hory-Pařenec localities. In general the measurements confirmed the main advantage of IP measurements in frequency domain, that means a three times higher field work productivity and the possibility of obtaining sensible data in areas with high background noise caused by disturbing fields. The only disadvantage of the frequency domain IP method is the influence of induction for resistivities under 100 Ωm. The experience with the application of frequency domain IP measurements in Czechoslovakia were described in detail by Kněz (1980).

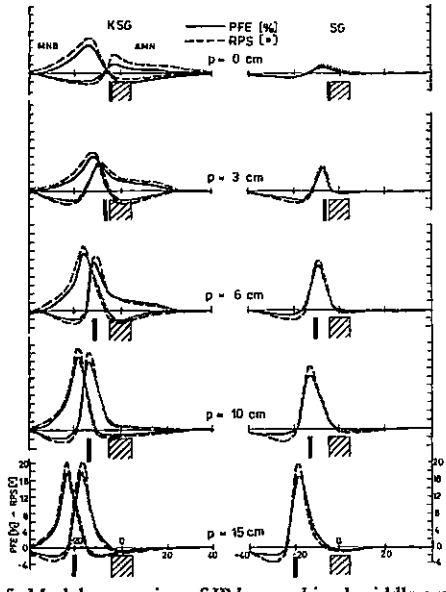

5. Model measuring of IP by combined middle gradient (KSG) and middle gradient (SG) above conductive and nonconductive sheets at variable mutual distance of the sheets *p*.

In order to achieve the greatest possible depth of investigation by the IP method, the electrode arrays with a fixed current circuit are the most advantageous. The corresponding methods are the combined middle gradient method (MG) or the

three-electrode gradient method. Besides the standard middle gradient method which was used at the Zámecký vrch and Bleskovec localities, also the in-line middle gradient method was applied at the Zlatý Chlum locality. Using the in-line middle gradient configuration, maximum IP anomalies can be detected as it was already proved by earlier laboratory model measurements (Kněz 1972).

The combined middle gradient modification represented another improvement in applications. This assumption was verified through a series of laboratory model measurements. The results of model monitoring confirmed the advantages of the combined middle gradient method over the classical middle gradient method, namely at resistivity inhomogeneous environment (Fig. 5). The IP anomalies obtained by the combined middle gradient method are more striking and the position of the conductive body can be much more accurately located by the point of intersection of both branches of the curve. These obvious advantages of the combined middle gradient method outweigh the only disadvantage as compared with the classical middle gradient method, which consists in a more complicated technology of field works (the third grounding electrode is placed in the "infinity"). The combined middle gradient method was used with success at the Supíkovice locality.

Another modification of IP measurements with fixed current circuit is the three-electrode (one pole) gradient profiling which, with regular intervals (200 m) between fixed current electrodes, makes it possible to present the results in the form of depth sections. The way of acquiring and processing the data was described in detail in previous publications and reports (e.g. Gruntorád - Kněz 1973). A number of such measurements were taken in the Zlaté Hory ore district and also at the Vidly locality.

There are several ways of transforming the results of measurements into vertical depth sections: situating the measured value of chargeability (resistivity) to various depths (according to the length of the array) below the current electrode, below the centre of potential electrodes or below the centre between the current electrode and the potential electrodes of the array. However, in all these cases the distribution of anomalous values in the depth section does not correspond to the real position of the sought body as it was proved by model monitoring. That is why another way of presenting the depth sections was sought that would correspond better to real positions of the studied objects. The suggested method of constructing multiple parameters sections makes use of the Komarov method (Komarov 1980) of interpreting the centres of isometric bodies (spheres) from two measurements with current electrodes at different positions (Fig. 6). The body

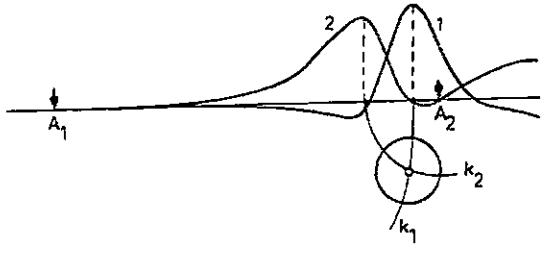

6. Determination of centre position of isometric bodies by IP method at two different positions of a current electrode.

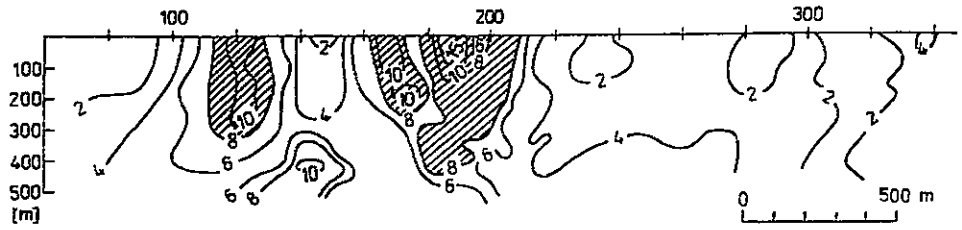

7. Vertical section of standardized polarizabilities at the locality Vidly.

centre lies at the point of intersection of circles whose centres lie in the corresponding current electrodes and the radii are given by the distance of the IP curve maximum. Generalizing this principle the points of intersection of individual circles can be attributed the value of normal product of chargeabilities at corresponding points of curves obtained from measurements in various positions of current electrodes. The values are used for construction of depth sections. This method was used for the processing of measured data at the Vidly locality (Fig. 7). In the depth interval 180 – 200 m the values in the product chargeability section correspond to known ore mineralization. The course of contours indicates its continuation to depth.

Processing of measured resistivity and IP data into vertical sections

The method of constructing vertical sections of apparent chargeability or of apparent resistivity was gradually developed and generalized also for other configurations with mobile current electrodes. To construct sections of normal chargeabilities or resistivities it is necessary to have two values from each point obtained by measurements with current electrodes or current dipoles at two different positions. The sections can therefore be constructed from data obtained by methods using composite arrangements, i.e. the above mentioned combined middle gradient method, combined profiling or dipole profiling.

While with the combined middle gradient method the analysis of both theoretical and model curves showed that the isometric inhomogeneity lies on the circle below the anomaly extreme, with other electrode configuration the curve differs from the circle (Fig. 8b).

The position of the anomalous object must therefore be sought at the point of intersection of the two curves corresponding to two different positions of grounding the current electrodes. It is possible to construct vertical normal pseudosections manually using the above mentioned curves but it is not suitable to process them by computer.

For computer processing it is convenient to record the values of normal chargeabilities at the points P_{ij} defined by positions x_{ij} on the profile and by depths h_{ij} below the measured profile

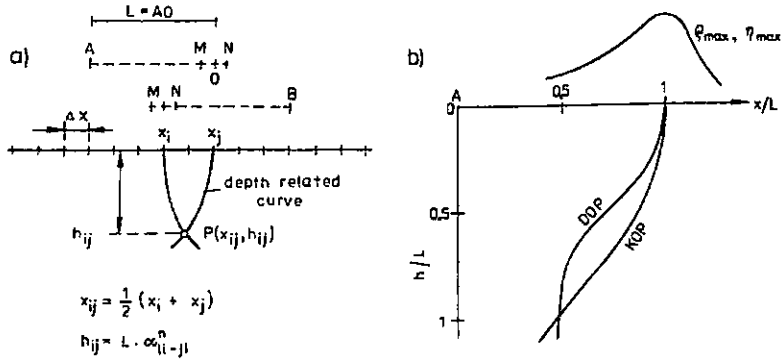

8. Principles of construction of vertical sections of standardized polarizabilities or standardized resistivities from a combined dipole-dipole profiling. a – position of points P_{ij} in vertical section below the measured profile, b – so called depth-related curves for localization of an isometric body below the anomaly extreme.

$$\eta_n = \frac{\eta_{zA}\,(x_j)\,.\,\eta_{zA}\,(x_i)}{\eta_{zO}}$$

or to record the values of normal resistivity

$$\rho_n = \frac{\rho_{zA}\,(x_j)\,.\,\rho_{zB}\,(x_i)}{\rho_{zO}}$$

where $\eta_{zA}\,(x_j)$ and $\rho_{zA}\,(x_j)$ correspond to measurements at the point x_j with grounding at point A (at dipole measurements it is the centre of current dipole) and the values $\eta_{zB}\,(x_i)$ and $\rho_{zB}\,(x_i)$ correspond to measurements at the point x_i with grounding at point B. The values η_{zO} and ρ_{zO} are the estimated mean values on a certain profile or in a certain area.

In the vertical sections below the profile the positions of points P_{ij} are specified by coordinates (Fig. 8a):

$$x_{ij} = \frac{1}{2}\,(x_i + x_j) = \frac{i+j}{2}\Delta x\,,\; x_i = i.\,\Delta x,\; x_j = j.\,\Delta x$$

$$h_{ij} = h_m = L.\,\alpha^n_{j-i} = L.\alpha^n_m\,,\; n = j - i,$$

where $n = L/\,\Delta\,x$ is the ratio of the measurement interval $\Delta\,x$ and the array length $L = AO = OB$ (with combined profiling) or $L = OO' = AM = BN$ (with dipole profiling). Depth coefficients α^n_m are derived from depth curves for isometric inhomogeneity and listed in Table 1.

Table 1. Depth-related coefficients α_m^n

combine profiling						dipole profiling					
m =	n =					m =	n =				
	3	4	5	6	7		3	4	5	6	7
0	0.00	0.00	0.00	0.00	0.00	0	0.00	0.00	0.00	0.00	0.00
1	0.54	0.47	0.42	0.39	0.36	1	0.38	0.32	0.28	0.25	0.23
2	0.77	0.66	0.60	0.54	0.50	2	0.54	0.46	0.42	0.38	0.34
3	0.99	0.92	0.73	0.66	0.62	3	0.92	0.58	0.50	0.46	0.42
4		0.99	0.85	0.77	0.72	4		0.91	0.62	0.54	0.49
5			0.99	0.88	0.80	5			0.91	0.66	0.56
6				0.99	0.89	6				0.92	0.68
7					0.99	7					0.91

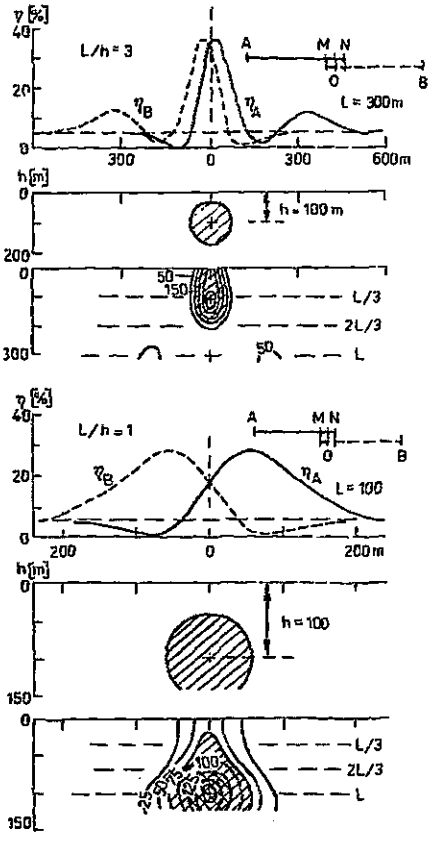

9. Standardized vertical pseudo-sections of polarizability derived from theoretical curves of combined profiling above isometric polarized body at two different ratios of the length of arrangement to the depth of body center *L/h*.

The above ways of the vertical section construction were verified by processing the chargeability curves above isometric bodies for various electrode arrangements (combined middle gradient and dipole profiling). For example, there are sections of normal chargeabilities above the sphere derived from combined profiling surveys in two different modifications :

a) for the array length L much greater than anomalous body depth (Fig. 9a), and

b) for the L, the same as the depth (Fig. 9b).

In both cases the contour patterns in normal chargeability sections correspond, unlike in classical sections, to the anomalous body shape. Extreme values in sections define almost precisely a centre of the disturbing body. This conclusion holds also for other electrode arrangements.

The distribution of normal chargeability values or of resistivities in sections correspond very well to an actual physical section even under very complicated circumstances. In Fig. 10 vertical section of normal resistivities from the locality Rejvíz is presented as an example, together with interpreted geological profile.

In conclusion the suggested way of processing tested in the Jeseníky Mts. areas promising as it is another step to objectivization of geophysical data interpretation.

Methodology of measurements by the transient EM method

The transient EM method is an inductive electromagnetic method for ore prospecting. It is one of electromagnetic methods which have recently undergone a rapid development both from the instrument and the interpretation point of view. The ground, airborne and well logging versions of this method are used worldwide. The method can be used for direct prospecting for conductive ore bodies and for resolving structural problems in sedimentary basins.

So far only ground variant of the method has been used in Czechoslovakia due to lack of instrumentation. The methodology was oriented towards direct prospecting for single conductive geological bodies (Vacek 1979). The time constant τ of the conductive body, which characterizes the quality of the conductor, was studied as a function of the conductive body shape. From profile curves it is possible to deduce, under favourable conditions, the shape, extent and depth of the conductive body. As interpretation processes and technical equipment abroad were improved, transient EM sounding is more and more used. The sounding can be carried out either in a far or in a near zone.

The principle of the transient EM sounding in the far zone is very similar to that of frequency sounding. Magnetic and electric field components of the horizontal field of the electric dipole are registered most frequently. The values of the electric field

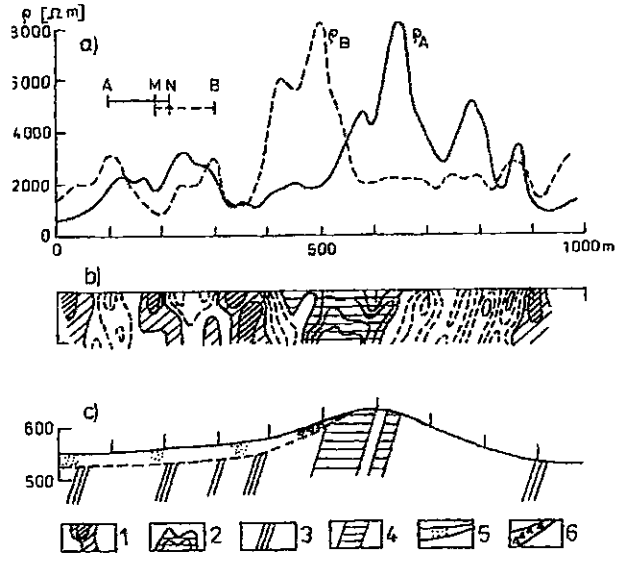

10. Example of standardized vertical resistivity pseudo-section derived from terrain measuring using combined profiling at the locality Rejvíz.
a – resistivity curves of combined profiling; b – vertical resistivity standardized section; c – interpreted geological section;
1 – conductors in isoohmic section; 2 – non-conductors in isoohmic section; 3 – interpreted conductive sheets (graphitized rocks); 4 – interpreted non-conductive sheets (quartzitic rocks); 5 – weathering products of graphitized rocks in eluvium; 6 – debris of quartzitic rocks.

component and time derivation of the magnetic field component do not depend on time in the wave zone. The wave zone is given by the equation:

$$u = r\sqrt{\frac{\sigma\mu}{2}t} >> 1$$

where r is the interval between the generating (electrical) and measuring (magnetic) dipole, the interval corresponding approximately to the depth of the investigated interfaces, σ is the conductivity, t is the time and μ is the magnetic permeability. The registration point is in the middle of the arrangement. At discrete times induced voltage $\varepsilon(t)$ is registered. Values $\varepsilon(t)$ for different times t and calculated resistivities ρ_τ correspond to various depths of investigation. For the interpretation asymptotes and extreme points on the curves are used.

In remote zone, sounding is, in regard to the large size of the arrangement, unsuitable. A way of measuring in near zone for small distances between source circuit and measuring circuit was therefore developed. At first, electric dipole was used as a source. Vertical magnetic element was measured. This methodology is very sensitive to changes in inclination of the underlying rock and therefore it was abandoned. Nowadays the loop-loop systems are largely used. The most common arrangement is a concrete configuration of emitting and receiving loops of equal dimensions. In this case EMS $e(t)$ induced in the measuring loop for $\mu << 1$ can be defined by the equation (valid only for thin conductive layer)

$$e(t) = \frac{3M_G M_M}{16S\pi} F, \quad F = \left(H + \frac{t}{\mu_0 S}\right)^{-4}$$

where $M_G = L^2 I$ and $M_M = l^2$ are the moments of the generating and measuring loops,

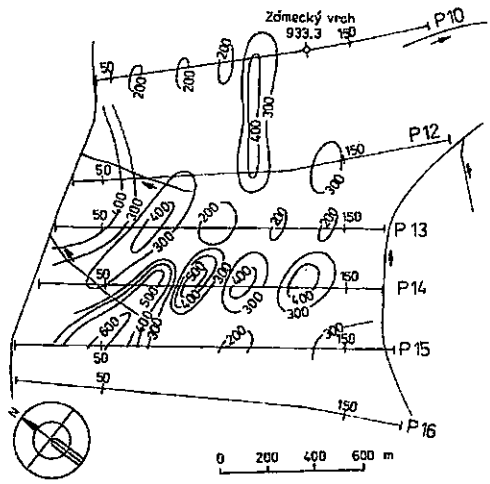

11. Transient electromagnetic method, map of isolines ρ_τ [Ω m] for t = 1 [ms], locality Zámecký vrch.

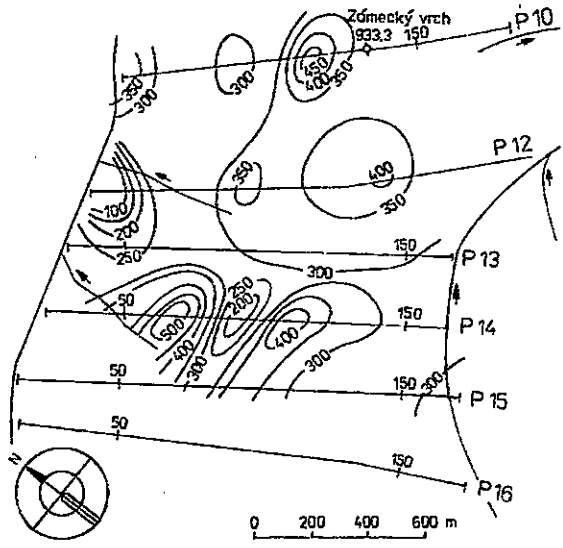

12. Transient electromagnetic method, map of isolines H_τ [m] for locality Zámecký vrch.

L and l are the side lengths of the generating and measuring loops and I is the current flowing through the generating loop. S is the longitudinal conductivity of the layer and H is the depth of the position of equivalent conductive layer. The solution of the $e(t_i)$ and $e(t_{i+1})$ set of equations provides us with expressions for longitudinal conductivity S and for the corresponding depth H (Isajev 1979).

$$S = \frac{2}{\mu_0}\left(\frac{2\pi}{3 M_G M_M \mu_0}\right)^{\frac{1}{3}} \left(\frac{t_{i+1} - t_i}{\frac{1}{e(t_{i+1})^{\frac{1}{4}}} - \frac{1}{e(t_i)^{\frac{1}{4}}}}\right)^{\frac{4}{3}}$$

$$H = \left(\frac{3 M_G M_M}{16 \pi S e(t_i)}\right)^{\frac{1}{4}} - \frac{t_i}{\mu_0 S}$$

In this case of sounding for isometric bodies and generally deposited sheet-like bodies extreme points on the sounding curve (t_{min}, $\rho_{\tau\,min}$) are used to determine the depth of conductive objects.

The measurements carried out at the Zámecký vrch locality in the Jeseníky Mts. exemplify the use of the above described method. The measurements were carried out along five profiles P10 – P15 using the Soviet device MPP-3 with a 100 x 100 m loop. Different kinds of gneisses are mapped on the whole territory. Only ends of profiles P10 and P12 reach the area where quartzites are mapped. In the study area the average noise

level was found out to be about 8 μV, which is quite low. In Fig. 11 the course of apparent resistivity ρ_τ is shown. The course of conductive structures depths is in Fig. 12 where the isolines H_τ are depicted. In the western part of the investigated area comparatively regular variations of conductive plane depths can be observed. It may be due to e.g. several slab-like or lenticular conductive bodies that are dipping roughly in the southeast direction. The conductive zone can occasionally be folded. In order to confirm the interpreted data, it would be necessary to carry out measurements in a denser grid and to measure the transition characteristics at earlier and later times which could be done with a better-quality Soviet device Impuls-C.

If the time constant τ, which reaches the maximum value of 9,6 ms on profile 15 at 150 m, is used for the interpretation there is either an inconspicuous ore mineralization or several conductive zones reflecting tectonic lines or resistivity inhomogeneities in rocks.

It can be said that the first results of sounding with the transient EM method suggest new possibilities of this method in ore prospecting and in resolving some structural-geological problems.

Conclusions

In the course of investigations in the area of the Jeseníky Mts. the following main results were obtained:

a) It was proved that the mathematical statistics methods can markedly contribute to the prognosis concerning the evaluation of areas where regional geophysical and geochemical data are at disposal. It is possible to evaluate the contribution of individual methods to the resolution of the given problem and to delimit prospective areas for detailed geophysical investigations.

b) The induced polarization method is the most important geoelectric method for ore prospecting. Advantages and disadvantages of IP frequency measurements were verified and higher productivity of field measurements using its modifications was proved. The method can successfully be applied also in areas with high industrial noise. In order to study the depth of polarizable bodies it is recommended to use either three-electrode gradient or combined middle-gradient profiling methods.

c) Vertical sections of normal resistivities and chargeabilities can be constructed using the data obtained by the three electrode gradient profiling, combined middle gradient method, and combined and dipole profiling. The proposed way of processing the data provides resistivity and chargeability patterns which are close to reality.

d) In the course of research in the methodology of TM measurements a new way of interpretation was proposed for the construction of contour maps of apparent resistivities and of depths to conductive bodies. Time constant can be used to determine the character of the studied conductor.

K tisku doporučil J. Daňko
Přeložila D. Maliková

References

Gruntorád, J. (1977): Geophysical research of the Jeseníky Mts. – Univ. Carol., Geol., 162. Praha.

Gruntorád, J. – Kněz, J. (1973): Parametrická měření metodou vyzvané polarizace v jižním pokračování zlatohorské rudní struktury. – Geofyzikální výzkum Jeseníků, Univ.Karl., 88-96. Praha.

Gruntorád, J. – Karous, M. – Kněz, J. (1986): Vertical cross-sections in the induced polarization method. – EAEG, 48th Meeting, Abstracts of Papers, 129-130. Ostende.

Isajev, G.A. (1979): Metoditcheskije rekomendaciji po komplexnoj interpretaciji geofizitcheskich dannych pri poiskach rudnych mestorozhdenij. – SNIIGGIMS, 77. Novosibirsk.

Kameneckij, F. M. (1976): Rukovodstvo po primeneniju metoda perechodnych processov v rudnoj geofizike. – Nedra, 127. Moskva.

Kněz, J. (1972): Současný stav a perspektivy rozvoje metody vyzvané polarizace v rudní prospekci. – Sborník Hornická Příbram ve vědě a technice, sekce užitá geofyzika, 12. Příbram.

Kněz, J. (1980): Zkušenosti s aplikací frekvenčního měření v ČSSR. – 7. celostátní konference geofyziků, sborník referátů, sekce geoelektrika a radiometrie, 5. Gottwaldov.

Komarov, V. A. (1980): Elektrorazvedka metodom vyzvanoj polarizacii. – Nedra, 392. Leningrad.

Rudová, A. (1980): Ocenění perspektivnosti průzkumu na základě statistického zpracování geofyzikálních podkladů. Rigorózní práce. – MS přírodověd. fak. Univ. Karl. Praha.

Stehlík, E. (1980): Vymezení oblastí nadějných na výskyt Cu-Pb-Zn ložisek na základě statistického zpracování geofyzikálních a ložiskově-geologických podkladů z oblasti Nízkého Jeseníku. Habilitační práce. – MS přírodověd. fak. Univ. Karl. Praha.

Vacek, V. (1979): Jednosmyčková varianta metody přechodových jevů. – Geol. Průzk., 21, 70-73. Praha.

Metodika geofyzikálních výzkumů v oblasti Jeseníků

(Resumé anglického textu)

Jan Gruntorád - Miloš Karous - Jaroslav Kněz - Vladimír Vacek

Předloženo 16. června 1988

V rámci metodických geofyzikálních výzkumů v Jeseníkách byly ověřeny možnosti metod matematické statistiky při prognózním ocenění ploch, na nichž jsou k dispozici kompletní geofyzikální a geochemické podklady. Byly použity metody sumárních informativností, diskriminačních funkcí a faktorové analýzy.

Dále byly rozpracovány geoelektrické metody s velkým hloubkovým dosahem, především metoda vyzvané polarizace a metoda přechodových jevů. Byly navrženy postupy měření vhodné ke konstrukci vertikálních řezů zdánlivých polarizovatelností. Bylo zjištěno, že nejlepší představu o skutečném rozložení odporů a polarizovatelnosti poskytují vertikální hloubkové řezy normovaných měrných odporů a polarizovatelností, konstruovaných nově navrženým způsobem.

Vysvětlivky k tabulce a obrázkům

Tabulka 1. Hloubkové koeficienty α_m^n.

1. Průnik ploch sledovaných příznaků. 1 – hranice zpracovávaného území,2 – státní hranice s Polskem,3 – kladný etalon, 4 – souřadnice kilometrové čtvercové sítě.
2. Mapa sumární podílové informativnosti příznaků 2, 3, 7, 8 a 10. 1 – hranice zpracovávaného území, 2 – státní hranice s PLR, 3 – souřadnice kilometrové čtvercové sítě, 4 – ložisko, 5 – rudní výskyt, 6 – rudní indicie, 7 – hodnoty sumární informativnosti.
3. Mapa izolinií fyzikálně chemického faktoru.
4. Mapa izolinií strukturně tektonického faktoru.
5. Modelová měření VP kombinovaným středovým gradientem (KSG) a středovým gradientem (SG) nad vodivou a nevodivou deskou při proměnné vzájemné vzdálenosti desek p.
6. Určení polohy středu izometrických těles metodou VP při dvou různých polohách proudové elektrody.
7. Hloubkový řez normovaných polarizovatelností na lokalitě Vidly.
8. Princip konstrukce vertikálních řezů normovaných polarizovatelností příp. normovaných měrných odporů z kombinovaného a dipólového profilování. a – poloha bodů P_{ij} ve vertikálním řezu pod měřeným profilem, b – tzv. hloubkové křivky pro lokalizaci izometrického tělesa pod extrémem anomálie.
9. Normované vertikální pseudořezy polarizovatelnosti odvozené z teoretických křivek kombinovaného profilování nad izometrickým polarizujícím se objektem při dvou různých poměrech délky uspořádání k hloubce středu objektu L/h.
10. Příklad normovaného vertikálního odporového pseudořezu odvozeného z terénního měření kombinovaným profilováním na lokalitě Rejvíz. a – odporové křivky kombinovaného profilování, b – vertikální odporový normovaný řez, c – interpretovaný geologický řez.
    1 – vodiče v izoohmickém řezu, 2 – nevodiče v izoohmickém řezu, 3 – interpretované vodivé polohy (grafitizované horniny), 4 – interpretované nevodivé polohy (kvarcitické horniny), 5 – zvětraliny grafitizovaných hornin v eluviu, 6 – sutě kvarcitických hornin.
11. Metoda PJ, mapa izolinií ρ_τ [Ω m], pro t = 1 [ms], lokalita Zámecký vrch.
12. Metoda PJ, mapa izolinií H_τ [m] , lokalita Zámecký vrch.

Sborník geologických věd	Užitá geofyzika 25	Pages 117–143	33 figs.	1 tab.	– pl.	Praha 1992 ISBN 80-7075-110-X ISSN 0036-5319

Detection of horizontal sheets by electromagnetic conductometers

Detekovatelnost horizontálních deskovitých těles pomocí elektromagnetických konduktometrů

Richard Záhora[1]

Received April 11, 1990

1 : 50,000
24 - 32, 24 - 33
25 - 13, 25 - 33

Electromagnetic prospection
Conductivity
Archaeological application

Záhora, R. (1992): Detection of horizontal sheets by electromagnetic conductometers. – Sbor. geol. Věd, užitá Geofyz., 25, 117–143. Praha.

Abstract: The electromagnetic method with small induction number is applied to direct and contactless measurement of apparent conductivity of magnetic dipoles in a near field. The detection of sufficiently large horizontal conducting and non-conducting sheets with vertical and horizontal magnetic dipoles is explained and the detectability curves are drawn. Detectability of small-size inhomogeneities is discussed and estimated. The method has been applied in archaeological prospection.

[1]*Geofyzika,a. s., Brno, Ječná 29a, 612 46 Brno*

Introduction

The direct contactless measurement of rock resistivities is based on the dependences of the measured components of electromagnetic field on apparent resistivity of an equivalent conducting half-space. These dependences are much more simple if the induction number $N = r/\delta$ is small (or if there is a near zone), i.e. the skin depth δ is much greater than the transmitter-receiver separation and than the thickness of a horizontally layered half-space, i.e.

$$N = \frac{r}{\delta} << 1\,, \quad \frac{h_i}{\delta} << 1 \tag{1}$$

where $\delta = \sqrt{2/\omega\mu\sigma}$ is the depth of skin.

Direct contactless measurement of apparent conductivity

Let us consider a vertical transmitter-receiver magnetic dipole array located on the surface of a horizontally layered conducting half-space, as it is illustrated in Fig. 1. The conductivity of the layers is σ_i and their thickness is h_i. Let us assume that the condition of a small induction number given by equations (1) is satisfied. Then approximately

$$\frac{\dot{v}}{v_0} = 1 + j\,\frac{\omega\,\mu\,\sigma_a}{4}\,r^2 \tag{2}$$

where $\dot{v}$ is complex amplitude of voltage in the receiver induced by the total vertical magnetic field,
v_0 amplitude of voltage induced in the receiver only by the primary (direct) magnetic field, i.e. in an entirely non-conducting space,
ω angular frequency of current I in the transmitter dipole,
r transmitter-receiver separation,
$\mu = \mu_0 = 4\pi \,.\, 10^{-7}\ H/m$ permeability of the medium,
and σ_a apparent conductivity for a horizontally layered conducting half-space (Fig. 1)

$$\sigma_a = \sum_{i=1}^{n} \sigma_i\, Q_i \tag{3}$$

Coefficients Q_i are called geometric factors (for the vertical component of the magnetic field) as they only depend on the thickness of individual layers h_i and on the distance r between the dipoles. They are given (Kaufmann-Keller 1983) by equations

$$Q_1 = 1 - R(\tau_1)$$

$$Q_i = R(\tau_{i-1}) - R(\tau_i) \tag{4}$$

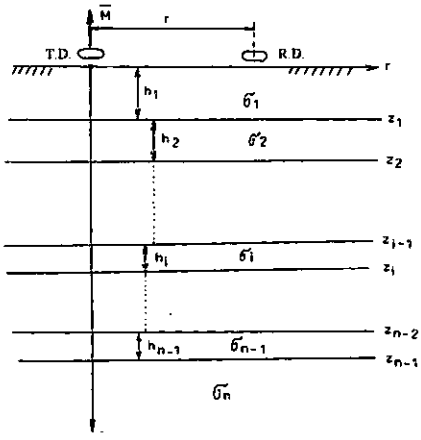

1. Vertical magnetic dipoles over a horizontally layered half-space.

for $i = 2, 3, 4 \ldots\ldots n-1$, $Q_n = R(\tau_{n-1})$
where the function $R(\tau_i)$ for vertical dipole array

$$R(\tau_i) = R_v(\tau_i) = \frac{1}{\sqrt{4\tau_i^2 + 1}} \tag{5}$$

where $\tau_i = z_i/r$ normalized depth level,
$z_i = h_1 + h_2 + \ldots\ldots h_i$ depth of the foot of i-th layer.

From equation (2) follows

$$\frac{\dot{v} - v_0}{v_0} = \frac{\Delta \dot{v}}{v_0} = \frac{\dot{H}_z^s}{H_z^0} = j \frac{\omega \mu \sigma_a}{4} r^2 = j \frac{H_z^s}{H_z^0}$$

i.e.

$$\sigma_a = \frac{4}{\omega \mu r^2} \frac{H_z^s}{H_z^0} = \frac{4}{\omega \mu r^2} \frac{|\Delta \dot{v}|}{v_0} \tag{6}$$

where $\dot{H}_z^s = j \frac{\omega \mu M}{16 \pi r} \sum_{i=1}^{n} \sigma_i Q_i$ (7)

is the complex amplitude of the vertical component of the secondary magnetic field in the receiver induced by eddy curents in a layered conducting half-space

$$H_z^0 = \frac{M}{4 \pi r^3} \tag{8}$$

is the amplitude of the vertical component of the primary magnetic field in the receiver induced by current in the transmitter only,

The secondary component of the magnetic field carries information on apparent conductivity. In regard to the primary component (current in the dipole) it is shifted in phase by $\pi/2$ and it is directly proportional to apparent conductivity. That is the principle of measurement of apparent conductivity with magnetic dipoles in the near field (induction conductometers). Induction conductometers are e.g. EM-31, EM-38, M-34 of Geonics Ltd., Canada and DIKO of Geofyzika Brno, Czechoslovakia. Their form depends on the required depth range. These devices facilitate geoelectric measurements at shallow depths in electromagnetic profiling and in some cases in electromagnetic sounding.

The input signal voltage $\Delta \dot{v}$ as well as the measured apparent conductivity (or vertical component of the secondary magnetic field $\dot{H}_z^s$) are given by the sum of n-terms (eqs. 3,6 and 7). Each term of the sum corresponds to a layer and is defined by its geometric factors and conductivity. We may afford this simplification because eddy currents in individual elementary horizontal layers of a conducting half-space are independent. The magnetic field of eddy currents in the surrounding medium, with small induction number, can be neglected. A change of conductivity in one horizontal layer will only cause a change of current in the layer and will affect neither the geometry of current lines, nor current densities in other layers. Therefore, the measured apparent conductivity is given by the sum of independent contributions of individual layers on the assumption that each contribution is dependent on the depth of the respective layer, its thickness and conductivity.

As it follows from eqs. (4), (7) or (3), the function R (τ_i) denotes a relative independent contribution to the secondary magnetic field (or measured apparent conductivity) of the medium as a whole under the normalized level τ_i. Its derivative then determines the dependence of the relative contribution of a unit layer at the normalized depth τ, which for vertical magnetic dipoles is

$$F_v(\tau) = \frac{4\tau}{\left[4\tau^2 + 1\right]^{\frac{3}{2}}} \tag{9}$$

Relationships analogous to eqs. (5) and (9), characterizing relative independent contributions, can be written for horizontal magnetic dipoles (coplanar):

$$R_H(\tau_i) = \sqrt{4\tau_i^2 + 1} - 2\tau_i \tag{10}$$

$$F_H(\tau) = 2 - \frac{4\tau}{\sqrt{4\tau^2 + 1}} \tag{11}$$

The above simplifications following from the condition of the so called "small induction number" considerably simplify solution of the direct problem, in this case calculation of apparent conductivity of the studied medium (particularly a horizontally layered half-space) as well as solution of the inverse problem in some simple cases.

Detectability of horizontal sheets

Functions $F_V(\tau)$ and $F_H(\tau)$ illustrated in Fig. 2 demonstrate that the depth of the layer affects each type of dipole array in different way. Functions $R_V(\tau_i)$ and $R_H(\tau_i)$ which are used for a simple calculation of apparent conductivity of a horizontally layered medium are illustrated in Fig. 3. The rather simple analytical representation of these curves greatly simplifies solution of many practical problems, e.g. the problem of detectability of horizontally layered conducting or non-conducting sheets.

Fig. 4 presents a model of this problem including assumed profiles of apparent conductivity for conducting and non-conducting bodies exhibiting rotational symmetry. Horizontal dimensions of sheet l with thickness d and depth h are considered sufficiently large compared with the distance between dipoles, i.e. $l >> r$. The maximum apparent conductivity σ_{aMAX} at $\sigma_2 > \sigma_1$ (conducting body) and the minimum apparent

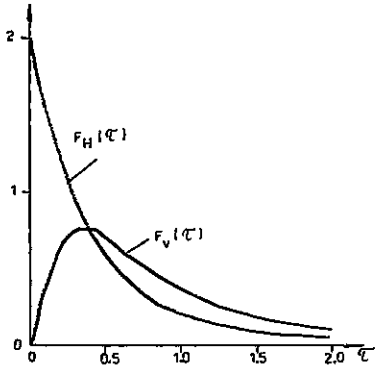

2. Dependence of the relative response to the secondary magnetic field of a unit layer on its normalized depth for vertical $F_V(\tau)$ and horizontal $F_H(\tau)$ magnetic dipoles.

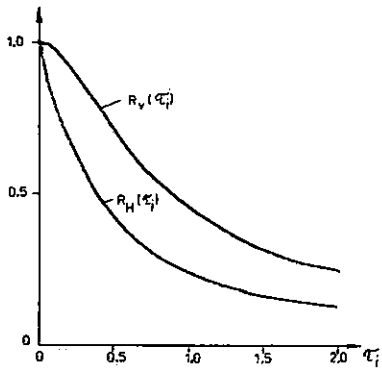

3. Relative contribution to the secondary magnetic field from below to normalized depth level τ_i for vertical $R_v(\tau_i)$ and horizontal $R_H(\tau_i)$ magnetic dipoles.

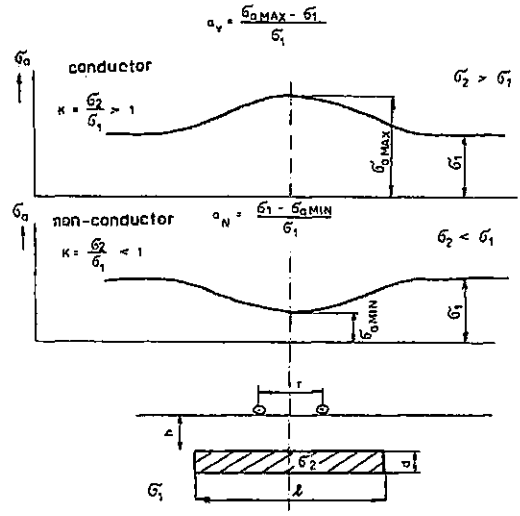

4. Model for specification of conditions for detecting a horizontally layered sheet.

conductivity σ_{aMIN} at $\sigma_2 < \sigma_1$ (non-conducting body) will obviously appear above the centre of the body (Fig. 4).
Let us denote

$$\frac{\sigma_2}{\sigma_1} = \frac{\rho_1}{\rho_2} = k \qquad \text{conductivity contrast}$$

$$H = \frac{h}{r} \qquad \text{normalized depth of the sheet}$$

$$\Delta = \frac{d}{r} \qquad \text{normalized thickness of the sheet} \quad (12)$$

The magnitudes of conductivity anomalies (amplitudes of anomalies) are defined by

$$a_v = \frac{\sigma_{aMAX} - \sigma_1}{\sigma_1} \quad (13)$$

for a conducting body (positive anomaly)

$$a_N = \frac{\sigma_1 - \sigma_{aMIN}}{\sigma_1} \quad (14)$$

for a non-conducting body (negative anomaly).

The conditions of detectability will be characterized by the dependence of the normal-

ized thickness of the sheet on its normalized depth for induction of a conducting anomaly of the fixed magnitude $a_v(a_N)$ at a given conductivity contrast k, i.e.

$$\Delta = f(H) \tag{15}$$

for parameters $a_v(a_N)$, k.

These dependences will be established for a conducting and for a non-conducting body, at vertical and horizontal magnetic dipole array.

Anomalies of conducting bodies

Above the centre of a sufficiently large sheet ($l >> r$) the apparent conductivity will presumably be the same as over a half-space formed by three layers with conductivities σ_1 and σ_2, and σ_1 the thickness of the middle layer d. Then the maximum apparent conductivity, regarding eqs. (3) and (4), is

$$\sigma_{aMAX} = \sigma_1 [1 - R(H)] + \sigma_2 [R(H) - R(H+\Delta)] + \sigma_1 R(H+\Delta)$$

Reducing it, with regard to (13), we get

$$R(H) - R(H+\Delta) = \frac{a_v}{k-1} = v \tag{16}$$

for $k > 1$.

A/ Vertical magnetic dipoles

From eqs. (16) and (5) it follows that

$$v = R_v(H) - R_v(H+\Delta) = \frac{1}{\sqrt{4H^2+1}} - \frac{1}{\sqrt{4(H+\Delta)^2+1}}$$

Hence

$$\Delta = -H + \frac{1}{2} \sqrt{\frac{4H^2+1}{\left[1 - \frac{a_v}{k-1}\sqrt{4H^2+1}\right]^2} - 1} \tag{17}$$

The limits of changes of argument H follow from the inequations $\Delta > 0$

$$1 > \frac{a_v}{k-1}\sqrt{4H^2+1}$$

hence

$$H \leq \frac{1}{2}\sqrt{\left(\frac{k-1}{a_v}\right)^2 - 1} = H_{MAX} \tag{18}$$

For amplitudes of anomalies and conductivity contrasts corresponding to real conditions the obtained H_{MAX} is sufficiently large and always exceeds the actual depth range of vertical magnetic dipoles.

B/ Horizontal magnetic dipoles

From eqs. (16) and (10) follows

$$v = \frac{a_v}{k-1} = R_H(H) - R_H(H+\Delta) = \sqrt{4H^2+1} - 2H - \left[\sqrt{4(H+\Delta)^2+1} - 2(H+\Delta)\right]$$

hence

$$\Delta = \frac{\left(\frac{a_v}{k-1}\right)^2 - 2\frac{a_v}{k-1}\sqrt{4H^2+1}}{4\left[2H + \frac{a_v}{k-1} - \sqrt{4H^2+1}\right]} \tag{19}$$

To satisfy the condition $\Delta > 0$

$$\left(\frac{a_v}{k-1}\right)^2 < 2\frac{a_v}{k-1}\sqrt{4H^2+1} \quad , 2H + \frac{a_v}{k-1} < \sqrt{4H^2+1}$$

must be true, or inverse inequations, which will never be satisfied for the considered magnitudes of anomalies and conductivity contrasts. Then

$$H < \frac{1 - \left(\frac{a_v}{k-1}\right)^2}{4\frac{a_v}{k-1}} = H_{MAX} \tag{20}$$

In this way limited depths are sufficient and in almost all cases exceed the maximum depth of horizontal dipoles, which is generally half the depth of vertical dipoles.

Anomalies of non-conducting bodies

A non-conducting sheet (if $l >> r$) induces minimum apparent conductivity (Fig. 4) above its centre. The minimum can be defined by a three-layer model. Then

$$\sigma_{a\,MIN} = \sigma_1 [1 - R(H)] + \sigma_2 [R(H) - R(H+\Delta)] + \sigma_1 R(H+\Delta)$$

Considering eq. (14)

$$R(H) - R(H+\Delta) = \frac{a_N}{1-k} = u \tag{21}$$

for $k<1$.

Equations (16) and (21) differ only by constants u, v on their right-hand sides. Substituting u for v for vertical magnetic dipoles (if $k<1$), we get

$$\Delta = -H + \frac{1}{2}\sqrt{\frac{4H^2+1}{\left[1-\frac{a_N}{1-k}\sqrt{4H^2+1}\right]^2} - 1} \tag{22}$$

$$H \leq \frac{1}{2}\sqrt{\left(\frac{1-k}{a_N}\right)^2 - 1} = H_{MAX} \tag{23}$$

for $k<1$.

Similarly for horizontal magnetic dipoles

$$\Delta = \frac{\left(\frac{a_N}{1-k}\right)^2 - 2\frac{a_N}{1-k}\sqrt{4H^2+1}}{4\left[2H + \frac{a_N}{1-k} - \sqrt{4H^2+1}\right]} \tag{24}$$

$$H < \frac{1-\left(\frac{a_N}{1-k}\right)^2}{4\frac{a_N}{1-k}} = H_{MAX} \tag{25}$$

All electromagnetic methods detect conductors much better than non-conductors. It is so with our electromagnetic method for direct and contactless measurement of apparent conductivity. Let us consider two sheets with the same geometry and depths. First of them is conducting ($k > 1$), the second is non-conducting ($k < 1$). The conductivity contrast in (16) for a conducting sheet will be $k = k_V > 1$ and in (21) for a non-conducting sheet $k = k_N < 1$.

Then

$$R(H) - R(H+\Delta) = \frac{a_V}{k_V - 1} \text{ (for } k_V>1), \qquad R(H) - R(H+\Delta) = \frac{a_N}{1-k_N} \text{ (for } k_N<1).$$

The left-hand sides of the equations are equal, assuming that their thicknesses Δ and depths H are the same. We shall also assume that in regard to the surrounding medium both sheets have the same, though reciprocal, conductivity contrasts, i.e. $k_V = 1/k_N > 1$.

Then

$$\frac{a_V}{k_V - 1} = \frac{a_N}{1-k_N} = \frac{a_N}{1-\frac{1}{k_V}} = \frac{k_V a_N}{k_V - 1} \tag{26}$$

i.e. $a_v = k_v \, . \, a_N$.

The conducting body induces k_v-times larger anomaly than the non-conducting body at the conductivity contrasts $k_v = 1/k_N > 1$.

Small-size sheets

The detectability problem for small bodies whose size is comparable or smaller than the distance between dipoles will be considerably more difficult to resolve as it requires use of multidimensional models. Záhora in Hašek et al. (1988) calculated the response for induction conductometers of a small cylindrical body with rotational symmetry whose axis is identical with the axis of the transmitter dipole, and discussed its detectability. Apparent resistivity over a model consisting of n rotational symmetry areas Ω_i; in a conducting finite cylindrical body of the normalized height τ_N , shown in Fig. 5, approximating a non-finite conducting half-space, is given by the relationship

$$\sigma_a = \sum_{i=1}^{n} \sigma_i \, W_i$$

where $$W_i = \frac{1}{\varphi_N} \iint_{\Omega_i} g\,(\xi, \tau)\, d\xi \, d\tau \qquad (27)$$

is the geometric factor for the i-th area Ω_i.

Then

$$g\,(\xi, \tau) = 2 \frac{\xi}{\left[\xi^2 + \tau^2\right]^{3/2}} \cdot \frac{1}{\sqrt{(1+\xi)^2 + \tau^2}} \left[K(\nu) + \frac{\xi^2 - 1 - \tau^2}{(1-\xi)^2 + \tau^2} E(\nu) \right] \qquad (28)$$

where $K(\nu)$, $E(\nu)$ are elliptic 1st and 2nd kind integrals

$$K_{(\nu)} = \int_0^{\pi/2} \frac{d\alpha}{\sqrt{1 - \nu^2 \sin^2 \alpha}} \qquad E_{(\nu)} = \int_0^{\pi/2} \sqrt{1 - \nu^2 \sin^2 \alpha} \; d\alpha$$

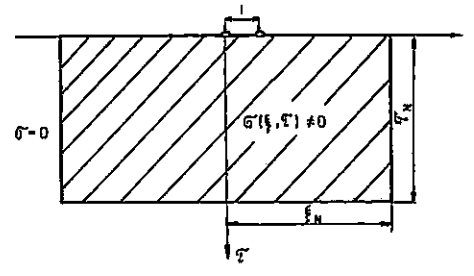

5. Model substituting the conducting half-space under the measuring dipole system.

where

$$\nu = \frac{2\sqrt{\xi}}{\sqrt{(1+\xi)^2 + \tau^2}}$$

By numerical integration it has been confirmed that for sufficiently high surface integral upper limits τ_N, ξ_N (over 10)

$$\varphi_N = \varphi(\xi_N, \tau_N) = \int_{\tau_L}^{\tau_N} \int_0^{\xi_N} g(\xi, \tau)\, d\tau \quad \rightarrow \pi$$

where ξ, τ..... cylindrical coordinates (normalized variables)

τ_L..... an arbitrary small positive number.

Then

$$R(\tau_i) = 1 - \frac{1}{\varphi_N} \int_{\tau_L}^{\tau_i} \int_0^{\xi_N} g(\xi, \tau)\, d\xi\, d\tau \tag{29}$$

Equation (29) for a sufficiently high ξ_N is in agreement with the corresponding function for the 1-D model given by equation (5). Substituting (28) into (27), we get the geometric factor for small-size inhomogeneities having small, even negative, values. It implies poor detectability of small-size, namely non-conducting inhomogeneities. Such bodies can induce conductivity inversion, depending on their thickness and depth. It means that a conducting inhomogeneity produces a negative anomaly and a non-conducting inhomogeneity a positive anomaly. The conductivity inversion is due to a negative geometric factor. This relates to the geometry of an inhomogeneity and to the considered measuring system, as it is obvious from the distribution of the secondary magnetic field increases in the receiver dipoles due to eddy current conductors within the inhomogeneous body and in the surrounding environment. Inversion does not take place in vertical dipoles (e.g. in well-logging), and does not relate to non-linear dependence of the quadrature component of the secondary magnetic field on apparent conductivity when with increasing real conductivity of the environment over a certain limit the measured apparent conductivity decreases to negative values (as it can be observed in field measurements with induction conductometers).

In a conducting inhomogeneity the absolute value of the anomaly is

$$a_v = |a| = |W| \quad |k-1| \gg |W| \qquad \text{for } k \gg 1$$

while a non-conducting inhomogeneity induces the anomaly

$$a_N = |a| = |W| \quad |1-k| < |W|$$

The maximum absolute value of an anomaly induced by a non-conducting inhomogeneous body ($k<1$) is always limited by the corresponding geometric factor $|W|$. Anomalies due to conducting bodies are generally large.

To estimate the detectability of small horizontal sheets, we shall introduce some

simplifications. First, we shall assume a cylindrical body with the diameter l. It will also be assumed that the space under the dipoles, from the greater part (e.g. 90%) contributing to the secondary magnetic field, is cylindrical with the diameter p. Further we shall assume that all elementary parts of a particular elementary cylinder of the diameter p, height dh and depth h equally participate in the relative contribution of this elementary cylinder, with weight coefficients σ_1 or σ_2. On these rather "rough assumptions" the maximum apparent conductivity (for $p > l$) of a conducting body ($k > l$) is given by the relationship

$$\sigma_{a\,MAX} = \sigma_1 [1 - R(H) + R(H+\Delta)] + [R(H) - R(H+\Delta)] \frac{\sigma_2 \frac{\pi}{4} l^2 + \sigma_1 \frac{\pi}{4} (p^2 - l^2)}{\frac{\pi}{4} p^2} \tag{30}$$

and its minimum value for a non-conducting body ($k < 1$) is given by the same relationship when $\sigma_{a\,MAX}$ on the left-hand side is substituted by $\sigma_{a\,MIN}$
Reducing (30), we get

$$R(H) - R(H+\Delta) = v_p \qquad \text{for } k > 1 \tag{31}$$

$$\text{where } v_p = \frac{a_V m^2}{k-1} = m^2 v \tag{32}$$

$m = p/l$ and

$$R(H) - R(H+\Delta) = u_p \qquad \text{for } k < 1 \tag{33}$$

$$\text{where } u_p = \frac{a_N m^2}{1-k} = m^2 u. \tag{34}$$

Equations (31), (16) and (33), (21) characterizing anomalies of conducting and non-conducting bodies differ by constants v, v_p, u, u_p only. Equations for "infinite" bodies can therefore be used for estimating the detectability of small bodies by substituting v_p for v and u_p for u.

Detectability curves

The detectability curves defined by eqs. (17), (19), (22) and (24), and by corresponding equations for $m>1$ were calculated with the HP 9845A computer for conducting and non-conducting bodies and for both dipole arrays for large ranges of anomaly amplitudes, conductivity contrasts and coefficients m. Some of the curves are presented in Figs. 6 to 24.

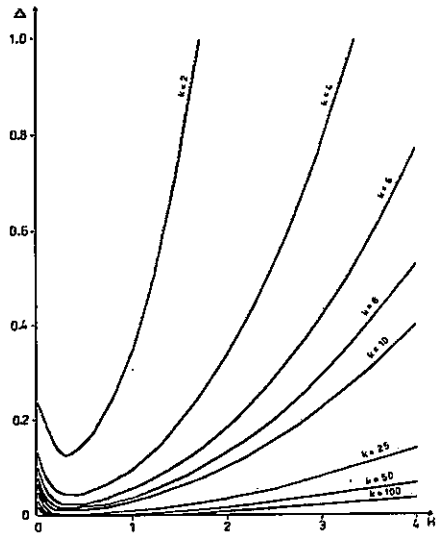

6. Dependence of the normalized thickness of a conducting body on its normalized depth for anomaly $a = 0.1$, $m = 1$ and conductivity contrasts $k = 2$, 4, 6, 8, 10, 25, 50, 100. Vertical magnetic dipoles.

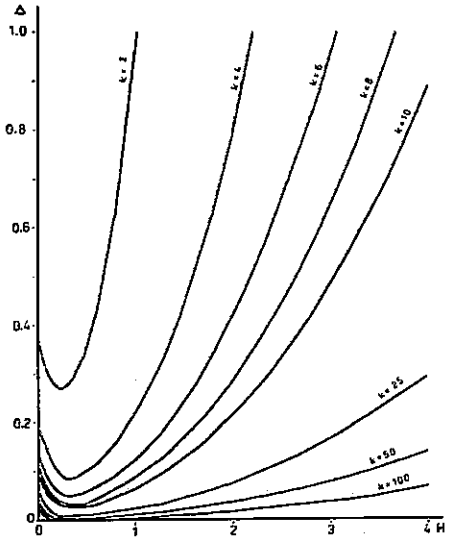

7. Dependence of the normalized thickness of a conducting body on its normalized depth for anomaly $a = 0.2$, $m = 1$ and conductivity contrasts $k = 2$, 4, 6, 8, 10, 25, 50, 100. Vertical magnetic dipoles.

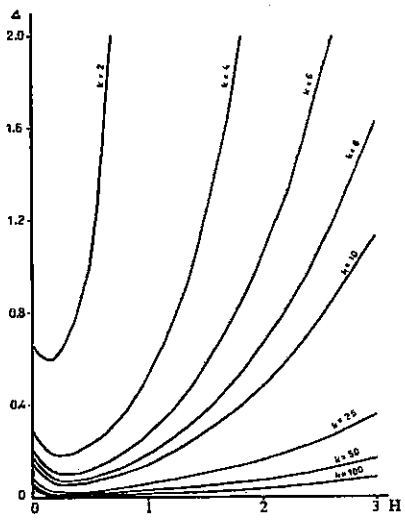

8. Dependence of the normalized thickness of a conducting body on its normalized depth for anomaly $a = 0.4$, $m = 1$ and conductivity contrasts $k = 2$, 4, 6, 8, 10, 25, 50, 100. Vertical magnetic dipoles.

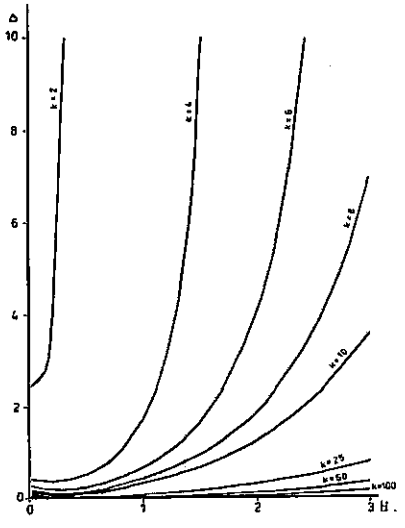

9. Dependence of the normalized thickness of a conducting body on its normalized depth for anomaly $a = 0.8$, $m = 1$ and conductivity contrasts $k = 2$, 4, 6, 8, 10, 25, 50, 100. Vertical magnetic dipoles.

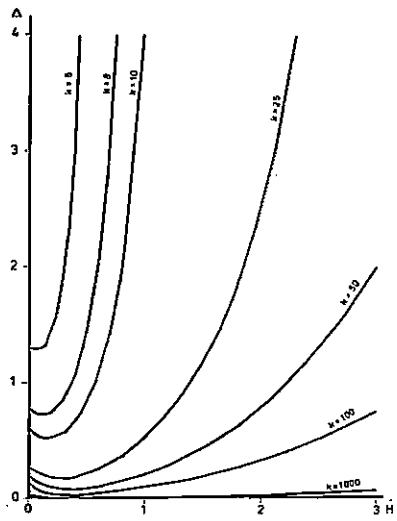

10. Dependence of the normalized thickness of a conducting body on its normalized depth for anomaly $a = 0.2$, $m = 4$ and conductivity contrasts $k = 6$, 8, 10, 25, 50, 100, 1000. Vertical magnetic dipoles.

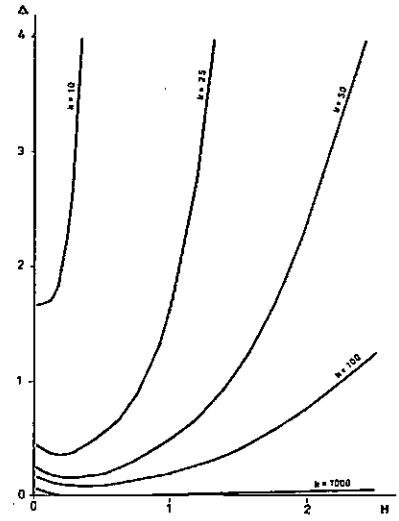

Fig. 11. Dependence of the normalized thickness of a conducting body on its normalized depth for anomaly $a = 0.4$, $m = 4$ and conductivity contrasts $k = 10$, 25, 50, 100, 1000. Vertical magnetic dipoles.

The coefficient m characterizes the horizontal dimension of a body exhibiting rotational symmetry. It is $m = 1$ for $l >> r$. Greater values of m correspond to small bodies whose horizontal dimension is comparable or smaller than the distance between coils. Figures 6 to 11 show the detectability curves for conducting bodies at vertical dipole array, amplitudes $a_V = 0.1$, 0.2, 0.4, 0.8 and a large range of conductivity contrasts. Two values of parameter m are taken for comparison – 1 and 4.

Figs. 12 and 13 demonstrate the considerable influence of amplitude and parameter m on detectability curves if $k = 10$.

For horizontal dipoles and conducting bodies similar curves are drawn in figs. 14, 15, 16 and 17 for $m = 1$, 2, 5, amplitudes 0.2 and 0.6, and for the corresponding range of conductivity contrasts. Detectability curves for non-conducting bodies for both dipole configurations for amplitudes $a_N = 0.05$, 0.1 and 0.2, coefficients $m = 1{,}2$ and conductivity contrasts 1/2, 1/4, 1/6, 1/10, 1/50, 10^{-6} are in Figs. 18 to 24.

The dependence on amplitude and coefficient m can be observed on all curves, see Figs. 12 and 13, and in the case of conducting bodies also on the conductivity contrast k. For instance, with vertical magnetic dipoles at $m = 1$, $k_N = 1/50$ a large negative anomaly $a_N = 0.2$ over a nonconducting sheet at the relative depth $H = 1$ can be created if the relative thickness of the body $\Delta = 1$, for $a_N = 0.1$ over a sheet at the same depth the thickness $\Delta = 0.36$ (i.e. 2.8 times smaller) and for $a_N = 0.05$ the thickness must be only $\Delta = 0.16$ (i.e. 6.3 times smaller). All curves confirm that it is much easier to detect conducting rather than non-conducting bodies. For instance, in the case of vertical

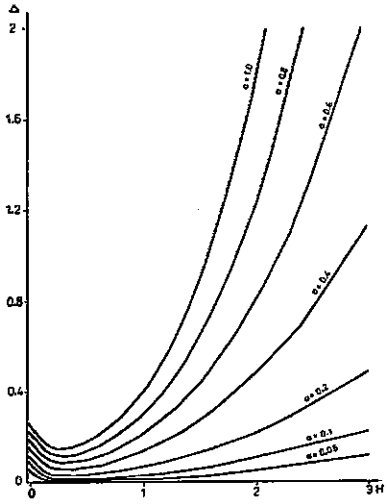

12. Dependence of the normalized thickness of a conducting sheet on its normalized depth for conductivity contrast $k = 10$, $m = 1$ and anomalies $a = 0.05, 0.1, 0.2, 0.4, 0.6, 0.8, 1$. Vertical magnetic dipoles.

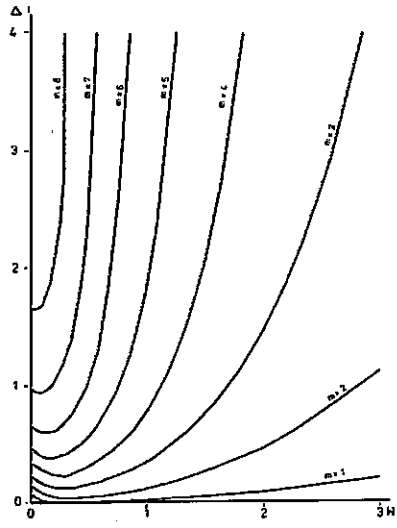

13. Dependence of the normalized thickness of a conducting sheet on its normalized depth for anomaly $a = 0.1$,conductivity contrast $k = 10$ and $m = 1, 2, 3, 4, 5, 6, 7, 8$. Vertical magnetic dipoles.

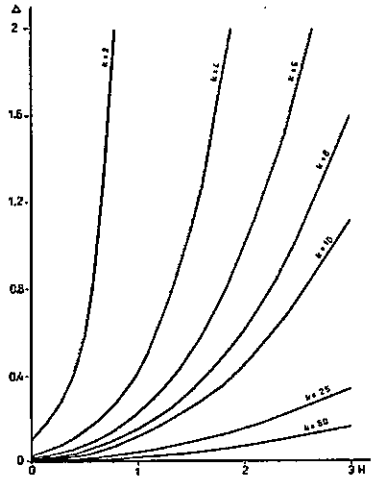

14. Dependence of the normalized thickness of a conducting body on its normalized depth for anomaly $a = 0.2$, $m = 1$ and conductivity contrasts $k = 2, 4, 6, 8, 10, 25, 50$. Horizontal magnetic dipoles.

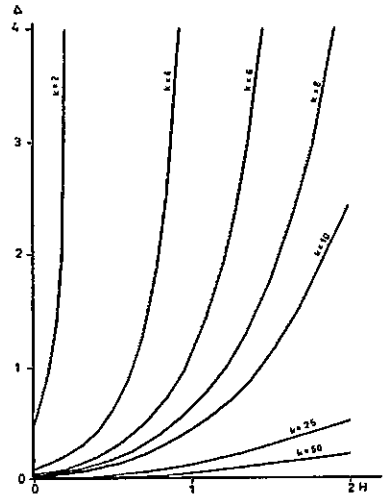

15. Dependence of the normalized thickness of a conducting body on its normalized depth for anomaly $a = 0.6$, $m = 1$ and conductivity contrasts $k = 2, 4, 6, 8, 10, 25, 50$. Horizontal magnetic dipoles.

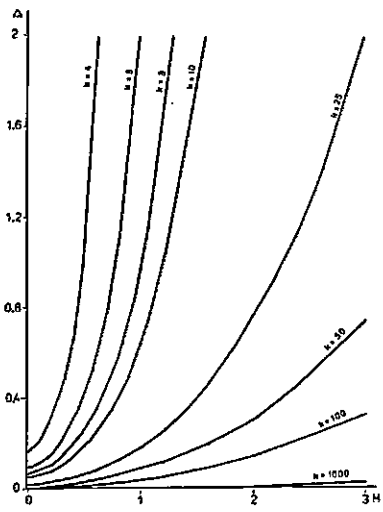

16. Dependence of the normalized thickness of a conducting sheet on its normalized depth for anomaly $a = 0.2$, $m = 2$ and conductivity contrasts $k = 4$, 6, 8, 10, 25, 50, 100, 1000. Horizontal magnetic dipoles.

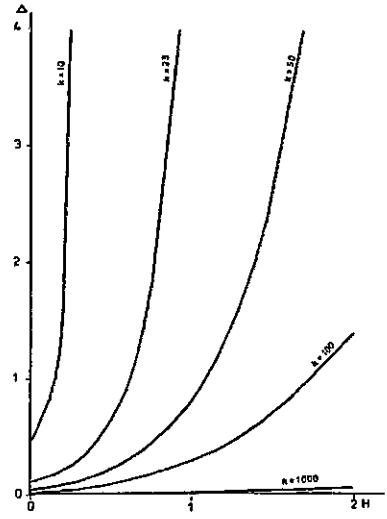

17. Dependence of the normalized thickness of a conducting sheet on its normalized depth for anomaly $a = 0.2$, $m = 5$ and conductivity contrasts $k = 10$, 25, 50,100, 1000. Horizontal magnetic dipoles.

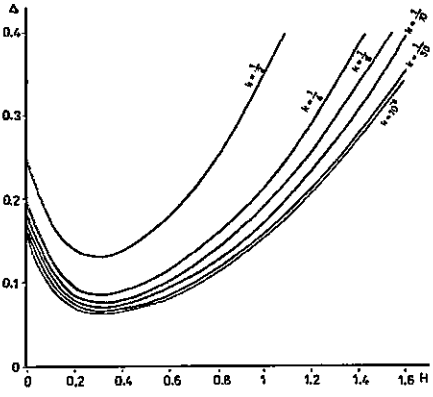

18. Dependence of the normalized thickness of a non-conducting sheet on its normalized depth for anomaly $a = 0.05$, $m = 1$ and conductivity contrasts $k = 1/2$, 1/4, 1/6, 1/10, 1/50, 10^{-6}. Vertical magnetic dipoles.

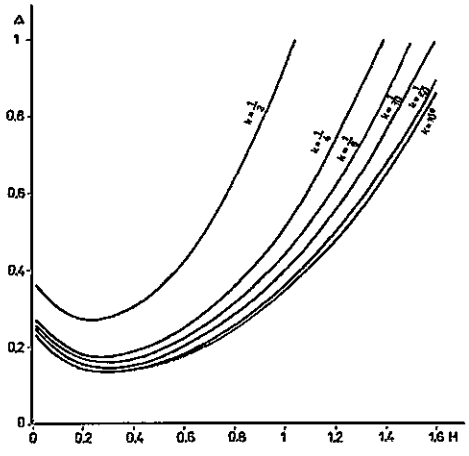

19. Dependence of the normalized thickness of a non-conducting sheet on its normalized depth for anomaly $a = 0.1$, $m = 1$ and conductivity contrasts $k = 1/2$, 1/4, 1/6, 1/10, 1/50, 10^{-6}. Vertical magnetic dipoles.

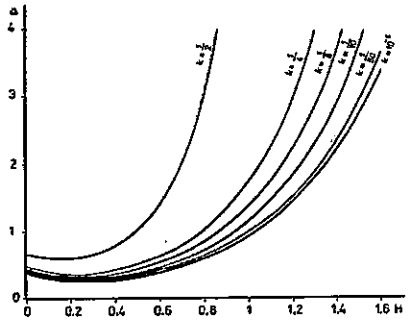

20. Dependence of the normalized thickness of a non-conducting sheet on its normalized depth for anomaly $a = 0.2$, $m = 1$ and conductivity contrasts $k = 1/2, 1/4, 1/6, 1/10, 1/50, 10^{-6}$. Vertical magnetic dipoles.

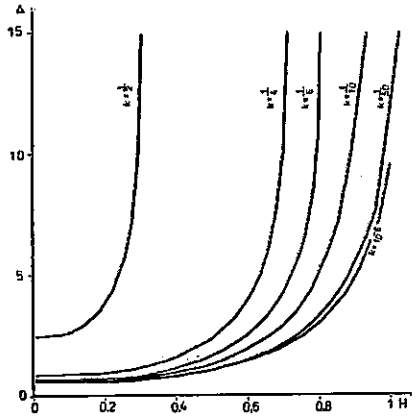

21. Dependence of the normalized thickness of a non-conducting sheet on its normalized depth for anomaly $a = 0.1$, $m = 2$ and conductivity contrasts $k = 1/2, 1/4, 1/6, 1/10, 1/50, 10^{-6}$. Vertical magnetic dipoles.

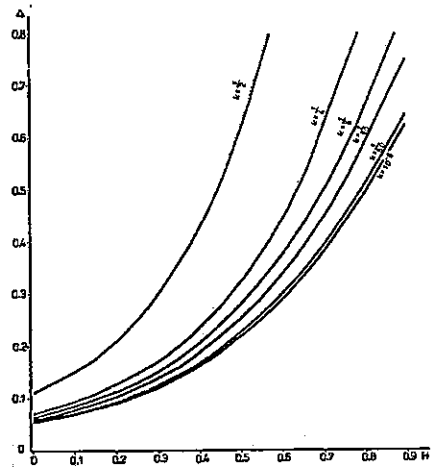

22. Dependence of the normalized thickness of a non-conducting sheet on its normalized depth for anomaly $a = 0.1$, $m = 1$ and conductivity contrasts $k = 1/2, 1/4, 1/6, 1/10, 1/50, 10^{-6}$. Horizontal magnetic dipoles.

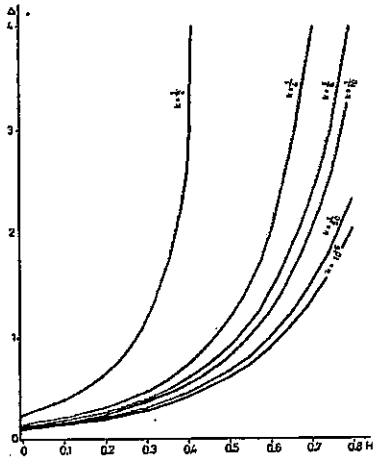

23. Dependence of the normalized thickness of a non-conducting sheet on its normalized depth for anomaly $a = 0.2$, $m = 1$ and conductivity contrasts $k = 1/2, 1/4, 1/6, 1/10, 1/50, 10^{-6}$. Horizontal magnetic dipoles.

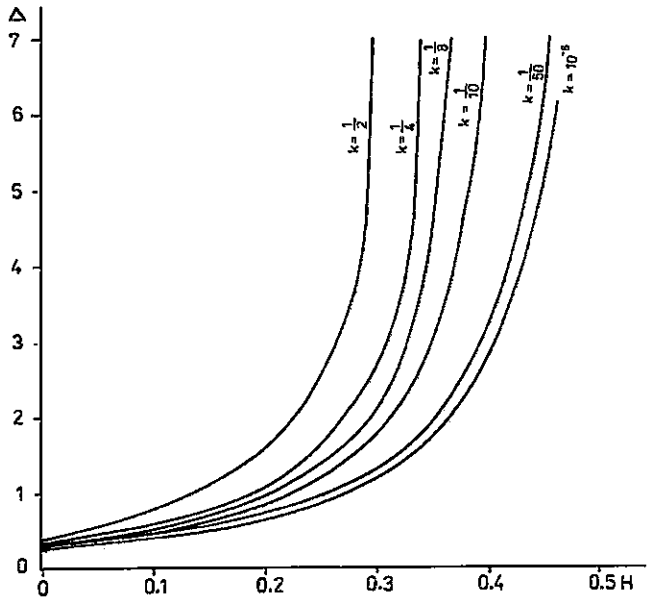

24. Dependence of the normalized thickness of a non-conducting sheet on its normalized depth for anomaly $a = 0.1$, $m = 2$ and conductivity contrasts $k = 1/2, 1/4, 1/6, 1/10, 1/50, 10^{-6}$. Horizontal magnetic dipoles.

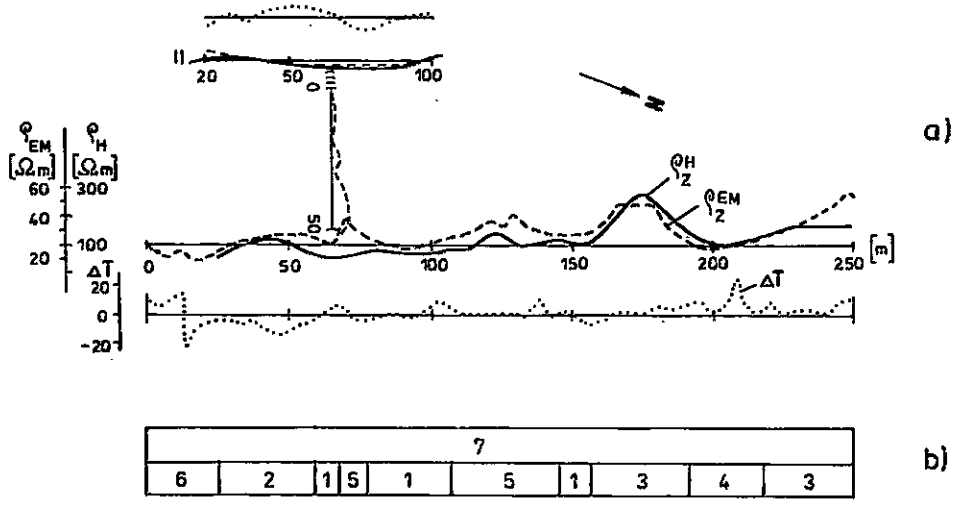

25. Resistivities distribution in Milovice, district Břeclav. a) map of resistivity lines, b) subsurface geological section; 1 – Tertiary clay, 2 – Tertiary gravel, 3 – Tertiary clastics, 4 – turbid matter, 5 – erosion scar, 6 – embankment, 7 – loess.

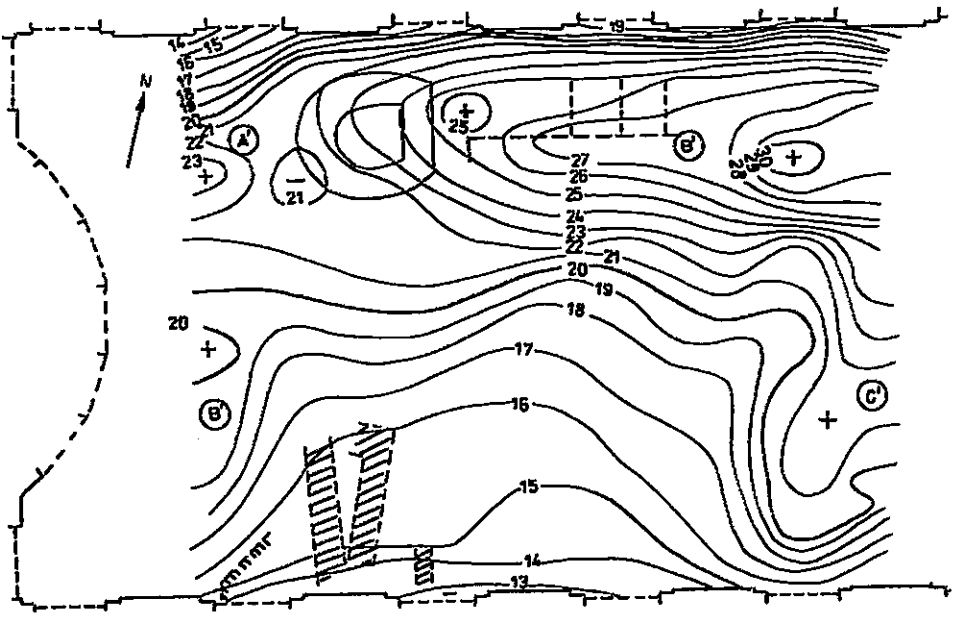

26. Map of ρ_z^{EM} contours according to measurement by the DIKO induction conductometer in Slavkov, district Brno-venkov.

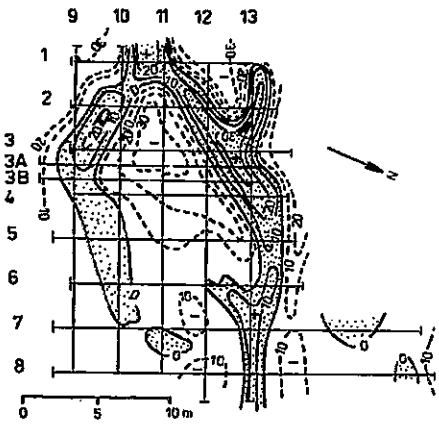

27. Map of ρ_Z^{EM} contours according to measurement in Předklášteří near Tišnov, district Brno-venkov.

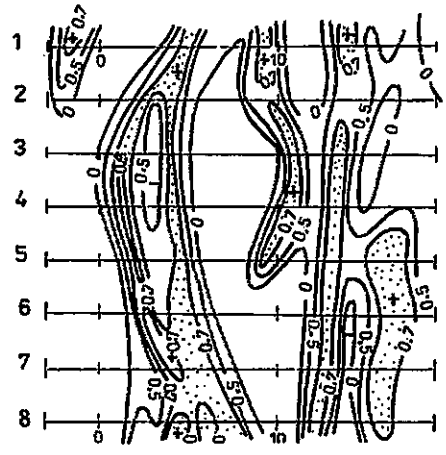

28. Map of mutual correlation coefficient according to measurement in Předklášteří near Tišnov, district Brno-venkov.

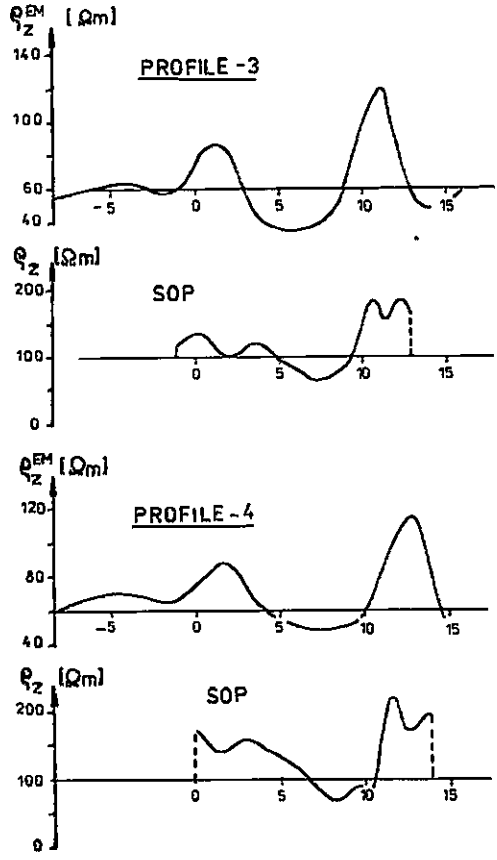

29. Comparison of profile curves $\rho_{Z(OP)}$ and ρ_Z^{EM} according to measurement in Předklášteří near Tišnov, district Brno-venkov.

magnetic dipoles with $m = 1$, a positive anomaly $a_V = 0.2$ of a conducting body at the relative depth $H = 1$, conductivity contrast $k = 50$ will be induced if the relative thickness $\Delta = 0.0115$, at the contrast $k = 10$ the relative thickness $\Delta = 0.065$ (i.e. 5.6 larger). However, for a negative anomaly a_N=0.2 over a non-conducting body with $k = 1/50$ the thickness must be $\Delta = 1$, if $k = 1/10$ the thickness $\Delta = 1.17$. In the case of non-conducting bodies the conductivity contrast $k<1/10$ affects the curves only very slightly. If the coefficient values are low, the effect can be neglected. On the contrary, in the case of conducting bodies the thickness Δ of the sheet markedly decreases with increasing conductivity contrast. For $m = 1$, i.e. for large-scale bodies, the detectability curves reflect the reality quite well. For smaller bodies, i.e. for $m > 1$ the curves offer rather a qualitative judgement on the possibilities of detection. The different curve for vertical magnetic dipoles on the one hand, and for horizontal magnetic dipoles on the

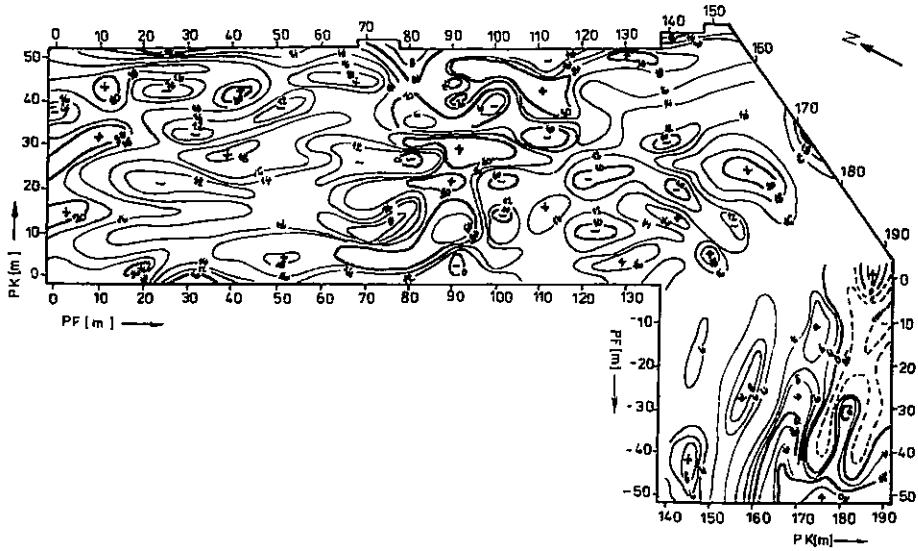

30. Map of ρ_2^{EM} contours according to measurement in Rybárna, area A, Staré Město near Uherské Hradiště.

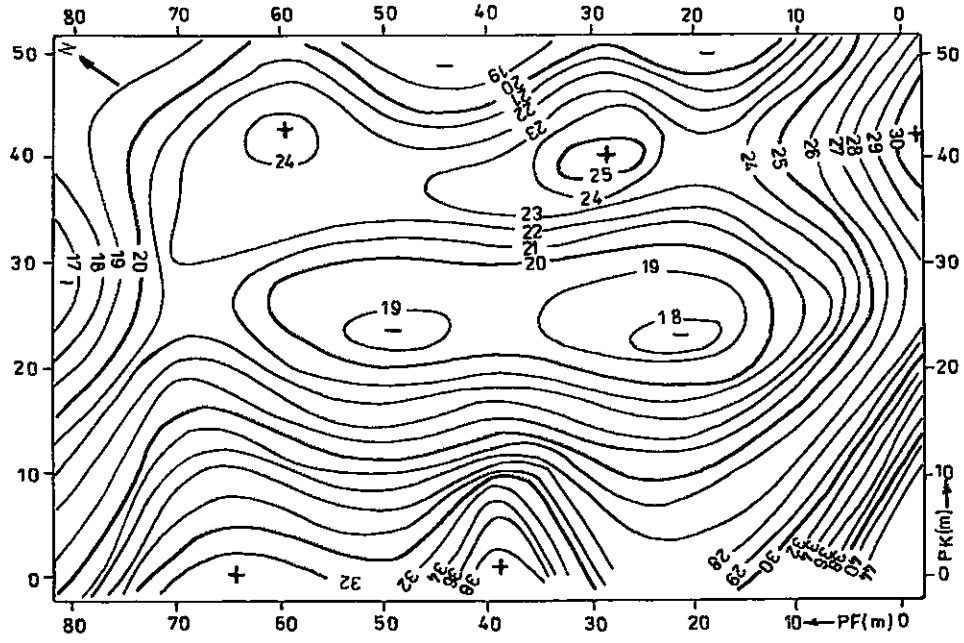

31. Map of ρ_2^{EM} contours according to measurement in Rybárna, area B, Staré Město near Uherské Hradiště.

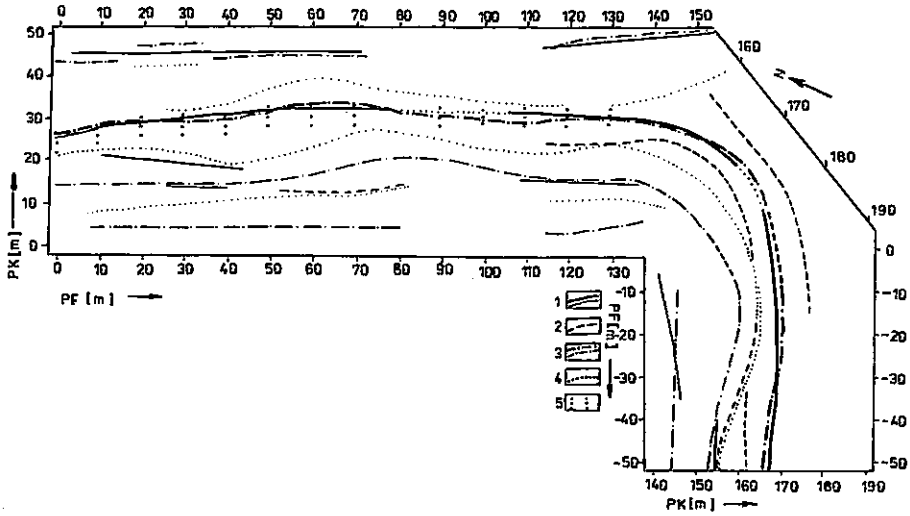

32. Comparison of geophysical measurement in Rybárna, area A, Staré Město near Uherské Hradiště. 1 – DEMP axes of non-conducting zones, 2 – DEMP axes of conducting zones, 3 – axes of positive Δ T anomalies, 4 – axes of negative Δ T anomalies, 5 – extent of morphological elevation structures.

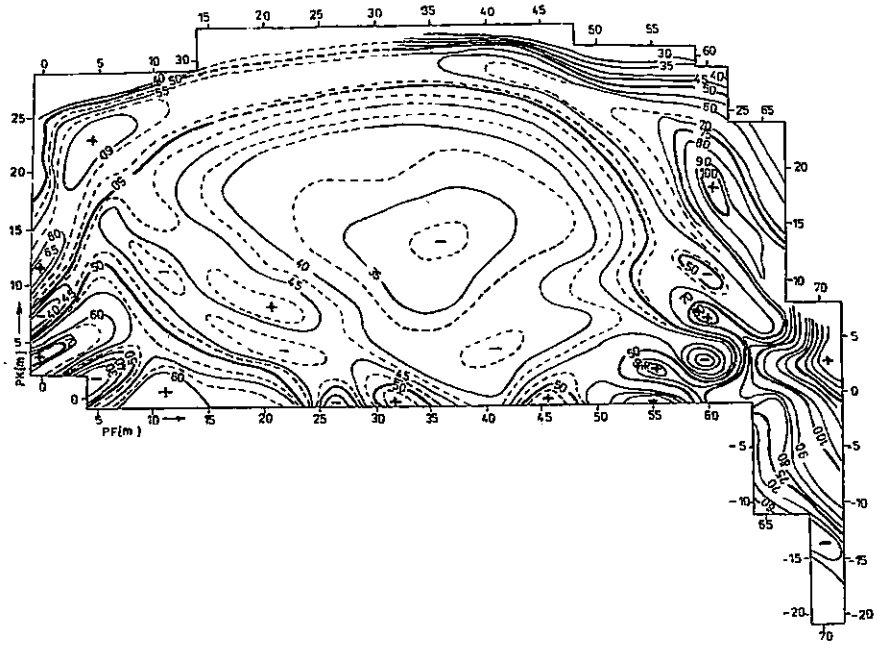

33. Map of ρ_Z^{EM} contours according to measurement in Přerov, Horní náměstí (Upper Square).

other with small H (from 0 to approx. 0.5) reflect the different effects of near-surface layers on the secondary magnetic field in the receiver at respective configurations (Fig. 2).

The sharp growth of curves for non-conducting bodies ($m > 1$) suggests a very poor or zero detectability of small non-conducting bodies from certain limit depth.

Field measurements with induction conductometers

The prototype of a device for direct and contactless apparent conductivity measurements (DIKO) has been developed in Geofyzika Brno. It is similar in principle to the EM-31 from Geonics Ltd., Canada. The prototypes are used for geophysical measurements in archaeological prospection, e.g. at Předklášteří, Staré Město, Uherské Hradiště, Bítov, Moravské Knínice, Milovice, Buchlov, Přerov-Zábřeh. Some results from reports by Hašek et al. (1988,1989) are presented here.

At the locality Milovice (district Břeclav) experimental geophysical measurements (DEMP – induction conductometer, VLF, magnetometry) were aimed at mapping of assumed erosion furrows and occurrences of Tertiary clastics in the Quaternary basement which are related with an assumed Palaeolithic settlement. A detailed geologic survey conducted along a profile running across interpreted occurrences of rocks exhibiting increased resistivity revealed two erosion furrows and a layer of Tertiary clastics (Fig. 25).

In the environs of the Slavkov u Brna castle conductivity measurements were carried out over an area of 26x20 m in a grid of 3x1 m in search for the stone foundations of the studied object. Results of measurements were processed into map of ρ_z^{EM} isolines (Fig. 26) in which a number of local anomalies can be found. Increased resistivity zones (e.g. A') well correlate with magnetic data.

Resistivity profiling and conductivity measurements at Předklášteří near Tišnov were conducted to verify the assumed site of a church in the area of the museum was reconstructed. ρ_z^{EM} isolines (Fig. 27) and the map of correlation coefficients (Fig. 28) indicated foundations of a small oval stone object. Results of measurements on profiles PF3 and PF4 (Fig. 29) show a good correlation between data obtained by both methods (resistivity profiling configuration was A2 M1 N2 B).

Measurements at Staré Město u Uherského Hradiště (locality "Rybárna") were aimed at defining the course of a fortification revealed by archaeological prospection.The measurements were conducted over two areas – A (200x50 m) and B (80x80 m) in a grid of 5x2 m. The results were processed into a map of ρ_z^{EM} isolines (Figs. 30 and 31) and into DEMP and magnetometry correlation diagrams (Fig. 32). Increased resistivity areas revealed by conductivity measurements correspond with positive ΔT anomalies which may indicate remnants of stone masonry and a bank.

Conductivity measurements on 15 profiles (30 m each) at Horní square in Přerov were aimed at defining the course of a 10th century ditch revealed by archaeologists in the vicinity of profile 15, station 25 m. The map of ρ_z^{EM} isolines (Fig. 33) and comparison with archaeological findings showed that the fortification is indicated by increased

apparent resistivities mainly in the northern part of the measured area, i.e. around 20–30 m. Decreased ρ_2^{EM} values indicated a filled in fountain.

Conclusions

If the condition of small induction number (or a near field) is satisfied, there is almost linear dependence of the secondary component of the magnetic field induced by eddy currents on apparent conductivity of a conducting half-space. The measured component of the secondary magnetic field in the receiver is shifted in phase by $\pi/2$ in regard to the primary magnetic field. Devices based on this principle (so called induction conductometers) enhance geoelectric investigations at small depths particularly in areas affected by human activity. They are applied in electromagnetic profiling, partly also in sounding to solve many practical tasks.

The present article concentrates on detection of horizontal conducting and non-conducting sheets at depth, using vertical and horizontal magnetic dipoles. The relatively easy handling of the task is due to the simple analytical representation of the relative contributions of elementary horizontal layers to the total apparent conductivity. It is conditioned by mutual independence of eddy currents in individual horizontal layers of the near field. The detectability curves were calculated using a one-dimensional model, which is suitable for sufficiently large horizontal bodies (i.e. for $l >> r$). To calculate the detectability of smaller bodies whose dimensions are comparable or less than the separation of dipoles, a multidimensional model is required. In the present article, simplified assumptions were used for detectability estimation.

Positive anomalies induced by conducting bodies prevail (they are k-times larger) over negative anomalies induced by non-conducting bodies. The calculated detectability curves show dependence on amplitude, and for conducting bodies on conductivity contrast. In the case of non-conducting bodies the influence of contrast $k < 1/10$ on the curves is very little. For $m = 1$ when horizontal dimensions of the body many times exceed the distance between dipoles, the detectability curves reflect reality quite well. For small bodies ($m > 1$) the curves, with regard to simplifying starting arguments, provide rather a qualitative idea about the detectability and testify to the very poor chance of detecting smaller non-conducting bodies by means of this method.

Field measurements with the developed induction conductometer prototypes confirm the positive features of the method when used at small depths. It is also obvious from the presented examples of measurements by means of induction conductometers at archaeological sites.

K tisku doporučil J.Chyba
Přeložila D. Maliková

References

Kaufmann, A. A. - Keller, G. V. (1983): Frequency and transient soundings. – Elsevier. Amsterdam.
Záhora, R. in Hašek, V. et al. (1988): Geofyzikální příprava těžby hnědého uhlí. – MS Geofyzika, a.s. Brno.

Záhora, R. (1989): Využitelnost přímého bezkontaktního měření zdánlivé vodivosti pro účely archeologické prospekce. Sbor. Geofyzika v archeologii a moderní metody terénního výzkumu a dokumentace. – MS Geofyzika, a.s. Brno.

Hašek, V. - Měřínský, Z. (1989): IRB při archeologickém výzkumu a archeogeofyzikálním průzkumu na Moravě v letech 1986–1988. Sbor. Geofyzika v archeologii a moderní metody terénního výzkumu a dokumentace. – MS Geofyzika, a.s. Brno.

Hašek, V. et al. (1989): Geofyzikální příprava terénního archeologického výzkumu. Etapa 1989. – MS Geofyzika, a.s. Brno.

Detekovatelnost horizontálních deskovitých těles pomocí elektromagnetických konduktometrů

(Resumé anglického textu)

Richard Záhora

Předloženo 11. dubna 1990

Příspěvek pojednává o elektromagnetické metodě s malým indukčním číslem, kdy hloubka vniku (skinu) značně převyšuje vzdálenost mezi vysílacím a přijímacím dipólem. Tato metoda realizovaná magnetickými dipóly v blízké zóně je využívána pro bezkontaktní určování odporových vlastností hornin. Přímé a bezkontaktní měření zdánlivé vodivosti je v tomto případě podmíněno monotónní, téměř lineární závislostí sekundární složky magnetického pole, vybuzené vířivými proudy na zdánlivé vodivosti vodivého poloprostoru. Vyhodnocovaná složka sekundárního magnetického pole v místě přijímacího dipólu je navíc fázově posunuta o $\pi/2$ oproti primárnímu magnetickému poli. Aparatury, které využívají tento efekt (tzv. indukční konduktometry) značně zefektivňují geoelektrický průzkum malých hloubek zejména v oblastech s intenzívní lidskou činností. Využívají se při elektromagnetickém profilování a částečně i sondování, které pro mnoho praktických úloh je dostačující.Jsou to např. přístroje EM-31, EM-38,EM-34, vyráběné kanadskou firmou Geonics, Ltd. a DIKO a.s. Geofyzika Brno, jejichž provedení závisí zejména na požadovaném hloubkovém dosahu.

Hlavní pozornost článku je věnována hloubkové detekovatelnosti horizontálně uložených vodivých a nevodivých deskovitých nehomogenit při vertikálním a horizontálním uspořádání magnetických dipólů. Hloubkovou detekovatelnost definujeme závislostí normované mocnosti Δ deskovité nehomogenity na normované hloubce H jejího uložení pro vytvoření vodivostní anomálie fixované velikosti a_v (a_N) při daném kontrastu vodivostí k, tj. závislostí $\Delta = f(H)$ pro parametry a_v (a_N), k.

Poměrně snadné řešení této úlohy vyplývá z jednoduchého analytického vyjádření relativních nezávislých příspěvků elementárních horizontálních vrstev k celkovému sekundárnímu magnetickému poli či celkové měřené zdánlivé měrné vodivosti.Tyto příspěvky jsou charakterizovány funkcemi $F_V(\tau)$ či $F_H(\tau)$ nebo $R_V(\tau)$ a $R_H(\tau)$ pro vertikální a horizontální uspořádání magnetických dipólů, které jsou znázorněny na obr. 2 a 3. Jednoduché vyjádření těchto funkcí (viz rovnice 5, 9, 10 a 11) vyplývá ze vzájemné nezávislosti vířivých proudů v jednotlivých horizontálních vrstvách blízké zóny.

Pro stanovení křivek detekovatelnosti je využit jednorozměrný model,který je oprávněný pouze pro dostatečně rozlehlé nehomogenity v horizontální rovině, tj. pro $l >> r$ (viz obr. 4). Úloha detekovatelnosti menších nehomogenit, jejichž rozměry jsou přibližně stejné jako rozestup mezi dipóly nebo menší, je podstatně složitější, neboť vyžaduje řešení vícerozměrných modelů. Pro přibližné hodnocení detekovatelnosti menších horizontálních deskovitých nehomogenit byly zavedeny značně zjednodušující předpoklady.

Křivky detekovatelnosti byly vyčísleny pro vodivé a nevodivé nehomogenity a obě

uspořádání dipolů pro značná rozmezí amplitud anomálií, vodivostních kontrastů a koeficientů m. Některé z těchto křivek jsou vyneseny na obr. 6–24. Koeficient m charakterizuje horizontální rozlehlost nehomogenity, která je uvažována rotačně symetrická, pro $l >> r$ je $m = 1$. Větší hodnoty m odpovídají menším nehomogenitám, jejichž horizontální rozměr je porovnatelný s rozestupem mezi cívkami nebo menší.

Popisovaná elektromagnetická metoda pro přímé a bezkontaktní měření zdánlivé vodivosti detekuje podle očekávání daleko výrazněji vodiče než nevodiče, jak dokumentují všechny křivky. Kladné anomálie vytvořené vodivými nehomogenitami převyšují k-krát amplitudy záporných anomálií nevodivých nehomogenit při jejich stejné geometrii i hloubce uložení. Všechny křivky vykazují očekávanou poměrně značnou závislost na amplitudě anomálie a koeficientu m (jak je patrno z obr. 12 a 13) a u vodivých nehomogenit na poměru vodivostí k. U nevodivých homogenit při $k < 1/10$ poměrně málo ovlivňuje průběh všech křivek, při $k << 1/10$ je jeho vliv prakticky zanedbatelný.

Pro $m = 1$, tj. pro značně rozlehlé nehomogenity, odpovídají křivky detekovatelnosti vcelku dobře skutečným poměrům. Pro menší nehomogenity při $m>1$ poskytují příslušné křivky s ohledem na značně zjednodušené výchozí předpoklady pouze orientační údaje.

V závěru příspěvku jsou uvedeny výsledky měření s popsanou elektromagnetickou metodou při archeologickém průzkumu lokality Milovice, okr.Břeclav, zámku Slavkova u Brna, v Předklášteří u Tišnova, ve Starém Městě a v Přerově. Výsledky těchto měření potvrdily efektivnost a výhodnost této elektromagnetické metody při průzkumu malých hloubek.

Vysvětlivky k obrázkům

1. Vertikální magnetické dipóly nad vrstevnatým poloprostorem.
2. Závislost relativního příspěvku (odezvy) k sekundárnímu magnetickému poli jednotkové vrstvy na normované hloubce jejího uložení pro vertikální $F_V(\tau)$ a horizontální $F_H(\tau)$ magnetické dipóly.
3. Relativní příspěvek k sekundárnímu magnetickému poli celého prostředí nalézajícího se pod normovanou hloubkovou úrovní τ_i pro vertikální $R_V(\tau_i)$ a horizontální $R_H(\tau_i)$ magnetické dipóly.
4. Model pro stanovení podmínek detekovatelnosti horizontálně uložené deskové nehomogenity.
5. Model nahrazující nekonečný vodivý poloprostor pod měřicím dipólovým systémem.
6. Závislost normované mocnosti vodivé deskové nehomogenity na normované hloubce jejího uložení pro anomálii $a = 0{,}1$, $m = 1$ a poměry vodivostí $k = 2, 4, 6, 8, 10, 25, 50, 100$. Vertikální magnetické dipóly.
7. Závislost normované mocnosti vodivé deskové nehomogenity na normované hloubce jejího uložení pro anomálii $a = 0{,}2$, $m = 1$ a poměry vodivostí $k = 2, 4, 6, 8, 10, 25, 50, 100$. Vertikální magnetické dipóly.
8. Závislost normované mocnosti vodivé deskové nehomogenity na normované hloubce jejího uložení pro anomálii $a = 0{,}4$, $m = 1$ a poměry vodivostí $k = 2, 4, 6, 8, 10, 25, 50, 100$. Vertikální magnetické dipóly.
9. Závislost normované mocnosti vodivé deskové nehomogenity na normované hloubce jejího uložení pro anomálii $a = 0{,}8$, $m = 1$ a poměry vodivostí $k = 2, 4, 6, 8, 10, 25, 50, 100$. Vertikální magnetické dipóly.
10. Závislost normované mocnosti vodivé deskové nehomogenity na normované hloubce jejího uložení pro anomálii $a = 0{,}2$, $m = 4$ a poměry vodivostí $k = 6, 8, 10, 25, 50, 100, 1000$. Vertikální magnetické dipóly.
11. Závislost normované mocnosti vodivé deskové nehomogenity na normované hloubce jejího uložení pro anomálii $a = 0{,}4$, $m = 4$ a poměry vodivostí $k = 10, 25, 50, 100, 1000$. Vertikální magnetické dipóly.
12. Závislost normované mocnosti vodivé deskové nehomogenity na normované hloubce jejího uložení pro poměr vodivostí $k = 10$, $m = 1$ a anomálie $a = 0{,}05, 0{,}1, 0{,}2, 0{,}4, 0{,}6, 0{,}8, 1$. Vertikální magnetické dipóly.
13. Závislost normované mocnosti vodivé deskové nehomogenity na normované hloubce jejího uložení pro anomálii $a = 0{,}1$, poměr vodivostí $k = 10$ a $m = 1, 2, 3, 4, 5, 6, 7, 8$. Vertikální magnetické dipóly.

14. Závislost normované mocnosti vodivé deskové nehomogenity na normované hloubce jejího uložení pro anomálii a =0,2, m =1 a poměry vodivostí k =2, 4, 6, 8, 10, 25, 50. Horizontální magnetické dipóly.
15. Závislost normované mocnosti vodivé deskové nehomogenity na normované hloubce jejího uložení pro anomálii a =0,6, m =1 a poměry vodivostí k =2, 4, 6, 8, 10, 25, 50. Horizontální magnetické dipóly.
16. Závislost normované mocnosti vodivé deskové nehomogenity na normované hloubce jejího uložení pro anomálii a =0,2, m =2 a poměry vodivostí k =4, 6, 8, 10, 25, 50, 100, 1000. Horizontální magnetické dipóly.
17. Závislost normované mocnosti vodivé deskové nehomogenity na normované hloubce jejího uložení pro anomálii a =0,2, m =5 a poměry vodivostí k =10, 25, 50, 100, 1000. Horizontální magnetické dipóly.
18. Závislost normované mocnosti nevodivé deskové nehomogenity na normované hloubce jejího uložení pro anomálii a =0,05, m =1 a poměry vodivostí k =1/2, 1/4, 1/6, 1/10, 1/50, 10^{-6}. Vertikální magnetické dipóly.
19. Závislost normované mocnosti nevodivé deskové nehomogenity na normované hloubce jejího uložení pro anomálii a =0,1, m =1 a poměry vodivostí k =1/2, 1/4, 1/6, 1/10, 1/50, 10^{-6}. Vertikální magnetické dipóly.
20. Závislost normované mocnosti nevodivé deskové nehomogenity na normované hloubce jejího uložení pro anomálii a =0,2, m =1 a poměry vodivostí k =1/2, 1/4, 1/6, 1/10, 1/50, 10^{-6}. Vertikální magnetické dipóly.
21. Závislost normované mocnosti nevodivé deskové nehomogenity na normované hloubce jejího uložení pro anomálii a =0,1, m =2 a poměry vodivostí k =1/2, 1/4, 1/6, 1/10, 1/50, 10^{-6}. Vertikální magnetické dipóly.
22. Závislost normované mocnosti nevodivé deskové nehomogenity na normované hloubce jejího uložení pro anomálii a =0,1 , m = 1 a poměry vodivostí k =1/2, 1/4, 1/6, 1/10, 1/50, 10^{-6}. Horizontální magnetické dipóly.
23. Závislost normované mocnosti nevodivé deskové nehomogenity na normované hloubce jejího uložení pro anomálii a =0,2, m =1 a poměry vodivostí k =1/2, 1/4, 1/6, 1/10, 1/50, 10^{-6}. Horizontální magnetické dipóly.
24. Závislost normované mocnosti nevodivé deskové nehomogenity na normované hloubce jejího uložení pro anomálii a =0,1, m =2 a poměry vodivostí k =1/2, 1/4, 1/6, 1/10, 1/50, 10^{-6}. Horizontální magnetické dipóly.
25. Rozložení odporů v Milovicích, okr.Břeclav.
    a) mapa odporových profilů, b) podpovrchový geologický řez; 1 – terciérní jíl, 2 – terciérní štěrk, 3 – terciérní klastika, 4 – splachové sedimenty, 5 – erozní rýha, 6 – navážka, 7 – spraš.
26. Mapa izolinií ρ_Z^{EM} podle měření s indukčním konduktometrem DIKO ve Slavkově u Brna.
27. Mapa izolinií ρ_Z^{EM} z měření v Předklášteří u Tišnova,okr. Brno - venkov.
28. Mapa koeficientů vzájemné korelace z měření v Předklášteří u Tišnova,okr. Brno-venkov.
29. Porovnání profilových křivek $\rho_{Z\,(OP)}$ a ρ_Z^{EM} z měření v Předklášteří u Tišnova,okr. Brno-venkov.
30. Mapa izolinií ρ_Z^{EM} z měření v Rybárně, plocha A, Staré Město u Uherského Hradiště.
31. Mapa izolinií ρ_Z^{EM} z měření v Rybárně, plocha B, Staré Město u Uherského Hradiště.
32. Korelační schéma z měření v Rybárně, plocha A, Staré Město u Uherského Hradiště.
    1 – osy nevodivých pásem z metody DEMP, 2 – osy vodivých pásem z metody DEMP, 3 – osy pozitivních anomálií ΔT, 4 – osy negativních anomálií ΔT, 5 – rozsah morfologických elevačních struktur.
33. Mapa izolinií ρ_Z^{EM} z měření v Přerově na Horním náměstí.

SBORNÍK GEOLOGICKÝCH VĚD
JOURNAL OF GEOLOGICAL SCIENCES

užitá geofyzika

applied geophysics

25

Vydal Český geologický ústav
Praha 1992

Vědecký redaktor: RNDr. Karel Cidlinský, CSc.

Obálku navrhl M.Cihelka
Odpovědná redaktorka: V. Čechová
Technická redaktorka: J. Pavlíčková
Sazbu programem Ventura 4.0 provedlo vydavatelství ČGÚ,
Malostranské nám. 19, Praha 1
Tisk: Tercie, s.s r.o., V Šáreckém údolí 39, Praha 6

Vydání I. — 144 stran, 12,63 AA — 12,83 VA
Náklad 500 výtisků — 03/9— 446-421-92
ISBN 80-7075-110-X ISSN 0036-5319